ABSTRACT

Title of Document: ANALYTICAL STUDY OF THE BEHAVIOR OF COMPOSITE DOVETAIL METAL DECKING FLOOR SYSTEMS FOR THE DEVELOPMENT OF PRACTICAL DESIGN GUIDELINES

Tara Leigh Pase, Doctor of Philosophy, 2022

Directed by: Professor Brian M. Phillips, Ph.D.
Department of Civil and Environmental Engineering

Prior testing and industry practice have shown composite metal floor systems – floors systems constructed from concrete composite with metal decking – behave stiffer than the current state-of-the-practice simplified calculations and estimations predict. Specifically, the dovetail decking does not have the quantity of available research and universal design guidance compared to the more common trapezoidal composite decking; this lack of a more accurate design standard has made the calculation of the non-linear stiffness behavior of the dovetail composite deck floor systems under small to intermediate strains inaccurate, and therefore limits its use for long-span configurations where deflection limits (i.e., serviceability limits) control the design.

The objective of this research is to create an analytical model of the flexural behavior of re-entrant dovetail composite decking floor systems for service (i.e.,

deflection) and strength (i.e., ultimate capacity) limit states and to understand the unique mechanical behavior of the slab system. By creating a more accurate analytical model of the flexural behavior of the dovetail composite deck system, a robust design guide table for engineering use is developed for a multitude of variables typically seen in construction, including but not limited to: various loads, deck gauges (thicknesses), concrete strength, concrete depths, etc.

The flexural behavior of the composite metal deck is modeled based on its material properties and the following base assumptions: the composite slab is in pure bending; plane sections remain plane and are orthogonal to the neutral axis; the laws of static equilibrium apply; and loads are assumed to be static. Application of this composite theory to determine the moment-curvature relationship using a numerical strain-compatibility computer-based solver is compared against physical tests to validate and calibrate the theoretical assumptions that make up the basis for the calculations. The resulting flexural behavior derived from this numerical strain-compatibility method has a multitude of uses including but not limited to: the derivation of a robust design table for a number of decking gauges, common slab thickness values, concrete strength ranges, and so forth; and variable stiffness properties for use in simplified finite element plate models.

The real-world purpose for this new numerical strain-compatibility model is to provide robust design guidance and engineering resources for practicing structural engineers, without a time-consuming and expensive finite element model. With the numerical strain-compatibility analysis, an engineer can

accurately analyze and specify composite concrete slabs in building projects without being limited by shorter spans or thicker slabs due to inaccuracies in deflection calculations.

ANALYTICAL STUDY OF THE BEHAVIOR OF COMPOSITE DOVETAIL METAL DECKING FLOOR SYSTEMS FOR THE DEVELOPMENT OF PRACTICAL DESIGN GUIDELINES

By

Tara Leigh Pase

Dissertation Submitted to the Faculty of the Graduate School of the
University of Maryland, College Park, in partial fulfillment
of the requirements for the degree of
Doctor of Philosophy
2022

Advisory Committee:
Brian M. Phillips, Co-Chair
Chung C. Fu, Chair (Co-Chair)
Michelle T. Bensi
Peter W. Chung, Dean's Representative
Marcus Zupan

Dedication

To my husband, Brian, who supported and encouraged me throughout this research and my engineering profession, and my children, Zane, Rye, and Arabella, without whom this research would have been completed five years earlier.

To my dad, Walter Pase, who shared my love of engineering and inspired and encouraged learning and education throughout my life.

To my mom, Marilyn, the benevolent nursing professor, who helped me realize very early in life that the medical profession is not a good fit for someone with an aversion to needles and an aversion to high levels of stress.

Table of Contents

Table of Contents iii
List of Figures v
List of Tables vii
1 Introduction 1

1.1 Composite Concrete Systems in Construction 1
1.2 Analysis and Testing of Steel Decking for Composite Systems 3
1.3 Existing Design Procedures for Composite Decking 5
1.4 Research Objective 6

2 Literature Review 7

2.1 Historical Context 7
2.2 Composite Concrete Theory 9
2.3 Design Code Development 11

2.3.1 The Pre-qualified Section Method 14
2.3.2 The Shear Bond Method 14
2.3.3 The Ultimate Strength Method 15
2.3.4 Other Tests, Methods, and Theories 17

2.4 Modeling the Behavior of Composite Slabs 18
2.5 Experimental Methods for Composite Concrete Slabs 20
2.6 Gaps in Prior Research and Design Methods 24

3 Dovetail Composite Slab Testing 27

3.1 Experimental Test Overview 27
3.2 Test Apparatus, Setup, and Instrumentation 30
3.3 Test Procedure 33
3.4 Load Test Results 34

4 Computational Strain-Compatibility Analysis 40

4.1 Strain-Compatibility Method Theory 40
4.2 Material Stress-Strain Models 47

4.2.1 Concrete Material Modeling Introduction 47
4.2.2 Concrete Compression Model 48
4.2.3 Concrete Tension Model 51
4.2.4 Steel Decking and Steel Reinforcement 56

4.3 Computational Analysis Methodology 58

4.3.1 Computational User Input 60
4.3.2 Numerical Integration for Computational Analysis 67
4.3.3 Steel Deck Strain Slip 69
4.3.4 Computational Analysis Solver 72
4.3.5 Moment-curvature Relationship 73
4.3.6 Deflection Calculation using the Moment-Area Method 75

4.4 Numerical Strain-Compatibility Model Validation with Test Data . 79

4.4.1 Computation of Deck Slip Strain 84

4.5 Practical Applications of Numerical Strain-compatibility Model for Dovetail Composite Slabs 98

5 Analysis of In-Situ Dovetail Composite Slab 100

5.1 5.1 In-situ Test Procedure 102
5.2 In-situ Test Results 105
5.3 Comparison of Numerical Strain-Compatibility Model with Other Simplified Methods 106

5.3.1 ASCE 3-91 Stiffness Calculation Method 106
5.3.2 Other Equations for Stiffness Calculation 108
5.3.3 Stiffness Calculation with Numerical Strain-compatibility Model 110
5.3.4 Comparison of Calculated Stiffness Models 112

5.4 Finite Element Plate Model of In-situ Composite Dovetail Decking Slab Implementing the Numerical Strain-compatibility Model 114

6 Development of Design Tables Utilizing the Numerical Strain-compatibility Model 129

6.1 Design Table Introduction 129
6.2 Practical Scope of the Design Table 130

6.2.1 Common Material and Geometric Properties 131

7 Conclusions 137
8 References 141

List of Figures

Fig. 1.1 Dimensions of the dovetail decking profile (Canam, 2016). 3
Fig. 1.2 Example of a trapezoidal decking profile (Canam, 2010). 3
Fig. 3.1 Composite concrete specimen profile (a) and dovetail decking geometric profile (b). 29
Fig. 3.2 Load frame apparatus with specimen loaded diagram. 32
Fig. 3.3 Load frame apparatus with specimen loaded and sensors installed. 32
Fig. 3.4 Free-body diagram of test specimens. 35
Fig. 3.5(e) Load-deflection results from tests, Spec. 6 38
Fig. 4.1 Dovetail decking profile for analysis and geometric definitions a, b, c, d, s, w, h_d, and definition of the neutral axis. 43
Fig. 4.2 Linear strain profile under very small strains and corresponding stress profile; materials' stress-strain relationships are still within the elastic range. 43
Fig. 4.3 Linear strain profile under increasing strains and corresponding stress profile; materials' stress-strain relationships are non-linear. 44
Fig. 4.4 Segmental geometric definitions of concrete for cross-sectional stress computations. 47
Fig. 4.5 Concrete compressive stress-strain model. 51
Fig. 4.6 Concrete macro-crack and fracture process zone location. 52
Fig. 4.7 Cohesive stress at the fracture process zone. 53
Fig. 4.8 Concrete tension stress-strain model with tension softening. 55
Fig. 4.9 Alternative tension stress-strain model based on Damjanic and Owen Model. 56
Fig. 4.10 Stress-strain elastic, perfectly plastic model for steel. 58
Fig. 4.11 Dovetail composite slab with geometry definition for example spreadsheet calculation. 61
Fig. 4.12 Flexural strain description for tabular input in analytical model. 66
Fig. 4.13 Stress-strain relationship of Zone I concrete; numerical integration of compressive stress region. 68
Fig. 4.14 Stress-strain relationship of Zone II concrete; numerical integration of tensile stress region above the flutes. 68
Fig. 4.15 Stress-strain relationship of Zone III concrete; numerical integration of tensile stress region in the flutes. 69
Fig. 4.16 Stress-strain relationship of Zone IV concrete; numerical integration of tensile stress region in the flutes. 69
Fig. 4.17 Strain distribution profile including slip strain of decking. 70
Fig. 4.18 Free-body diagram of frictional force between concrete and decking. 72
Fig. 4.19 Generic representative moment-curvature diagram for a generalized composite concrete slab. 74
Fig. 4.20 Moment, M(x), diagram along a simply-supported beam with a constant distributed load. 76

Fig. 4.21 Curvature diagram showing the numerical analysis for the moment-area method. 78
Fig. 4.22(a) Load-deflection model with no slip comparison with test specimen. 81
Fig. 4.23 Deck slip strain relationship with corresponding effective stiffness of composite slab, results from specimen 3. 86
Fig. 4.24 Deck slip strain relationship with corresponding flexural curvature angle of composite slab, results from specimen 3. 88
Fig. 4.25 Specimen end slip movement differential from (a) zero at initiation of test and (b) 1 mm at final loading of test. 90
Fig. 4.26(a) Load-deflection model comparison with test specimen 2. 92
Fig. 4.27 Deck slip factor vs. depth of composite dovetail decking slab. 97
Fig. 5.1 Structural floor plan of in-situ composite slab. 101
Fig. 5.2 Initial condition of composite slab. 104
Fig. 5.3 Initial placement and tare of dial indicators. 104
Fig. 5.4 Measured deflection vs vertical load across in-situ composite slab. 105
Fig. 5.5 Load deflection relationship at each quarter point, “A,” “B,” and “C,” along the composite slab span. 106
Fig. 5.6 Calculated moment-curvature diagram of in-situ composite slab. 112
Fig. 5.7 Calculated stiffness, EI, of in-situ composite slab. 114
Fig. 5.8 Flat plate model of in-situ slab in RISA 3D. 116
Fig. 5.9 Weak-axis bending of in-situ composite slab in Ansys. 118
Fig. 5.10 Strong-axis simplified moment diagram of continuous composite slab. 121
Fig. 5.11 Composite slab reinforced for negative flexure. 121
Fig. 5.12 In-situ slab material stiffness variations under self-weight and first load step. 124
Fig. 5.13 In-situ slab material stiffness variations under self-weight and second load step. 124
Fig. 5.14 In-situ slab material stiffness variations under self-weight and third load step. 125
Fig. 5.15 In-situ slab material stiffness variations under self-weight and fourth load step. 125
Fig. 5.16 In-situ slab material stiffness variations under self-weight and fifth load step. 126
Fig. 5.17 In-situ slab material stiffness variations under self-weight and sixth load step. 126
Fig. 5.18 In-situ slab material stiffness variations under self-weight and seventh load step. 127
Fig. 5.19 Numerical Strain-compatibility Model vs. In-situ Test Data 128
Fig. 6.1 Sample design table for dovetail decking composite slab. 135
Fig. 6.2 Moment - effective stiffness diagram for sample design of dovetail decking composite slab. 136

List of Tables

Table 2.1. Concrete Flexural Testing: Standards and Recommendations 22
Table 2.2. Flexural Testing: Composite Slab Research 23
Table 2.3. Gaps in Prior Research and Design Methods 24
Table 3.1. Dimensional properties of test specimens 30
Table 4.1. Table for steel deck geometry input. 62
Table 4.2. Table for concrete geometry input. 62
Table 4.3. Input for deck material properties. 64
Table 4.4. Input for concrete material properties in compression. 64
Table 4.5. Input for steel reinforcement properties. 64
Table 4.6. Deck Slip Factors 96
Table 5.1. Calculated moment-curvature-stiffness relationship of the in-situ composite slab 111
Table 5.2. Weak-axis flexural properties for in-situ composite slab 118
Table 5.3. In-situ composite dovetail decking slab effective stiffness for FE model 122
Table 5.4. Numerical Strain-compatibility Method FE Deflection vs. In-situ Test Data 128

1 Introduction

An introductory overview of the significance of composite decking in construction, the inaccuracies or gaps in the current design procedures for dovetail composite decking, and the purpose of developing a rational strain-compatibility method for the design of dovetail composite decking systems.

1.1 Composite Concrete Systems in Construction

Residential and commercial building design trends demand higher ceiling layouts and thinner, lighter floor systems, driving the requirements of structural floor systems beyond the capabilities of traditional structural steel and cast-in-place concrete. Composite metal decking appears to be a qualified response to these industry demands, but its current simplified design criteria limits it to shorter spans or thicker slabs. As a consequence, shorter spans compromise the architectural layout, creating a trade-off between higher ceilings versus longer clear-spans. However, based on prior testing and industry practice, the performance of composite metal floor systems – floors constructed from concrete composite with metal decking – is stiffer than the current state-of-the-practice simplified calculations and estimations predict.

The properties of the composite floor system are unique to the metal decking manufacturer's custom geometries and the physical interaction with the concrete slab. Composite behavior of the metal deck and concrete floor systems under flexural loading can be determined via testing and mathematical analysis to develop a distinctive design table. Two common types of corrugated metal decking geometries are trapezoidal (Fig. 1.2) and dovetail (Fig. 1.1); the benefits to the trapezoidal decking in manufacturing and in installation is the ease of stacking sheets without nesting, whereas dovetail must be stacked and unstacked by sliding from the ends . However there is an aesthetic architectural and ease-of-construction benefit to using dovetail once it is in place as part of the structure; the acute angles made by the dovetail configuration allows for non-penetrating hangers to be installed for HVAC systems, electrical systems, plumbing systems, hung ceilings, and other architectural finishes. The quantity of available performance research and, consequently, universal design guidance for the trapezoidal decking is far more extensive than for the dovetail decking; this lack of an accurate analysis method has made the calculation of the non-linear stiffness of the dovetail composite deck floor systems under small to intermediate strains grossly overstated, and limits its use for long-span

configurations where the code imposed deflection limits (i.e., serviceability limits) control the design.

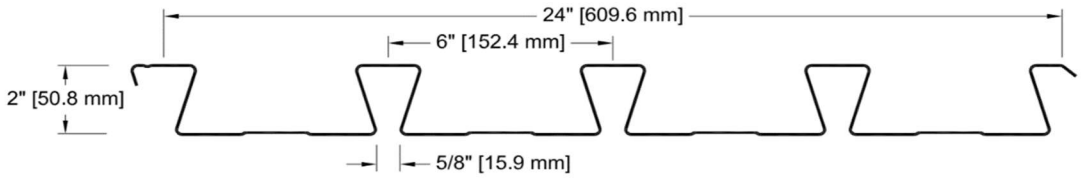

Fig. 1.1 Dimensions of the dovetail decking profile (Canam, 2016).

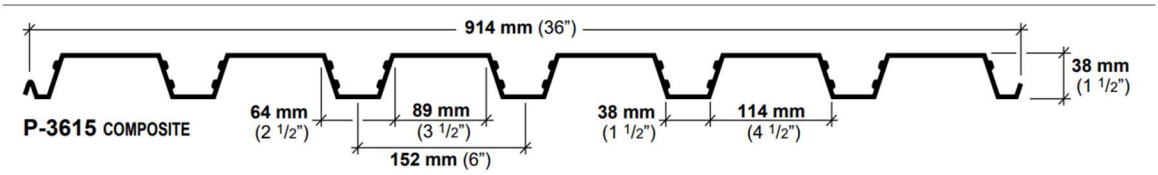

Fig. 1.2 Example of a trapezoidal decking profile (Canam, 2010).

1.2 Analysis and Testing of Steel Decking for Composite Systems

The testing and design recommendations of composite decking with a trapezoidal profile conclude that the decking does not effectively yield before partial delamination of the concrete-decking interface, which is referred to as a "bond slip" (Chen, 2010), and therefore its ultimate strength failure occurs before

the full ductile advantage of the steel is utilized. The re-entrant geometric profile of the dovetail deck cannot separate and pull away from the concrete the way that the trapezoidal decking separates when it slips; this is because the geometric configuration of the dovetail decking provides a mechanical interlocking into the concrete such that it makes the decking flex with the same curvature angle as the concrete, as it cannot pull away vertically from the concrete. This characteristic of the dovetail deck, alone, indicates that there must be an additional stiffness advantage in comparison to the more traditionally utilized trapezoidal composite decking.

The current absence of available models, design tables, full-scale tests, and literature for the dovetail specific decking configurations has limited the use of the dovetail decking design to short spans for some decking manufacturers, thereby ultimately limiting the efficiency and sustainability of the floor system. Prior studies and testing of composite concrete slabs with profiled steel decking, which utilizes the trapezoidal, obtuse angle corrugations, demonstrate a desirable ductile behavior with failure mechanisms commonly caused by slipping of the shear bond between the decking and the concrete. Historic studies using un-embossed dovetail decking show slip-failures are inevitable without the application of end-anchors, such as pins installed at the end of the spans near

the supports (Patrick, 1990); however, modern manufacturing of embossments rolled into the decking at the time of production do not exhibit the sudden end-slip failure in the same manner. A key distinction between the dovetail, re-entrant metal decking and the obtuse profile decking is the inherently interlocking nature of the decking into the concrete; this geometry makes its failure and slip mechanism fundamentally different from the debonding at the steel-concrete interface of the trapezoidal decking.

1.3 Existing Design Procedures for Composite Decking

Current American design procedure recommends analysis from the American Concrete Institute (ACI) 318, for reinforced concrete slabs, and the Steel Deck Institute (SDI), to determine the effective moment of inertia based on the cracked condition (American Concrete Institute, 2014), (Steel Deck Institute, 2017). The SDI and ACI provides a conservative and simplified calculation procedure, but also allows an alternative by permitting, instead, a rational *strain-compatibility analysis*. Currently, the rational strain-compatibility method of analysis for dovetail decking composite slabs lacks available research and test validation.

A rational strain-compatibility analysis and flexural testing of full-scale specimens are implemented and developed through this study. The full-scale test of the composite metal decking system validates the analytical model with the tested specimens.

1.4 Research Objective

The objective of this research is to better understand and model the flexural behavior of the re-entrant dovetail composite decking floor systems for service (i.e., deflection) and strength (i.e., ultimate capacity) limit states. By creating a more accurate analytical model of the flexural behavior of the dovetail composite deck system, a robust design guide table for engineering use is then developed for a multitude of variables typically seen in manufacturing and construction, including but not limited to: various common design loads, deck gauges (thicknesses), concrete material strength, and concrete slab depths. This design table was validated by physical testing.

2 Literature Review

A brief history of composite decking in construction practice, composite concrete theory of analysis, development of current design standards, various modeling methods for flexural behavior of composite concrete systems, historical composite decking experimentation, and gaps in current research in regards to analysis and modeling the behavior of composite dovetail decking systems.

2.1 Historical Context

The earliest patent for corrugated metal decking as a recognized construction component was documented in 1829 by Henry Palmer. Palmer's patent defined this innovative product as "fluted, indented or corrugated metallic sheets or plates [for] the roofs, and other parts of buildings;" his corrugated metal sheets served as roofs in the London Docks, built in the 1830s. Palmer later sold his patent to Richard Walker who continued to manufacture the corrugated decking until the mid1850s (Thorne, 2009). Upon expiration of the patent in 1843, other manufacturers broadened the use and availability for corrugated metal sheathing, prominently used as roofs for "railway trainsheds, dockyard buildings, and markets" (Thorne, 2009).

Across the Atlantic, in the United States, the Steel Roof Deck Industry Technical Committee was organized in 1939 to produce its first “Design Specification for Steel Roof Decking;” this committee was renamed the Metal Roof Deck Technical Institute in 1947, and then changed again in 1964 to the Steel Deck Institute (SDI), which is the name they still hold today (Steel Deck Institute, 2014).

The use of the corrugated metal in building and bridge construction evolved through time from a light-weight, self-supporting sheathing material for buildings to stay-in-place concrete formwork, and eventually to a contributory structural element of the concrete composite slab. This evolution in the United States occurred from the first use of composite construction in the form of concrete encased beams was in 1894, leading up to the first testing of welded shear studs – also commonly known as Nelson® studs – on composite steel beams at the University of Illinois in 1954, and to the inclusion of metal decking in a composite floor system appearing in the 1950s (Ahmed & Tsavdaridis, 2019). The composite metal decking provides many benefits in the construction process as a working platform, as temporary bracing for beams and walls, and as the permanent concrete formwork; benefits in the final composite design stage

include where the metal decking aids as part of the external reinforcement of the concrete slabs.

2.2 Composite Concrete Theory

Composite concrete design and analysis assumes that the steel and the concrete materials behave as a monolithic unit. Composite action will allow the horizontal shear forces developed in the longitudinal planes of a composite beam or a composite slab segment to transfer from one material to the other without slipping between the contact surfaces such that this assumption will be valid. The interconnecting elements between the horizontal shear force planes must be designed and analyzed to successfully resist this shear where, generally, slipping between the planes does not occur under flexural loads. For composite metal decking, dimples or “embossments” are formed in one or more of the ridge faces to resist slipping between the metal and the concrete; trapezoidal shaped decking, the more common geometric decking style, is prone to slipping at larger flexural strains thereby limiting the capacity of the composite slab system (Chen, 2010). This slip occurs when there is “overriding of [the] concrete against the embossments on the web surface when concrete slips under bending” in the trapezoidal decking (Abdullah & Easterling, 2008). Some metal decking profiles

are prone to slipping and a common method to define their shear bond interaction with the concrete is to perform a shear-bond test on a specimen with a defined geometric decking profile, and determine an additional reduction factor that is applied to the moment strength (Steel Deck Institute, 2017). This is referred to as the flexural strength determination of composite deck-slabs by the Shear Bond Method.

Theoretical analysis of composite concrete systems assume that the horizontal shear planes do not slip and are designed to adequately resist the horizontal shear forces, and there is no warping of the vertical planes under bending loads and therefore flexural strain is linear across the vertical planes of the beam or slabs. This assumption is typically described with the statement “plane sections remain plane.” Because the elements of the steel and concrete presumably behave monolithically, the stiffness of the composite system as a whole becomes greater than the sum of stiffness of its individual parts, which in turn increases efficiency of strength, stiffness, and materials.

Theoretically, one assumes a perfectly planar stain distribution along the depth of the slab with the composite action, but this condition is dependent upon the bond between the concrete and the steel deck interface being in perfect cohesion. The differing material properties of the steel and the concrete make

this shear bond more intricate and difficult to properly define in theory; steel can be characterized as an elastic-perfectly plastic material and concrete is a complex nonlinear material having different properties in tension and compression, as well as possessing complexities of tensile cracking.

By simplifying the flexural strain as perfectly linear, the stress profile and neutral bending axis at any point along the composite slab system can be defined based on the materials' stress-strain relationships. The composite floor system fails when a maximum stress limit state is met (known as a strength limit state), or when an unserviceable condition occurs, such as overall deflection of the span (known as a serviceability limit state).

2.3 Design Code Development

The design parameters of a structural flooring system are contingent upon meeting strength limit requirements, as well as service limit requirements while being subjected to a defined set of occupancy and environmental loading conditions. The strength limitations require, in general, that the composite floor system can be flexed until the steel has yielded and until the concrete has reached its maximum compressive stress, provided that the shear-bond strength has not been exceeded such that significant slipping occurs between the

concrete and steel materials. The service limitations require, in general, that the composite floor system not deflect beyond a pre-defined deflection limit; other service limits include sound transmission and vibrations, although these are not topics of discussion in this research report.

Design of composite concrete decking in the United States is currently under the direction of the Steel Deck Institute (SDI). The Steel Deck Institute first published their Steel Deck Institute Design Manual for Floor Decks and Roof Decks which included “Recommendations for the Design of Composite Steel Floor Deck” in 1978, Publication No. 23 (Steel Deck Institute, 2014). The American Society of Civil Engineers’ (ASCE) Standard for the Structural Design of Composite Slabs ANSI/ASCE 3-91 (American Society of Civil Engineers, 1994) is an older standard that is still referenced in some jurisdictions along with the SDI C-2017, however the SDI does not reference the ASCE 3-91 within its standard.

The current state-of-the-practice for designing long-span floor slab with composite metal decking includes design for strength capacity utilizing the Steel Deck Institute standards for composite decking (SDI C-2017 or earlier). The SDI C-2017 references the American Concrete Institute (ACI) 318-14 building code requirements (American Concrete Institute, 2014), and the American Society for

Civil Engineers (ASCE) 7-16 Minimum Design Loads for Building and Other Structures, among many other American standards; it does not reference the older ASCE 3-91 standard, however they both the SDI C-2017 and the ASCE 3-91 reference the standards of the ACI 318 of differing years. The SDI C-2017 provides a conservative estimate of calculated properties of the composite floor slab system due to its application of design analysis and procedures from the American Concrete Institute's Building Code Requirements for Structural Concrete (ACI 318) for reinforced concrete slabs. The SDI C-2017 acknowledges that the methods for determining the section properties of composite deck slabs "will provide conservative results for slabs with reinforcing," and that "the designer may choose to use alternate methods that consider the contribution of the reinforcing steel in this case" (citation). Those properties include: determination of the composite neutral axis, the moment of inertia of the cracked section, the moment of inertia of the uncracked section, and the moment of inertia of the composite section for deflection calculations. The SDI C-2017 procedures for determining the flexural resistance of a slab include: the pre-qualified section method, the shear bond method, the ultimate strength method, a full scale performance test as per SDI-T-CD, and other methods approved by the authority having jurisdiction.

2.3.1 The Pre-qualified Section Method

The pre-qualified section method to determine flexural strength utilizes empirical data from testing of various geometric configurations of embossments, which are the physical up-sets or dimpling of the metal decking. Based on the geometric pattern of the embossment, a variable called p_{sn}, where n is a number between 1 and 3 representing a limited number of embossment patterns, determines the embossment factor, and becomes part of the flexural strength equation. This method to determine strength is based on the ACI methods for determining flexural strength in reinforced concrete slabs and diminishing the strength value by an empirically calculated factor, k, less than or equal to 1.0. This k factor is called the "ordinate intercept of reduced experimental shear-bond line" and it determined empirically from shear-bond tests (ASCE 3-91 citation). There is no determination of service load properties from this method, which makes accurate calculations of deflections for checking against serviceability limits impossible.

2.3.2 The Shear Bond Method

The shear bond method utilizes empirical values from the shear bond resistance tests unique to the metal decking geometric and material properties,

or an alternative approach called the Force Equilibrium method which compares end- slip relationships to shear bond stress to more accurately describe the shear bond model (Abdullah et al, 2008). This testing and calculation methodology appears adequate for determining failures based on the capacity constraints of the shear bond between the concrete and trapezoidal decking, but it does not consider the benefit of the contribution of the concrete interlocking with the deck, which is inherent in re-entrant deck geometries; nor, does it focus on the behavior in the composite deck's lightly loaded, serviceable usage range. Generally, this method only provides a projected maximum strength determination of the composite slabs that focuses on shear bond failure of the trapezoidal profile, which for long-span slender dovetail decking composite slabs, is not typically the controlling limit state or failure mechanism.

2.3.3 The Ultimate Strength Method

The ultimate strength method calculates the composite flexural strength of the composite slab and the one-way shear strength; deflection calculations use a moment of inertia calculation of the direct average (equally weighted) of the full transformed section and the cracked composite section, conservatively assuming no contribution of stiffness from the concrete below the calculated neutral axis,

and conservatively assuming a constant stiffness across the entire length of the beam whether it is a single span or it is part of a continuous span. For continuous slabs, where the internal bending moments along the entire span transition between positive and negative moments, ASCE 3-91 offers the conservative option of assuming all spans are single, simply-supported, or using "a strength design of the cross section for conventional negative bending reinforcement" determination, but does not offer additional guidance for how this impacts the calculation of deflections (ASCE 3-91 citation). This ultimate strength method is certainly simplified and conservative in its estimate of deflections, which will cause an overly conservative design for slender slabs where deflection criteria failure occurs before strength failure.

The ASCE 3-91 commentary offers a more robust calculation for an effective moment of inertia, I_e, in relation to the moment applied to the composite concrete slab. Typical trapezoidal decking shapes at 1.5", 2", and 3" heights were tested in flexure and an empirical stiffness curve was developed by Lamport and Porter (1990). This calculation method offers a more accurate flexural behavior profile, however it does not properly apply to alternative geometric silhouettes, such as the dovetail deck shapes.

2.3.4 Other Tests, Methods, and Theories

The SDI code allows for alternate methods of design and analysis calculations for composite decking that are not specified within the code. This allowance provides an avenue for implementation of new and evolving theories, full scale testing of innovative geometric designs, and alternative methods of design utilizing technological advances.

Breaking away from traditional design practices for reinforced concrete where the composite slab system does not fully match with prior testing, real-world conditions, or common analytical procedures, can potentially have a greater benefit for strength and serviceability calculation accuracy in real-world applications. For example, a common design practice for reinforced concrete calculations is to conservatively neglect the stress-stain influence in tension once the concrete has cracked, (i.e., the point at which the outer most fiber in tension has reached the cracking strength, f_r, of concrete). This simplification provides decent results for ultimate strength design of typical reinforced concrete beams and slabs. However, if one considers the contribution of the confined tensile concrete material, utilizing a stress-strain model of the strain-softening behavior of the nonlinear quasi brittle material under small strain, serviceable loads, a

more accurate deflection model may be acquired (Kumar & Barai, Concrete Fracture Models and Applications, 2011).

2.4 Modeling the Behavior of Composite Slabs

The challenges of accurately and elegantly modeling the behavior of composite dovetail deck systems have inspired some variations of finite element analysis (FEA) studies. One particular challenge to finite element model (FEM) analysis is identifying an adequate method to define the bonding behavior between the steel deck and the concrete. The embossments on the flutes of the decking provide a mechanical interlock with the concrete to prevent slipping at the interface of the material and validate the assumption of composite theory that states *plane sections remain plane*; however, these embossments in trapezoidal decking are known to slip under higher flexural loads where the embossments pull out and detach from the concrete (Abdullah & Easterling, 2008). Early studies modeled the bond with connector elements or spring elements based on empirical values rendered from small scale shear push-out testing. The downside to using this method is that it does not factor the slenderness of the slabs (i.e., the ratio of the span length to the effective depth of the slab, defined as the distance measured from the top of the concrete to the centroid of the

decking) into the determination of bond strength and behavior (Abdullah et al 2009). Studies done by Abdullah et al (2009) defined the connector element between the steel shell element and the concrete 3D brick element with nonlinear properties based on test data. This study concluded that the slab slenderness has a considerable influence on the shear bond stresses and end-slips of the composite decking, and their finite element model validated the results of the test samples.

A similar study investigating the best methods to model the composite slab behavior using finite element analysis tools by Gholamhoseini (Gholamhoseini A. , 2018), determined that modeling results were reasonably comparable to test results. The finite analysis program, ATENA, was used and the slab system components were assumed with the steel decking as a “CC3D Bilinear Steel Von Mises” material, the concrete as a “CC3D Nonlinear Cementitious 2” material, and the composite bonding between the two as “CC3D Interface” material. The assumed steel deck properties included an elastic-fully plastic model. The concrete material comprised of at least four different stress conditions: linear elastic tension behavior before cracking, tension after cracking using crack-opening law and fracture energy theory, compression before peak stress, and concrete softening at compression after peak stress.

All finite element modeling verification testing and research identified above used the trapezoidal metal deck profile rather than a dovetail deck profile. The end-slip failure mechanism of the trapezoidal composite decking was highlighted and often quantified in prior tests and logically has a significant effect on the composite behavior of the slab system. Because the shear bond is unique to the perforations and the profile of the metal decking, a similar but stronger shear bond is anticipated for the dovetail decking profile in contrast to the trapezoidal profile.

2.5 Experimental Methods for Composite Concrete Slabs

The American standards by the Steel Deck Institute (SDI) and by the American Society of Civil Engineers (ASCE), the SDI T-CD-2017 and the ASCE 3-91, respectively, each provide their own published standard of testing for composite concrete slabs. The American Society for Testing and Materials (ASTM) ASTM C78/C78M-10 also provides testing standards for reinforced concrete flexural testing, but does not provide standards for composite concrete slabs, specifically.

Notable experiments regarding the flexural behavior and end-slip of trapezoidal geometries (Abdullah & Easterling, 2008) (Lamport & Porter, 1990)

(Gholamhoseini A. , 2018) and dovetail geometries with no embossments (Patrick, 1990) have been performed by various researchers. A summary of these testing standards, and the prior notable test methods are described in Table 2.1 and Table 2.2, respectively, for comparison of methods.

Table 2.1. Concrete Flexural Testing: Standards and Recommendations

Reference	Decking	Sample Width	Sample Length	Sample Depth	Span Length
SDI T-CD-2017	Unspecified	b_d	l	h	l
ASCE 3-91	Unspecified	18 in min.	l_i + 6 in min.	3.5 in min.	l_i
ASTM C78/C78M-10	No Decking	Unspecified	L+2 in min.	L/3	L

Reference	End Supports	Loading	Load Rate	Load Steps	Measurement Data
SDI T-CD-2017	Pinned-Roller; 1, 2 or 3-span	Four Point Loading	10% max load /min	Increments of 2% Max Load	Maximum Applied Load, Load/Deflection Data, and other
ASCE 3-91	Pinned-Roller	Four Point Loading or Uniform	150 psi/min compression stress	Increments of 1/10 Maximum Load	Midspan Load-deflection Data, End-slip Data, Load at First Visible Crack, and other
ASTM C78/C78M-10	Pinned-Roller	Four Point Loading (at Thirds)	125-175 psi/min tension stress	Unspecified	Maximum Applied Load, Modulus of Rupture, and other

Table 2.2. Flexural Testing: Composite Slab Research

Reference	Decking	Sample Width	Sample Length	Sample Depth	Span Length
Abdullah, Esterling 2009	Trapezoidal	305 mm	L + 200 mm	51 mm & 76 mm	1220 mm - 3660 mm
Gholsemini 2018	Trapezoidal	1200 mm	6900 mm	150 mm	3350 mm
Lamport, Porter 1990	Trapezoidal	24 in - 36 in	L + 6 in	3 in - 9 in	6 ft - 17 ft
Patrick 1990	Dovetail w/ end-anchors, no emboss.	Unspec.	Unspec.	Unspec.	5775 mm

Reference	End Supports	Loading	Load Rate	Load Steps	Measurement Data
Abdullah, Esterling 2009	Pinned-Roller; 1-span	Four Point Loading	Unspec.	Unspec.	Load-deflection Data, End-slip Data
Gholsemini 2018	Pinned-Roller; 2-span	Four-Point Loading	0.3 mm/min deflection	Unspec.	Load-deflection Data, End-slip Data
Lamport, Porter 1990	Pinned-Roller; 1-span	Four-Point Loading	Unspec.	Unspec.	Load-deflection Data
Patrick 1990	Pinned-Roller, 1-span	Approximated Uniform Loading	Unspec.	Unspec.	Load-deflection Data, End-slip Data

2.6 Gaps in Prior Research and Design Methods

Steel decking for composite concrete slab systems has been in use for decades and, in general, has a variety of testing, research, calculation methodology, and design standards done. However, there are notable gaps in all of this prior testing and research that this study and testing will address. Many of these gaps arise due to a lack of design guidance or standards on the specific geometric configuration of interest – the dovetail configuration. The gaps are summarized in Table 2.3.

Table 2.3. Gaps in Prior Research and Design Methods

Subject Matter	Citation	Summary of Research Gaps
Shear Bond Slip	Abdullah 2009	This study investigated the shear bond slip at the concrete/steel-decking interface for trapezoidal geometries of metal decking. The mechanism of the slip between the steel deck and the concrete is different for trapezoidal decking versus dovetail decking. The dovetail decking, specifically, is the focus of this research.
Deflection Calculations	Lamport & Porter 1990	This study concluded that their methodology of deflection calculations were not reasonably applicable at loading at or below the service load range; the calculations for deflection were too high

Subject Matter	Citation	Summary of Research Gaps
		at very small loads up to the design service loads. This research is focused on accuracy of the full range of deflection, especially at small service loads which are commonly the controlling design limit for very long span floor systems.
American Design Calculation Standards	ASCE 3-91	Design guidance is provided for common deck geometries of trapezoidal decking. An alternative calculation method for flexural capacity is valid for a plethora of trapezoidal deck geometries and embossment patterns. Other geometries of decking, such as the dovetail decking, do not comply with these design calculation methods.
American Design Calculation Standards	SDI C-2017	Similar to the ASCE 3-91, this design guide provides strength capacity methods and deflection calculation methods for common trapezoidal composite deck geometries and embossment styles. Dovetail decking does not apply to the calculation methods suggested.
Concrete Tension-stiffening Behavior	Stramandinoli & La Rovere 2008	This study recognized the benefit of formulating the constitutive model for reinforced concrete that takes into account the tensile behavior of the concrete. Their analysis and testing was limited to reinforced concrete beams, but was not applied to long-span composite concrete decking.
Shear Bond Slip	Abdullah &	This study noted unique web-curling at the

Subject Matter	Citation	Summary of Research Gaps
	Esterling 2008	embossments of the trapezoidal deck profiles under flexural loads. This is unique to the geometry of the trapezoidal decking, whereas the dovetail decking, which is the focus of this research, will not have the same web-curling phenomenon contributing to the slipping of the shear bond between the concrete and steel deck.

3 Dovetail Composite Slab Testing

A description of the preparation and implementation of physical flexural load tests performed on dovetail composite concrete slab specimens, the loading apparatus, the test procedure, and the results from the flexural load tests.

3.1 Experimental Test Overview

Full-scale bending tests were performed to determine the flexural behavior of a composite concrete and dovetail metal deck specimen under four-point loading. The purpose of the testing of these dovetail composite decking specimens is to verify and compare the test results to the new analytical method proposed in this study. The geometric shape and thickness of the metal decking, the RS2.0C fabricated by Canam (Canam, 2016), is depicted in Fig. 3.1; the nominal length of the composite deck was cut to 10'-0" (3.05 m) lengths and the width of the specimen was equal to the standard fabricated decking strip, 2'-1.125" (638 mm). Additional reinforcement for these specimens included 6x6 W2.0x2.0 welded wire mesh, which is commonly placed in composite concrete slabs as a standard construction practice, and as is required by ACI (American Concrete Institute, 2014) for temperature shrinkage and curing shrinkage control;

this reinforcement rests at the top of the flutes of the corrugated decking (Fig. 3.1).

A total of 13 slab specimens were cast to a nominal height of 5.5” (140 mm) with 4,000 psi (27.6 MPa) strength, normal weight concrete (approximately 145 lb/ft^3 or 22.8 kN/m^3). Because of the nature of variability the wood formwork, each specimen was measured to determine its as-constructed depth and width (Table 3.1). Any modeling and analysis of the test specimens could therefore be calculated using the actual depth and width measurement for higher resulting accuracy.

Concrete cylinder samples, of 6 in (152 mm) diameter, were cast at the beginning, middle and end of the concrete pour to verify the concrete strength of the batch. The specimens were rough finished and left to cure for more than 28 days; the 6-inch concrete cylinders were cured beside the slab specimens. The cylinders were sent to an independent test facility to determine their actual compressive strength, f'_c, where their strength was in the ranged from 5,620 psi (36.3 MPa) to 5,950 psi (41.0 MPa), with an average strength of 5,790 psi (39.9 MPa).

All composite slab specimens were cast and cured, fully supported on the ground so as to reduce any potential initial stresses in the steel decking. The

specimen loading into the apparatus was accomplished with a forklift at third points so as to also minimize stresses related to handling prior to the load test.

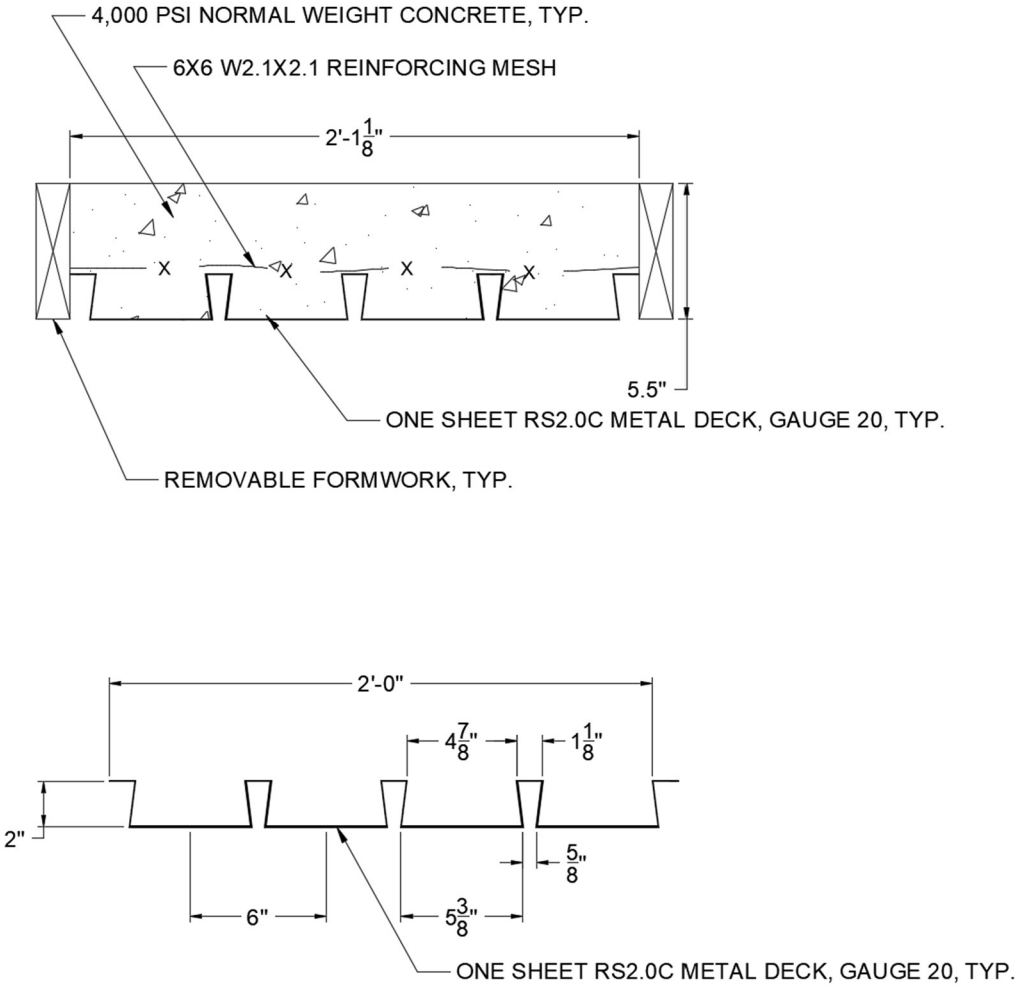

Fig. 3.1 Composite concrete specimen profile (a) and dovetail decking geometric profile (b).

Table 3.1. Dimensional properties of test specimens

Specimen	Depth (in)	Width (in)
1	5.5	25.5
2	5.625	26
3	6.75	26
4	5.75	25.75
5	6	25.5
6	5.75	25.375
7	5.875	25.75
8	6.25	25.75
9	5.75	25.75
10	5.75	25.25
11	5.75	25.75
12	5.625	25.75
13	5.625	25.75

3.2 Test Apparatus, Setup, and Instrumentation

A steel load frame apparatus was constructed to apply two point loads at a set distance on each of the identical specimens (Fig. 3.2 and Fig. 3.3). The square tubing supports provide a 2” seat at the ends of the slabs, which is the minimum seat requirement for the composite metal decking (Canam, 2010). A hydraulic jack, rated for use up to 40 k (178 kN), applied the load to the midpoint of a steel spreader beam, which reacts at two points on the slab specimen. The

jack is controlled with an air-to-hydraulic pump for use up to 10,000 psi (69 MPa); the rate at which the jack loads the frame is controlled using a foot switch. A calibrated load cell below the jack provides load application and rate of load data.

Deflection measurements are collected via three position sensors, one at midpoint, and two others at the locations shown in Fig. 3.2. Additional dial gauges were placed at the same deflection measurement locations to duplicate and verify sensor data at the displacement measurement points.

Two strain gauges were placed at the base of the steel decking (the bottom flute) within the constant moment/constant curvature region of the test specimen, between the point loads. A LVDT (Linear Variable Displacement Transducers) was placed on the top of the slab to measure the strain at the top of the concrete, mounted with non-destructive adhesion between the point loads. Two crack gauges are applied to the ends to measure the end-slip between the decking and the concrete.

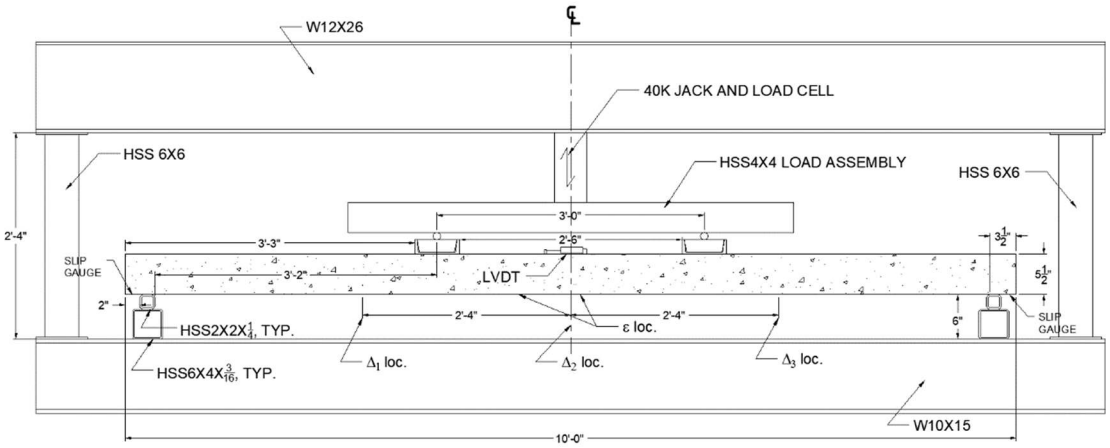

Fig. 3.2 Load frame apparatus with specimen loaded diagram.

Fig. 3.3 Load frame apparatus with specimen loaded and sensors installed.

3.3 Test Procedure

A single specimen was loaded in the load frame apparatus and all sensors and gauges were applied as depicted in Fig. 3.2 and Fig. 3.3. Distance measurements were taken which verified the correct placements of supports, load jack, and spreader beam as well as sensors. All sensors and gauges were tared.

The hydraulic jack applies the load at a rate of approximately 200 lb/min or less, within the maximum load rate requirements of the SDI T-CD-2017 (Steel Deck Institute, 2017), and similar to the loading rate used by Gholamhoseini (2014) which was a controlled deflection rate of 0.012 in/min (0.3 mm/min). The data acquisition system utilized, Labjack T4, records all sensor data for the duration of the load test at 8 second intervals. The digital dial gauge's measurements and the load cell read-out are also manually recorded at approximately 1,000 lb (4.45 kN) increments for redundancy and verification of the sensor data.

The specimens are loaded, quasi-statically, until the maximum resistive load is met and the samples deflect without resisting any higher load. Visible cracks and crack sounds are noted at first occurrence, and documented on the load-deflection data when they manifest. The location of cracking initiating within

the decking flutes was noted as “Zone III/IV” cracking, while cracking above the decking flutes was noted as “Zone II” cracking. These zones are regions of the composite slab profile that are defined and discussed further in Section 4.2.1 and in Fig. 4.4.

The samples are loaded to the deflection limit of approximately 1 inch (25 mm), which flexes the composite slab to approximately 30% of its original uncracked stiffness and at which point the end-slip of the test specimen is greater than 1 mm. Because this is well beyond the serviceable range of the composite slab system, it is adequate to terminate the test at this point.

3.4 Load Test Results

The primary data collected from the test is the load-deflection relationship curve, which is utilized to validate the computational analytical method for the composite dovetail-decking slab. The load applied by the hydraulic jack, P, is equally split by the load assembly steel tubes and the correlating maximum deflection, Δ_{max}, occurs at the center of the symmetrically loaded specimen. The free-body diagram of the load-frame on the test specimens is described in Fig. 3.4.

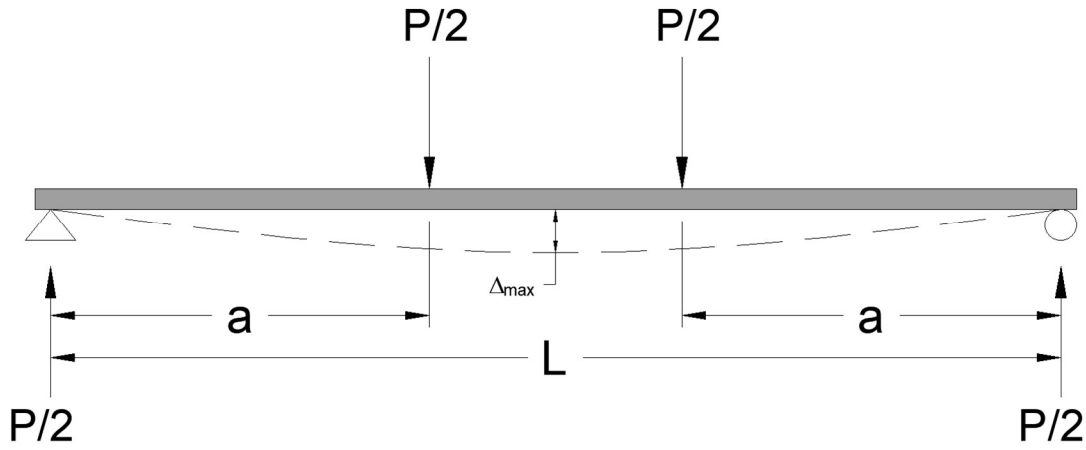

Fig. 3.4 Free-body diagram of test specimens.

The nonlinear load-deflection relationship measured from the test specimens is depicted in Fig. 3.5. Based on the various samples tested, the composite slabs appeared to consistently follow a trend of softening behavior at the initial indication of cracking, and experiencing a final end slip of the deck relative to the concrete around

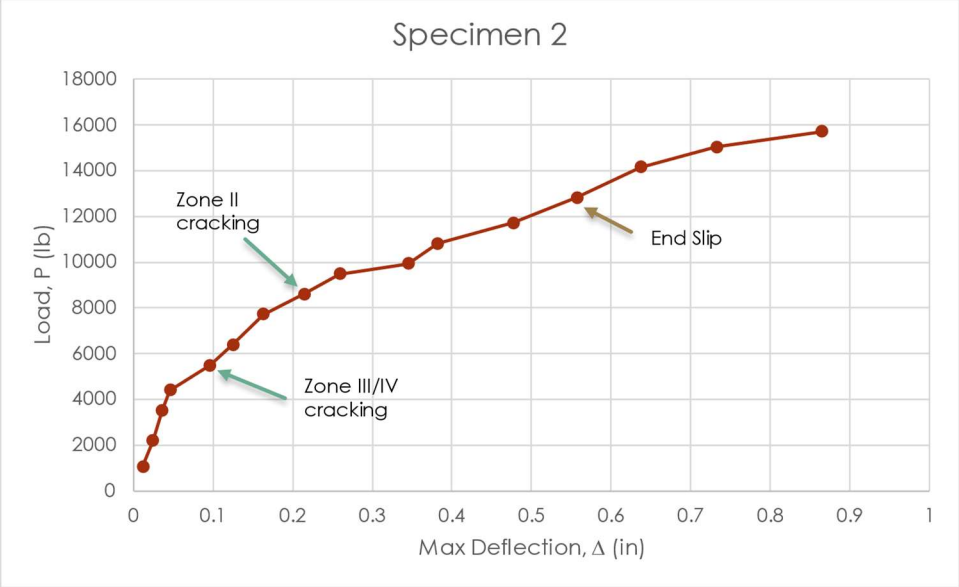

Fig. 3.5(a) Load-deflection results from tests, Spec. 2

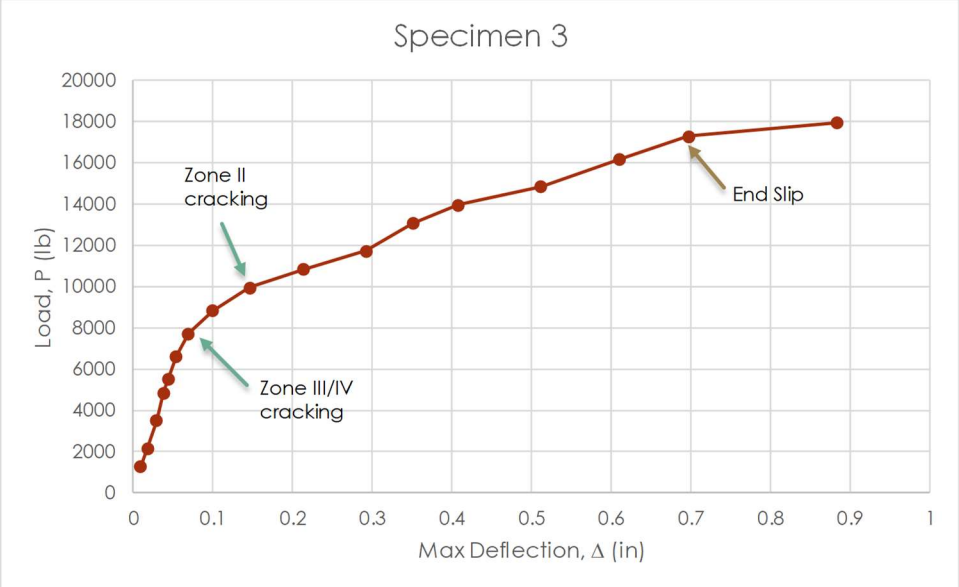

Fig. 3.5(b) Load-deflection results from tests, Spec. 3

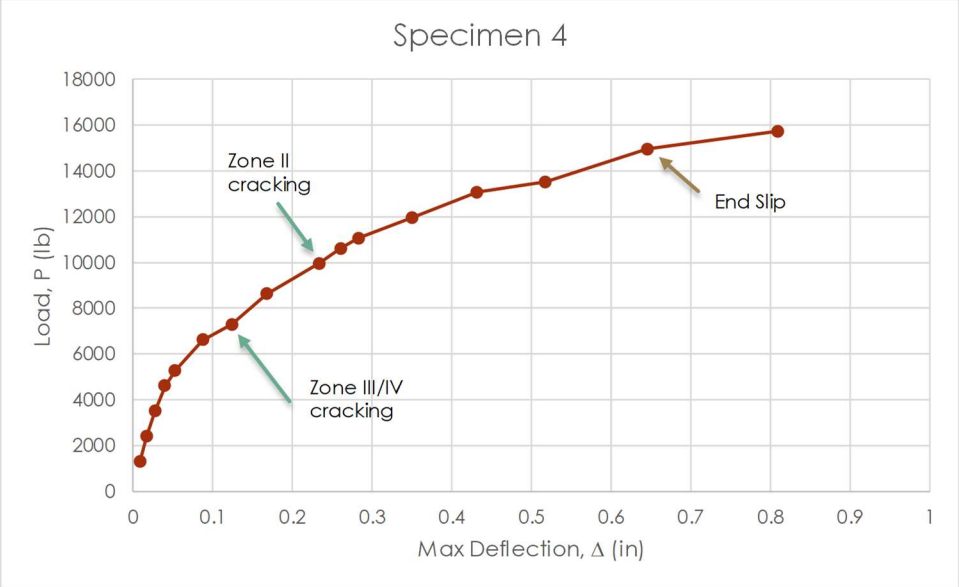

Fig. 3.5(c) Load-deflection results from tests, Spec. 4

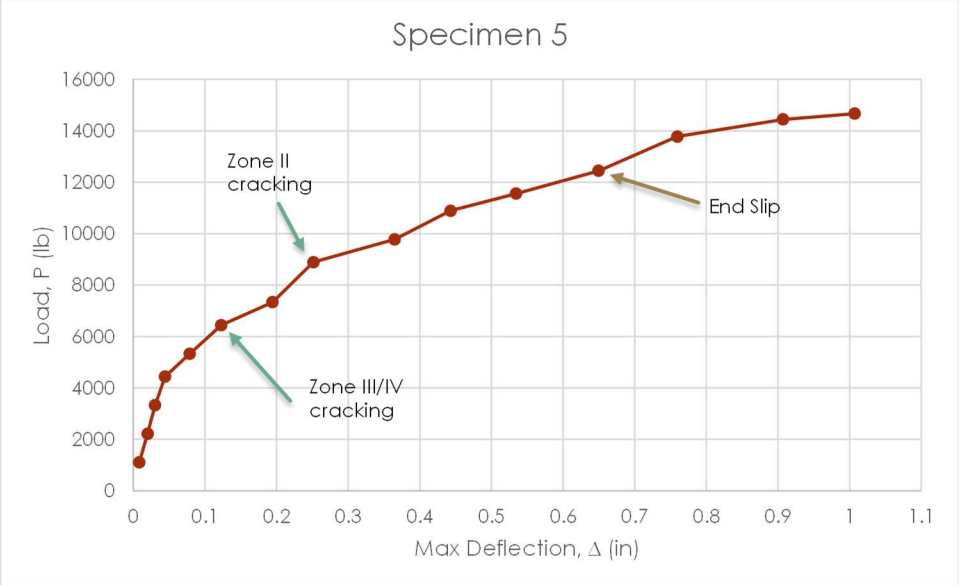

Fig. 3.5(d) Load-deflection results from tests, Spec. 5

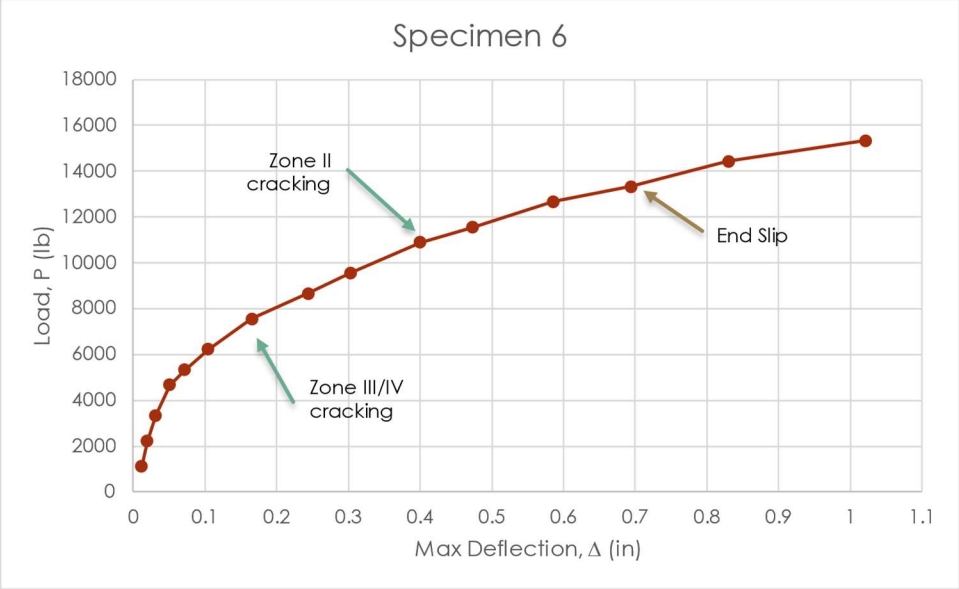

Fig. 3.5(e) Load-deflection results from tests, Spec. 6

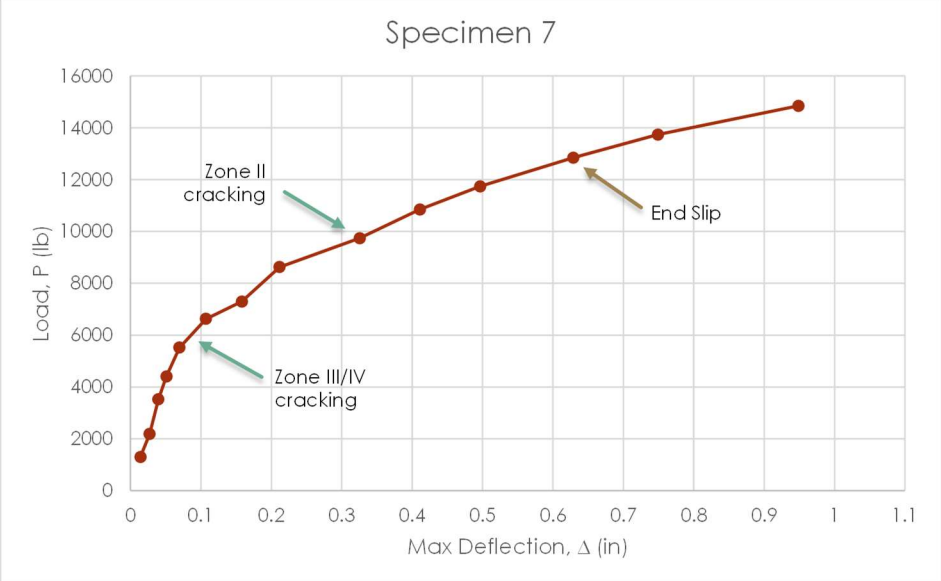

Fig. 3.5(f) Load-deflection results from tests, Spec. 7

Fig. 3.5(g) Load-deflection results from tests, Spec. 8

4 Computational Strain-Compatibility Analysis

The following sections describe strain-compatibility theory as applied to composite beams with reentrant, or dovetail, decking. The equations were assembled into a computer program that solves for static equilibrium with incrementally increasing flexural strain in the cross-section, producing a moment-curvature relationship for the given member properties. This procedure delivers a quick method for analysis and design in lieu of complex finite element models or experimental testing; the approach is compared to the experimental tests discussed in Section 4.4.

4.1 Strain-Compatibility Method Theory

A strain-compatibility based computational analysis of composite slab systems provides a rapid solution for engineers to design based on multiple changing variables without the need to produce unique finite element models for all possible scenarios on a structural design project, or conduct time consuming and expensive experiments. If reasonably accurate, a strain-compatibility based computational analysis can ultimately lead to the creation of a computational program that will quickly solve for the flexural behavior of the slab at small strains

where serviceability limitations control the design, thus expanding the usage of this composite floor system for longer spans.

The flexural behavior of the composite metal deck section can be analytically modeled based on its material properties and the following base assumptions: the composite slab is in pure bending; plane sections remain plane and are orthogonal to the neutral axis; the laws of static equilibrium apply; kinematic equations apply; and loads are static.

The geometry of the composite cross-section of the deck and concrete assembly is defined by the parameters depicted in Fig. 3.1 which match the specimens used for validation testing; the sample strain-compatibility analysis performed for this study will be compared to the results from the testing. Positive bending is evaluated first, and is defined with the top of the slab in flexural compression and the bottom of the slab in flexural tension. The composite concrete deck analysis is conducted for a single one-foot wide (305 mm) strip, which is a common width for analysis of one-way slabs in American standards (Fig. 4.1).

In strain-compatibility analysis, the flexural strain is defined incrementally from 0 to n at the top of the concrete slab and an associated moment is calculated at each increment; a value of n=0.003 was utilized based on ACI

standards for the maximum strain at crushing of concrete, although it can vary but is typically in the range of 0.003 to 0.004 for concrete members of “normal proportions, materials, and strength” (American Concrete Institute, 2014). At very small strain values, the associated concrete stresses in compression and tension, σ_c and σ_t, respectively, is nearly linear; the tension force in the deck is simplistically defined as T_d and is positioned at the centroid of the deck. The position of the neutral axis and the associated moments from the stress profile is calculated to satisfy the law of static equilibrium, $\Sigma F=0$, and the curvature, ψ, is defined by the set strain values and calculated location of the neutral axis (Fig. 4.2). As strains increase in magnitude, the neutral axis (N.A.) moves upward and the concrete stress distribution along the cross-section becomes more increasingly non-linear (Fig. 4.3). The associated internal moment from the flexural stresses is calculated for each increasing strain increment; at small strains when the curvature of the slab is very small, the resisting moment, M_r, of the dovetail decking is nearly zero, but as the curvature of the slab increases, the resisting moment also increases thereby playing a bigger role in the overall resisting moment of the composite slab system.

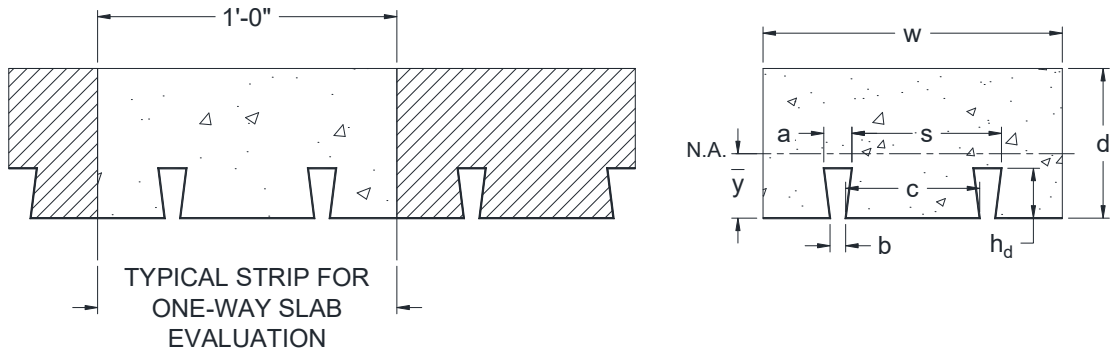

Fig. 4.1 Dovetail decking profile for analysis and geometric definitions a, b, c, d, s, w, h_d, and definition of the neutral axis.

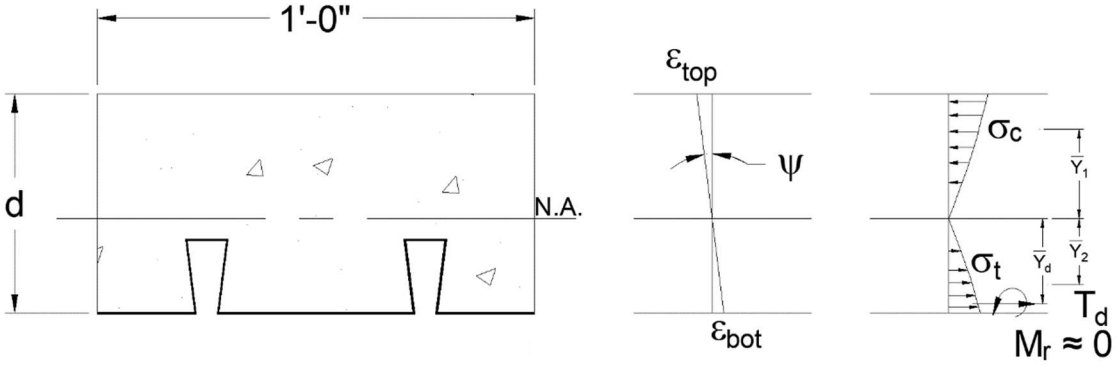

Fig. 4.2 Linear strain profile under very small strains and corresponding stress profile; materials' stress-strain relationships are still within the elastic range.

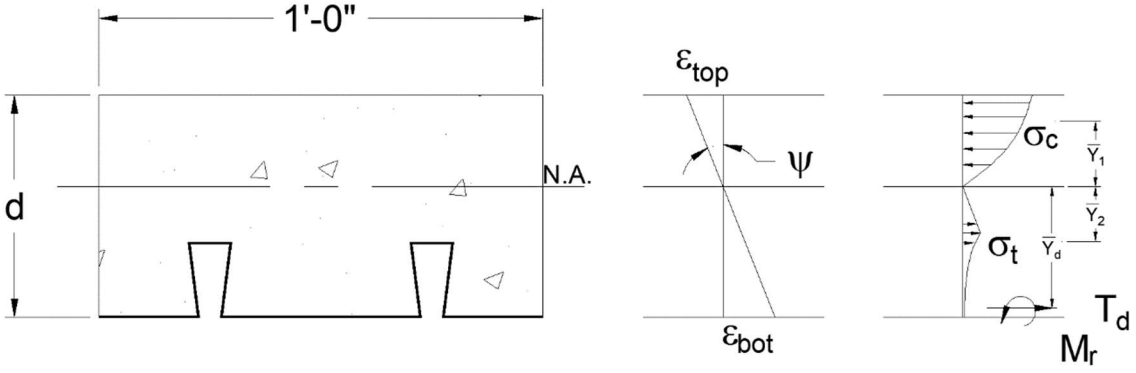

Fig. 4.3 Linear strain profile under increasing strains and corresponding stress profile; materials' stress-strain relationships are non-linear.

The strain-compatibility method employs the assumptions that strain remains linear and every finite orthogonal planar cross-section along the slab is balanced in equilibrium to determine the moment-curvature relationship of the flexural member. The moment-curvature relationship is specific for different configurations of the concrete composite deck system based on their unique geometric and material properties and is nonlinear. However, the equations for a linear moment-curvature relationship can be used to determine an effective elastic stiffness or secant stiffness, $(EI)_{eff}$, at discrete locations along a nonlinear composite slab using the following equations:

$$\Psi = \frac{\varepsilon}{y} \tag{1}$$

$$E = \frac{\sigma}{\varepsilon} \tag{2}$$

$$\sigma = \frac{M \cdot y}{I} \tag{3}$$

$$\psi = \frac{M}{EI} \tag{4}$$

$$EI_{eff} = \frac{M}{\psi} \tag{5}$$

ψ: curvature; the angle of rotation of the strain profile assuming plane sections remain plane

y: the perpendicular distance from the neutral axis

E: modulus of elasticity

σ: stress

ε: strain

EI_{eff}: effective stiffness in flexure

This effective stiffness, EI_{eff}, can be useful in simplified finite element models by segmenting the slab into discrete members or plates and applying a EI_{eff} based on its corresponding flexural moment. This method is further

discussed in Section 5.4Finite Element Plate Model of In-situ Composite Dovetail Decking Slab Implementing the .

The strength capacity of the composite slab is established by the maximum moment of the moment-curvature relationship curve; this maximum value is typically referred to as the nominal flexural strength, M_n (American Concrete Institute, 2014). For serviceability limit checks, the maximum deflection calculation is the important material behavior characteristic taken from the moment-curvature relationship; with this M-ψ association established for a unique composite deck profile, the deflection of the slab in flexural loading can be determined by the deflection equation defined in Equation (6).

$$\Delta(x) = \iint \psi(x)dx = \iint \frac{M(x)}{EI_{eff}(x)} dx^2 \tag{6}$$

Δ(x): vertical deflection as a function of x

ψ(x): curvature as a function of x

M(x): moment as a function of x

EI_{eff}(x): effective stiffness as a function of x

x: the distance as measured from the start of the member

4.2 Material Stress-Strain Models

4.2.1 Concrete Material Modeling Introduction

To calculate the stresses along the cross-section of the composite concrete slab, the concrete is divided into four different zones, Zone I,II, III, and IV. Fig. 4.4 illustrates the geometric definitions of the various zones.

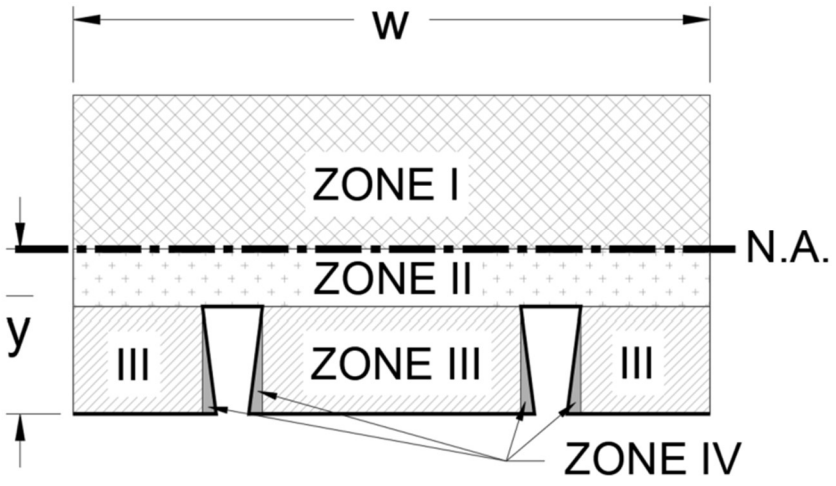

Fig. 4.4 Segmental geometric definitions of concrete for cross-sectional stress computations.

The concrete stress-strain behavior modeled in Zone I of the composite concrete deck profile is concrete in compression, as Zone I is defined as the

entire region of concrete above the neutral axis (N.A.), defined by the dimension $\bar{y}$ as measured from the base of the slab. Zones II, III, and IV are all below the neutral axis and are modeled using the concrete tensile stress-strain relationships. The strain and corresponding stress profile in Zone I requires an integral calculation to determine the compressive force for static equilibrium. A numerical integration method was implemented to simplify both the calculation of the compressive force and the calculation of the corresponding moment from the compressive force. Zone I was divided up *n=4* times, into equally spaced strips above the neutral axis, and the rectangle rule of numerical integration was implemented at the mid-height of each strip. Zones II, III, and IV similarly require an integral calculation to determine tensile force; these zones were likewise divided *n=4* times into equally spaced strips for numerical integration. To determine the flexural stresses along the concrete cross-section, two different concrete models are used to define their stress-strain constitutive relationships: a concrete compression model, and a concrete tension model.

4.2.2 Concrete Compression Model

Material stress-strain properties of concrete in compression can be defined by simplified models. The simplified model selected for this study is the

CEB-FIP Model Code 1990 nonlinear model for concrete compression stress-strain behavior under short-term loading (Comite Euro-International du Beton, 1993) (Fig. 4.5). This model was selected due to its simplicity and it is reportedly the most "global and most direct method" to model the "real behavior" of reinforced concrete structures (Favre & Charif, 1994). Prior studies investigating the material behavior of trapezoidal-profiled composite concrete slabs also utilized this simplified concrete compressive model such as Gholamhoseini (Gholamhoseini A. , 2018), and Gholamhoseini et al (Gholamhoseini, Gilbert, Bradford, & Chang, 2014).

In the CEB-FIP model, once the concrete has reached its maximum strength, f'_c, the compression strain-softening behavior of concrete commences and the concrete is no longer able to support higher stresses; this maximum strength occurs at a peak strain level, ε_c, which is the defined terminus point for the moment-curvature study. As stated in Section 5.1, the American concrete standard of an acceptable peak strain level for concrete, ε_c, is 0.003.

The CEB-FIP equations to define the concrete compressive stress-strain relationships up to maximum strength are:

$$\sigma = f_c' \frac{kx - x^2}{1 + (k-2)x} \tag{7}$$

$$x = \frac{\varepsilon}{\varepsilon_c} \tag{8}$$

$$k = \frac{E_c}{E_{c1}} \geq 1 \tag{9}$$

σ: the compressive stress of the concrete

f'_c: the maximum stress of the concrete material

x: the normalized strain factor

ε: the compressive strain of the concrete

ε_c: the strain at peak stress, f'_c

k: a shape parameter

E_c: the elastic modulus of the concrete

E_{c1}: the secant elastic modulus at the peak stress of the concrete

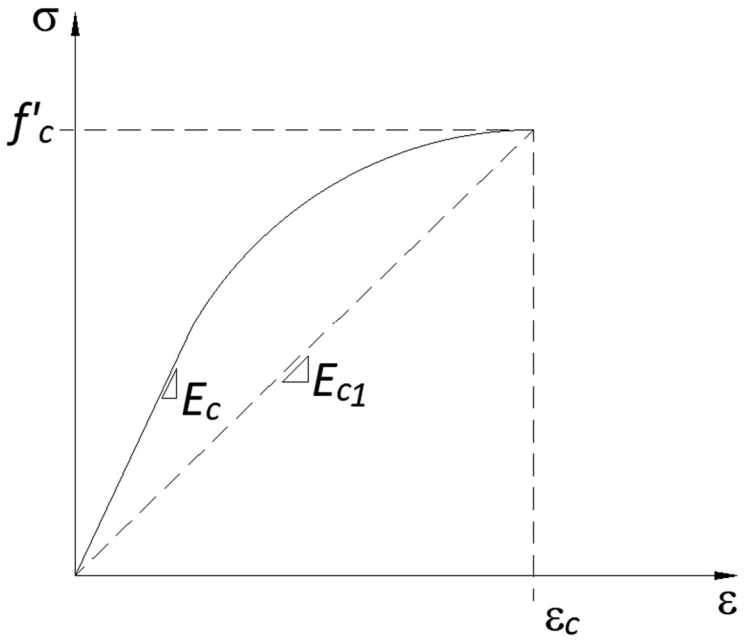

Fig. 4.5 Concrete compressive stress-strain model.

4.2.3 Concrete Tension Model

Concrete has a uniquely different stress-strain behavior in tension compared to compression. As a quasi-brittle material, it develops micro-cracks in direct tension which propagate into a localized macro-crack as the load increases. At its maximum tensile strength, f_t, a fracture process zone (FPZ) develops at the head of the crack where a "cohesive stress" acts perpendicular to the crack in an attempt to close it (Fig. 4.6 and Fig. 4.7). In this FPZ, concrete "undergoes progressive microcracking manifested by strain-softening" and the

shape and size of this zone is relatively large due to the size of the large aggregates in comparison to ductile materials, such as metals, which have a small FPZ (Bazant & Oh, 1983).

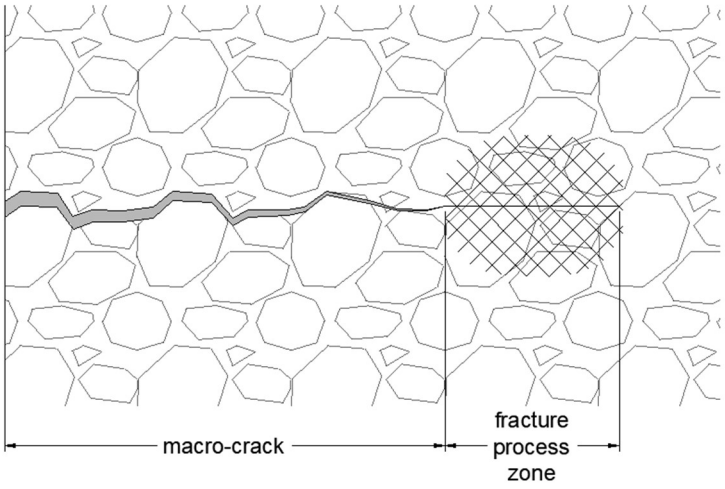

Fig. 4.6 Concrete macro-crack and fracture process zone location.

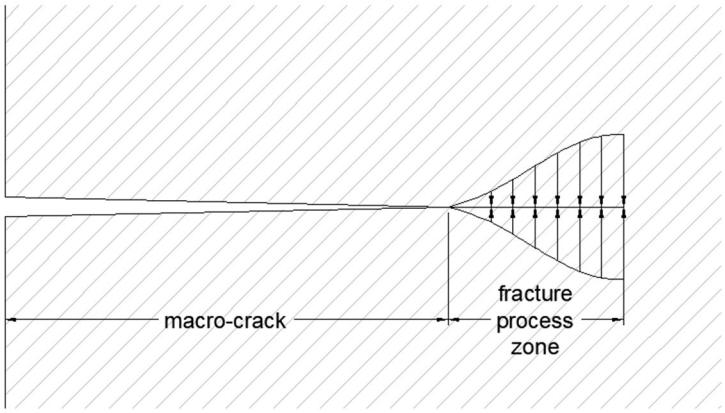

Fig. 4.7 Cohesive stress at the fracture process zone.

The concrete stress-strain relationship in tension is modeled employing this tension crack band theory, which is generalized by a “smeared crack band in which the material undergoes progressive microcracking characterized by a stress-strain relation that exhibits strain softening” (Bazant & Oh, 1983) (Fig. 4.8). This crack band model (CBM) expresses that concrete in tension assumes a linearity in the stress-strain behavior up to initial cracking – although testing has shown that it behaves nonlinearly but is approximately linear (Kumar & Barai, Concrete Fracture Models and Applications, 2011) – followed by a linear approximation defining the nonlinear tension softening region behavior from cracking. The CBM is mathematically simplified with the following equations:

$$\sigma_t = E_c \cdot \varepsilon, \ for\ 0 \leq \varepsilon \leq \varepsilon_p \tag{10}$$

$$\sigma_t = f_t + E_t(\varepsilon_p - \varepsilon), \ for\ \varepsilon > \varepsilon_p \tag{11}$$

$$\sigma_t \geq 0 \tag{12}$$

σ_t: the tensile stress of the concrete

ε: the tensile strain of the concrete

f_t: the maximum stress of the concrete in tension at the instant before initial fracture

ε_p: the strain of the concrete at f_t

E_c: the elastic modulus of concrete

E_t: the tangent strain-softening modulus

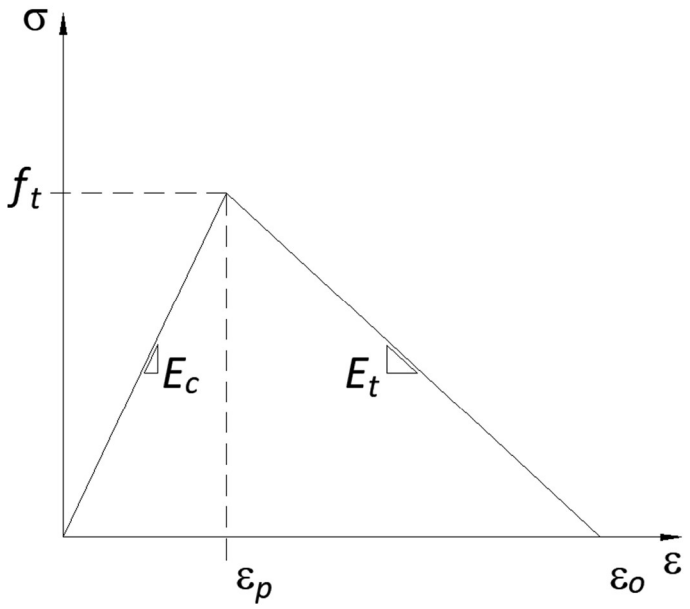

Fig. 4.8 Concrete tension stress-strain model with tension softening.

A similar concrete tension model proposed by Damjanic and Owen (1984) details the tensile behavior of concrete before and after cracking using dimensionless variables, α_1 and α_2, which range from 0 to 1 for α_1, and from 1 to infinity for α_2 Fig. 4.9. These a variables can be adjusted to match the desired tension-softening model; for example, an α_1 value of 0 and an α_2 value of $\varepsilon_o/\varepsilon_t$ will produce a stress-strain model equivalent to the simplified CBM model from Fig. 4.8. The model chosen for this computational analysis is Damjanic and Owen's alternative model with α_1 of 1 and α_2 of 15.

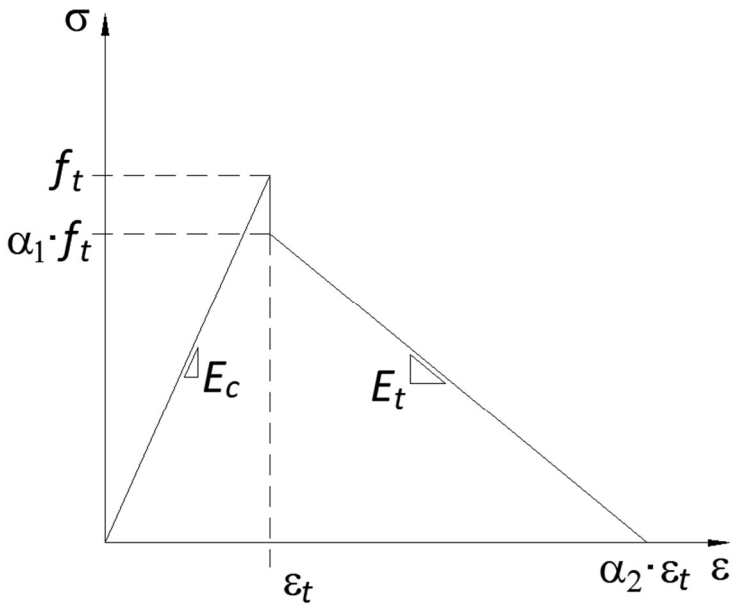

Fig. 4.9 Alternative tension stress-strain model based on Damjanic and Owen Model.

4.2.4 Steel Decking and Steel Reinforcement

The steel decking and any reinforcing mesh or reinforcing bar is assumed to act at its centroid as a single force vector in tension. In addition to this tensile force, the decking also provides a resistive moment, M_r, when flexed from the bending of the composite system (Fig. 4.2 and Fig. 4.3). Because of this inherent flexural resistance, the dovetail composite metal decking functions as the structural shoring while the concrete is being placed. Thus, the decking will

experience a pre-strain, ε_{so}, that is calculated based on the location of the shoring, length of the span, and weight of the uncured concrete. In industry practice, this initial pre-strain will be greater than zero, but for laboratory testing, the samples are fully supported during the casting of the concrete and the pre-strain and therefore the pre-stress of the metal decking will be equal to zero. The computational analysis can accommodate for a pre-stress in the metal decking if required by the construction shoring methods by including the pre-strain/pre-stress into the calculations.

The steel stress-strain model is assumed to be an elastic, perfectly plastic model (Fig. 4.10). This stress-strain model is used for steel in both tension and compression, but for this focused study of the composite slab in positive flexure, the decking will always be in tension and the reinforcement steel will be in tension or compression depending on its position in the slab.

$$\sigma = E_s \cdot \varepsilon, \quad for\ 0 \leq \varepsilon \leq \varepsilon_y \tag{13}$$

$$\sigma = F_y, \quad for\ \varepsilon > \varepsilon_y \tag{14}$$

σ: the stress of the steel deck or steel reinforcement
ε: the strain of the steel deck or steel reinforcement
F_y: the yield stress of the steel

ε_y: the strain of the steel at F_y

E_s: the elastic modulus of steel

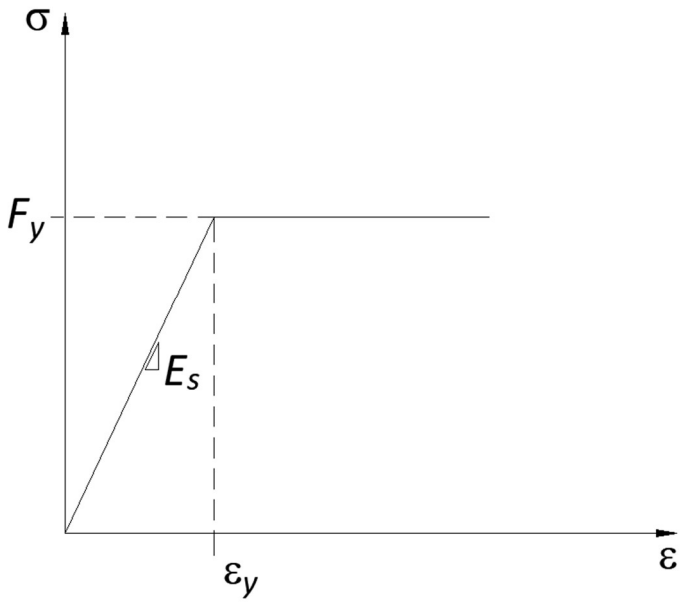

Fig. 4.10 Stress-strain elastic, perfectly plastic model for steel.

4.3 Computational Analysis Methodology

The use of a computer analytical program to determine an accurate moment-curvature behavior for any unique composite slab geometry, in lieu of multiple, complicated finite element models, benefits the designer through: ease of input, speed of input, ease of focused results, rapidity of performance based design results, speed of serviceability design results, and many other supportive

factors. For the computer-aided analysis, a computational solver is used to balance the statics equilibrium equation for all tension and compression forces of the cross-section at an incremental positive flexural strain to establish the corresponding location of the neutral axis. As the curvature of the strain increases, the location of the neutral axis gradually moves closer to the top of the slab to maintain static balance of this nonlinear composite system. Under the assumption that plane-section remain plane (i.e., there will be no warping and the flexural strain will remain linear), the strain-compatibility theory detailed in Section 4.1, is employed to produce a unique moment-curvature relationship for a defined composite dovetail slab.

Once the moment-curvature relationship is acquired for a defined composite slab specimen under incremental loading, the deflection relationship is then determined from the moment diagram profile based on the moment-area method of deflection calculation. This more complicated integral calculation is necessary because the moment across the flexural slab, M, is not typically a constant in realistic applications, and the stiffness relationship, EI_{eff}, is also not a constant, and therefore the simplified elastic deflection equations for beam members will not produce an accurate result.

4.3.1 Computational User Input

The computer analysis for this study was programmed using Microsoft Excel and its Visual Basic module. The various user-defined slab geometric properties and material properties entered into the spreadsheet and organized into the following categories: Deck Geometric Properties, Concrete Geometric Properties, Deck Material Properties, Concrete Material Properties, and Positive Moment Reinforcement Properties. Table 4.1 through Table 4.5 depict the geometric and material property inputs for a dovetail composite slab specimen; all user-defined input cells are highlighted and all colorless cells consist of labels, units, or calculated values based on the user-defined inputs. The spreadsheet as shown in these tables is representative example of a specific dovetail composite slab with a total height of 5.5 inches (140 mm), using 20-gauge dovetail decking (0.0358 inches, 0.9 mm) with a yield strength of 40,000 psi (276 MPa), steel welded-wire-mesh reinforcement of 6x6 W1.4xW1.4 with an area of steel equal to 0.0245 in^2 (15.8 mm^2) per 12 in (305 mm) and a yield strength of 60,000 psi (414 MPa), and normal weight concrete with a compressive strength of 5,600 psi (38.6 MPa). Fig. 4.11 shows a dimensioned drawing defining the input parameters of this example calculation set. The versatility of the

spreadsheet analysis allows the user to easily adjust the inputs based on any composite slab design using dovetail decking.

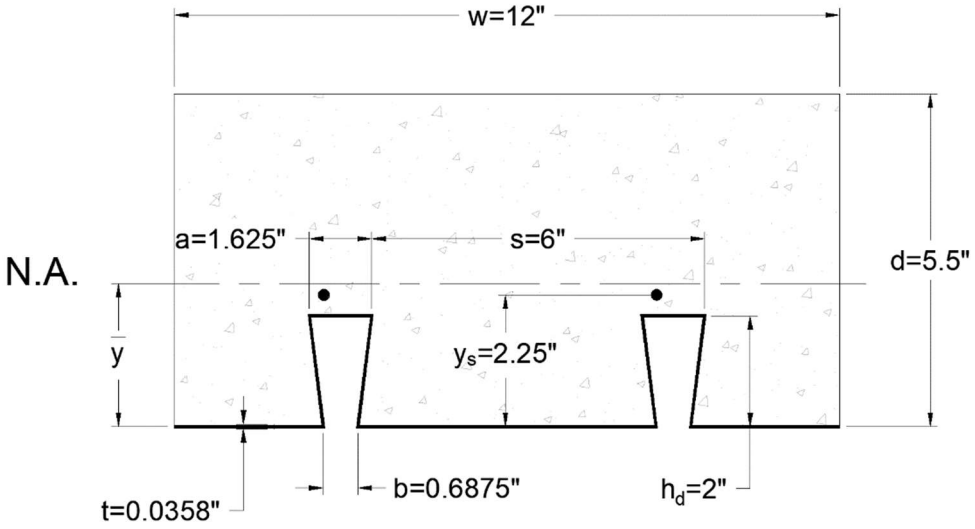

Fig. 4.11 Dovetail composite slab with geometry definition for example spreadsheet calculation.

Table 4.1. Table for steel deck geometry input.

Deck Geometric Properties		
h_d	2	in
s	6	in
t	0.0358	in
a	1.625	in
b	0.6875	in
c	5.3125	in
L	2.054	in
α	0.230	rad
L_s	11.046	in
A_d	0.791	in^2/ft
y_d	0.672	in
I_d	0.507	in^4/ft
PNA	0.790	in
Z_d	0.600	in^3

Table 4.2. Table for concrete geometry input.

Concrete Geometric Propertie		
d	5.5	in
A_1	38.33	in^2/ft
I_1	130.34	in^4/ft
y_1	3.90	in
A_2	3.67	in^2/ft
I_2	0.11	in^4/ft
y_2	2.15	in
A_3	17.50	in^2/ft
I_3	35.68	in^4/ft
y_3	1.00	in
A_4	1.88	in^2/ft
I_4	5.46	in^4/ft
y_4	0.67	in
Total A_c	61.38	in^2/ft
w	12	in

h_d: vertical height of deck

s: horizontal distance measure from dovetail bent-to-bent

t: thickness of metal decking

a: length of upper flute

b: length of lower gap between flutes

c: length of lower flute

L: length of the hypotenuse of the dovetail vertical legs

α: angle of the vertical leg as measured from the horizontal plane

L_s: total length of metal decking comprising one full dovetail bent

A_d: cross-sectional area of decking

y_d: centroid of the decking as measured from the bottom of the deck

I_d: moment of inertia of the decking about its centroid

PNA: the location of the plastic neutral axis of the decking

Z_d: the plastic section modulus of the decking

d: total height of composite slab

A_i: cross-sectional area of each concrete zone, *i*

I_i: moment of inertia of each concrete zone, *i*

y_i: local centroid of each concrete zone, *i*

A_c: cross-sectional area of all combined zones of concrete

w: horizontal width of the repeated form (12 inches based on American construction standards)

Table 4.3. Input for deck material properties.

Deck Material Properties		
F_y	40	ksi
E_s	29000	ksi
ε_{so}	0	
ε_y	0.00138	

Table 4.4. Input for concrete material properties in compression.

Concrete Material Properties		
f'_c	5.6	ksi
E_c	4265	ksi
f_t	561	psi
ε_c	0.003	
ε_p	0.000132	
E_{c1}	1867	ksi
k	2.29	
NW or LW	**NW**	

Table 4.5. Input for steel reinforcement properties.

Positive Moment Reinforcemer		
A_s	0.0245	in^2/ft
F_y	60	ksi
E_s	29000	ksi
ε_y	0.00207	
y_s	2.25	in

f'_c: the maximum stress of the concrete material

E_c: the elastic modulus of the concrete; calculated based on the ACI (American Concrete Institute) standard equation, Eqn. 19.2.2.1 (American Concrete Institute, 2014)

f_t: the maximum stress of the concrete in tension at the instant before initial fracture; calculated based on the ACI (American Concrete Institute) standard equation, Eqn. 19.2.3.1 ((American Concrete Institute, 2014)

ε_c: maximum crushing strain for concrete, typically in the range of 0.003 to 0.004 for standard strengths of concrete (American Concrete Institute, 2014)

ε_p: the concrete strain at f_t

E_{c1}: the secant elastic modulus at the peak stress of the concrete

k: a shape parameter

NW: normal weight concrete (approximately 145 lb/ft^3 by density)

LW: lightweight concrete (approximately 115 lb/ft^3 by density)

F_y: the yield stress of the steel material, for the decking and the reinforcement steel

E_s: the elastic modulus of steel, for the decking and the reinforcement steel

ε_y: the strain of the steel at F_y, for the decking and the reinforcement steel

ε_{so}: the pre-strain of the steel decking due uncured-concrete non-composite flexure

A_s: cross-section area of reinforcement steel

y_s: location of the centroid of the reinforcement steel as measured from the bottom of the composite slab

Multiple incremental flexural curvature conditions must be evaluated from zero flexure to a given maximum flexure, and therefore another critical user input is the increasing incremental strain conditions defining the extent of bending of the composite slab. This is best done by setting the strain values to increase at

the top, ε_{top}, from $0<\varepsilon_{top}<\varepsilon_c$, where ε_c is the maximum compressive strain in concrete allowed, and the corresponding location of the neutral axis, $\bar{y}$ or y in inches (Fig. 4.12).

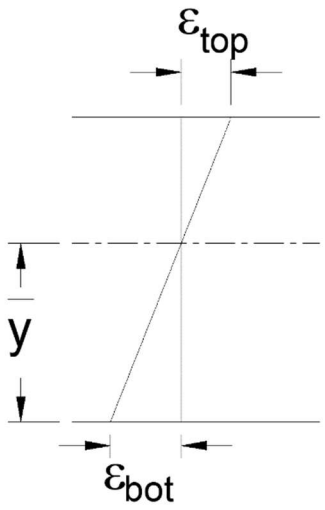

Fig. 4.12 Flexural strain description for tabular input in analytical model.

The straight-line strain assumption based on plane-section theory allows the strain at the bottom of the slab, ε_{bot}, to be calculated based on the given ε_{top} and $\bar{y}$ parameters; its corresponding values are solved in the analysis spreadsheet.

4.3.2 Numerical Integration for Computational Analysis

From the set strain flexural profile to the corresponding stress flexural profile, the resulting equilibrium forces are calculated and balanced using numerical integration methods. The summation of the tensile forces must equal the summation of the compression forces to satisfy static equilibrium of the composite slab. Numerical estimation of the integral of the stress curve is utilized to determine the equivalent vector force acting at the centroid of the area under the curve. The concrete zones, as defined in Concrete Material Modeling Introduction and depicted in Fig. 4.4, are evenly divided into *n* discrete segments and numerically integrated using the Riemann sum mid-point, rectangular method of integration; this creates a reasonably accurate integration result and also simplifies the moment calculation of each discrete segment. A graphic illustration of the four concrete zones partitioned into *n*=4 segments for numeric integration analysis are depicted in Fig. 4.13 through Fig. 4.16.

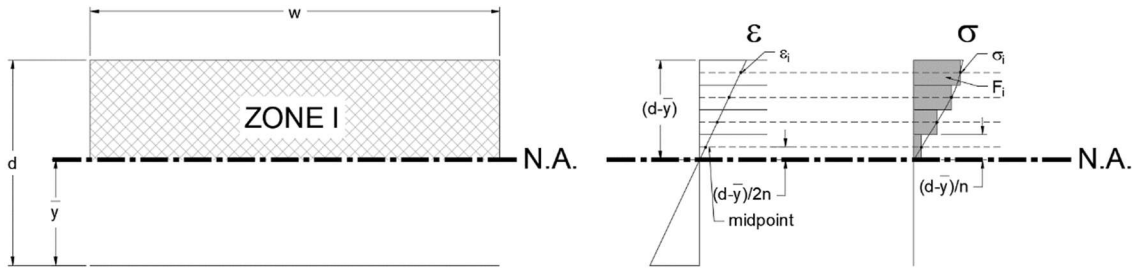

Fig. 4.13 Stress-strain relationship of Zone I concrete; numerical integration of compressive stress region.

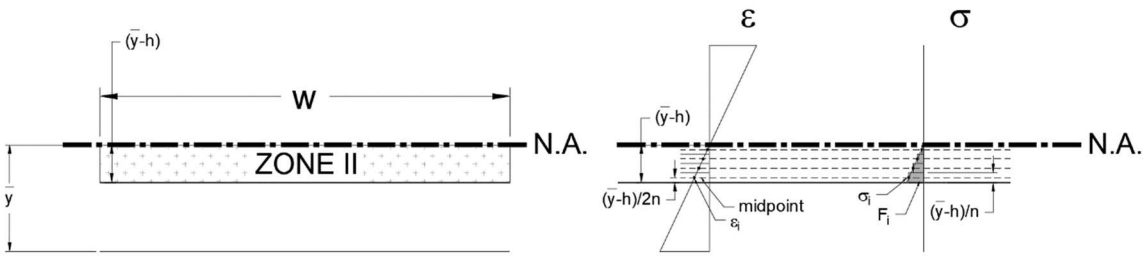

Fig. 4.14 Stress-strain relationship of Zone II concrete; numerical integration of tensile stress region above the flutes.

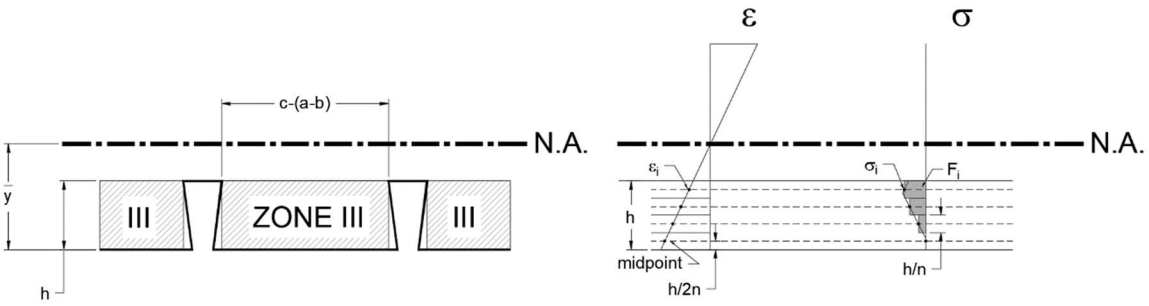

Fig. 4.15 Stress-strain relationship of Zone III concrete; numerical integration of tensile stress region in the flutes.

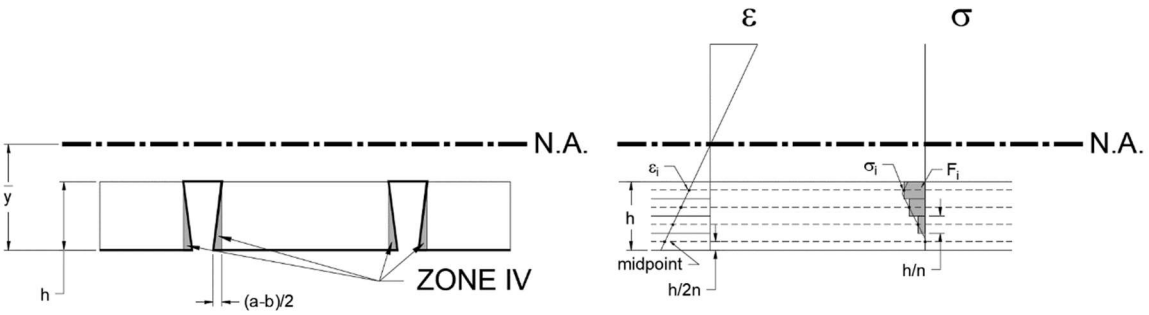

Fig. 4.16 Stress-strain relationship of Zone IV concrete; numerical integration of tensile stress region in the flutes.

4.3.3 Steel Deck Strain Slip

The interface between the steel deck and the concrete surfaces may be assumed to be perfectly bonded under the plane-sections-remain-plane strain-compatibility theory, but in reality the deck will slip relative to the concrete under flexural loading. The slip is of the deck relative to the concrete is shown in the

strain distribution diagram profile as a constant, ε_{sl}. The resulting strain of the steel deck under flexure is described by Equation (15) and depicted in Fig. 4.17.

$$\varepsilon_d = \varepsilon'_d - \varepsilon_{sl} \text{ and } \varepsilon_{sl} \geq 0 \tag{15}$$

ε_d: The strain of the steel decking at its centroid, y_d

ε_d': The strain of the steel decking assuming linear continuity from ε_{top} to ε_{bot}, at its centroid

ε_{sl}: The slip strain of the decking-concrete interface

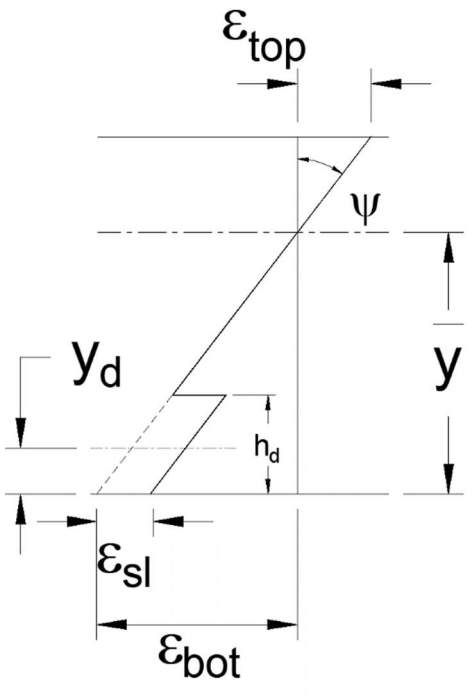

Fig. 4.17 Strain distribution profile including slip strain of decking.

There are multiple factors that determine the bond strength between the metal decking and the concrete surface. A simplified free-body diagram of the frictional forces between the concrete and decking surface is depicted in Fig. 4.18. In the composite decking slab systems, the shear frictional force is dependent the following: the friction coefficient of the concrete material against the steel decking surface; the surface area of contact of the decking and concrete per unit width; the geometry and placement of the decking embossments; and the normal force induced by the bending of the material which is dependent on the flexural stiffness of the decking. Based on the physics of shear friction, the following properties should increase the frictional forces between the two composite surfaces: increased surface roughness of the decking either by use of embossments or other means; increased contact surface area per width of decking by changing the geometry of the dovetail folds; and increased flexural stiffness, *EI*, of the decking thereby increasing the normal force between the surfaces.

It is logical to assume that when the first tensile fiber of concrete starts to crack, the composite frictional bond between the steel and the decking will alter, thus initiating the deck-slip, ε_{sl}. The reentrant upper corners of the dovetail decking is unique in the fact that it creates an interlocking track, forcing the

curvature angle of the concrete to be the same as the curvature angle of the deck even if the deck and concrete have slipped relative to each other. The quantifiable deck-slip that will occur from flexural loading must be calibrated from the physical tests to determine the numerical value to input into the computational solver, and to verify that the slip initiates at concrete cracking.

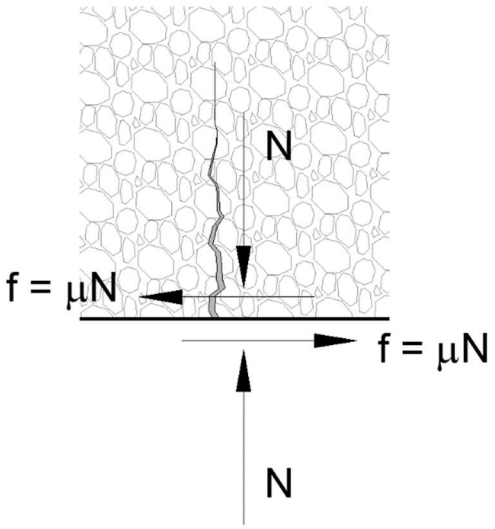

Fig. 4.18 Free-body diagram of frictional force between concrete and decking.

4.3.4 Computational Analysis Solver

A Generalized Reduced Gradient (GRG) nonlinear solver converges on the value for the neutral axis, $\bar{y}$, such that the compression force vectors are

equally balanced by the tension force vectors, or mathematically stated, the summation of compression vectors minus the summation of tension vectors is equal to zero. The solver's range is set to above the height of the deck, h_d, as a minimum and the total height of the slab, d, as a maximum value, and the precision is set to $1x10^{-6}$. The methodology established in this section assumes that the neutral axis occurs above the height of the deck. For all normal and practical uses of the dovetail decking for composite slabs, the neutral axis of the slab will always fall within these limits.

4.3.5 Moment-curvature Relationship

With the location of the neutral axis determined from equilibrium, the corresponding moment is calculated based on the discrete tension and compression vector forces and their perpendicular distances to a set point (e.g., the neutral axis, $\bar{y}$, was selected for this application). The summation of all of the force-distance products for a given curvature angle defines the relationship between the flexural resistance of the slab and its curvature. The relationship is summarized in both a tabular form and a graphic plot. The moment-curvature relationship is best utilized in tabular form as it provides a quick look-up tool for the user. The graphic plot is valuable to understand the complete and complex

behavior of each unique composite slab as it progresses through increasing stages of bending moment (Fig. 4.19). Because the development of the moment-curvature relationship involves a detailed stress-strain profile at small discrete increments of flexural curvature, the point on the moment-curvature diagram at which the composite slab first cracks in Zone III/IV (also commonly called "M_{cr}") and when it first cracks in Zone II can both be identified on the diagram.

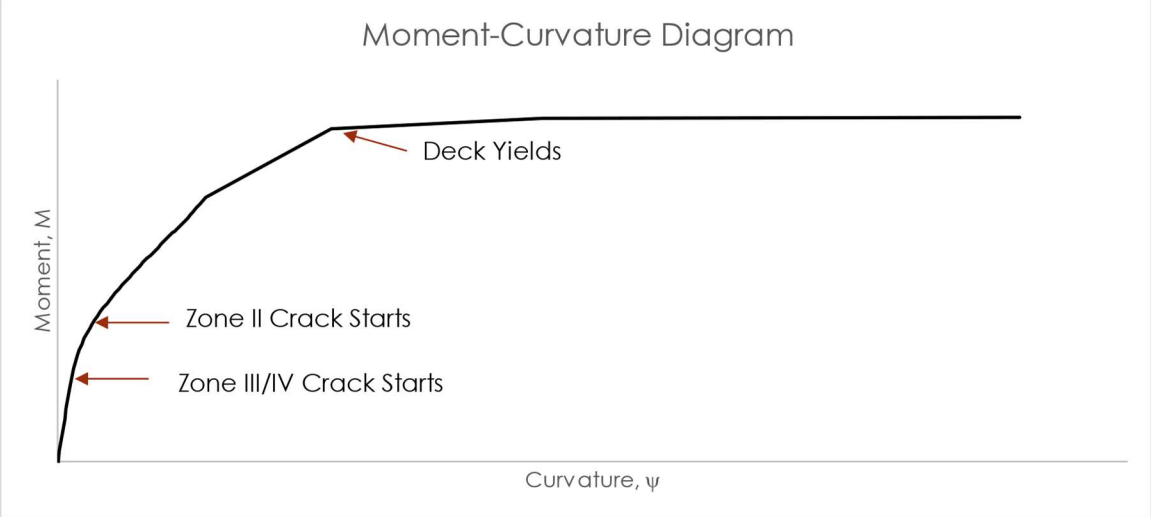

Fig. 4.19 Generic representative moment-curvature diagram for a generalized composite concrete slab.

The moment-curvature relationship of a composite slab system is useful for an analytical calculation of flexural stiffness as well as for a finite element plate analysis model.

4.3.6 Deflection Calculation using the Moment-Area Method

The moment-curvature relationship relates the flexural stiffness of the composite slab system, *EI*, to the applied moment, *M*. In flexural members that are linearly elastic and have a linear moment-curvature relationship, the deflection calculation is greatly simplified. An example of this is a structural steel beam under a uniform distributed load and simple pin-roller boundary conditions at its ends as portrayed in Fig. 4.20. In structural steel, the stiffness expression, *EI*, is a constant before yielding stress of the steel is reached, and therefore the double integral equation is simplified as the moment, *M(x)*, is the only variable function of distance along the member, x. For this case, the resulting deflection is at any point along the beam is therefore defined as:

$$\Delta(x) = \frac{wx}{24EI}(L^3 - 2Lx^2 + x^3) \tag{16}$$

Δ: vertical deflection at any point along the member
x: distance as measured from the start of the member

L: total length of the member

w: constant distributed load

EI: stiffness of elastic member with a constant moment of inertia; modulus of elasticity multiplied by the moment of inertia of the bending axis

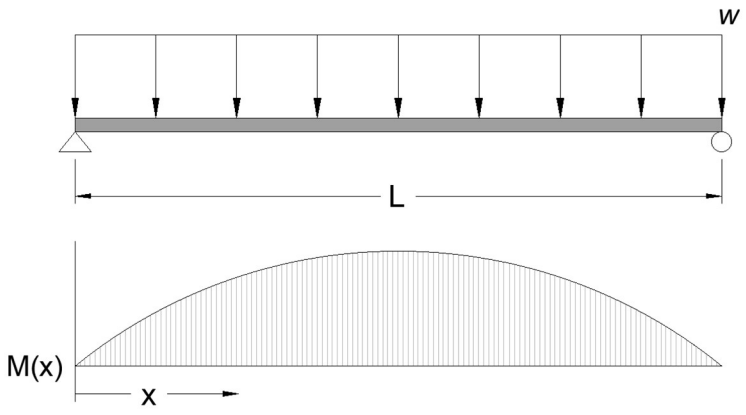

Fig. 4.20 Moment, M(x), diagram along a simply-supported beam with a constant distributed load.

To determine the deflection of a composite slab in flexure, which has a nonlinear moment-curvature relationship, solving the double integral of curvature would be complicated but for the use of numerical methods. The moment-area method is a graphic area calculation of determining the deflection based on the double integral of curvature, where the vertical deflection of the member is equal to the area under the curvature, ψ, curve and noting where the slope of tangent of the curve is equal to zero. For a simply-supported beam that has a symmetric

loading, the maximum deflection occurs at the center (mid-span) of the beam and therefore the deflection curve has a slope of zero at the center. If the moment diagram is known for the member, then the corresponding curvature diagram is also known. The method takes an incremental length, δx of the simply-supported flexural member to evaluate and multiplies it by the corresponding curvature; this "area" is then multiplied that by the distance of its centroid to the support, $\bar{x}$ (Fig. 4.21). The summation of the products of the areas and their distances up to the midpoint of the flexural member is equal to the deflection at that midpoint location, which is the maximum deflection in symmetric load cases.

For numerical calculation methods, by partitioning the curve into *n* finite segments and performing a numerical integration estimate, the deflection can be determined; accuracy of the solution is improved by increasing the number of segments. The deflection analysis of the test specimen, which has a span of approximately 9'-4" (284 cm), is split into 16 segments (*n*=16) at 7" (178 mm) each, with reasonably accurate results.

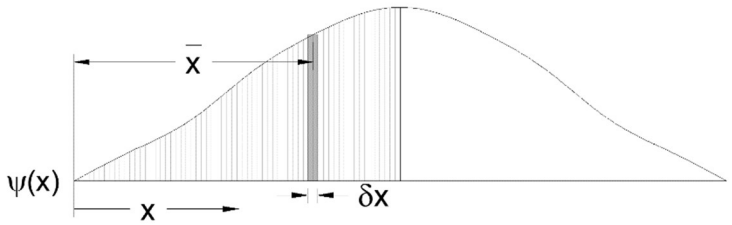

Fig. 4.21 Curvature diagram showing the numerical analysis for the moment-area method.

The test specimens have two load patterns: the self-weight of the specimen as an evenly distributed load, and an equal two-point loading pattern; both are symmetric loads. The most basic composite slabs specified for floor diaphragms in building design are required to have evenly distributed vertical loads applied perpendicular to the surface of the slab including, but not limited to: dead loads (those loads that are generally fixed such as weights of permanent construction materials), live loads (those loads that are not fixed and are specified based on the occupancy or use of the floor space), wind loads, snow loads, et cetera (International Code Council, Inc., 2020). Additional building design load requirements include single, isolated point loads positioned where they create the most severe condition, which occurs at the center of a simply-supported slab. The symmetric loading pattern of the specimen testing for this study, and the building code design load requirements both create a simple

moment-area method calculation for deflection. Special cases where a composite slab is required to support additional framing members such as walls or columns, or special loads from mechanical units, or other cases of asymmetric loading, the moment-area method for calculation of deflection can be used, but it becomes more complicated if the maximum deflection does not occur in the middle of the span. Additionally, the moment-area method for calculation of a continuous slab or slabs with overhangs is also possible, although the application of the method does also become increasingly complicated. In these cases, a finite element analysis plate model using the stiffness calculated from the moment-curvature (M-ψ) relationship is warranted; Section 5.4 is an example a plate finite element analysis using this M-ψ relationship.

4.4 Numerical Strain-Compatibility Model Validation with Test Data

To prove the validity of the numerical strain-compatibility model, applying the strain-compatibility theory described in Section 4.1, the computational analysis results are compared to the test data of the composite dovetail slab specimens under four-point flexural loading.

The measured geometric properties of each of the test specimens was entered as the input parameters for the computational to create a unique output

for each specimen. The numerical moment-area method for deflection calculated the resulting maximum deflection, Δ_2, at the middle as well as the intermediate deflections at each side, Δ_1 and Δ_3 (reference Fig. 3.2).

Without considering the deck-slip strain, the load-deflection results were compared to the analytical model. The analytical model closely follows the test results up until the initiation of the concrete cracking tensile strain; Fig. 4.22 (a) through (g) depicts the graphical results of that comparison.

Upon tensile cracking of the concrete, the bond between the metal decking and the concrete changes, causing a relative slip between the two surfaces and altering the formerly linear relationship of the flexural strain profile (recall Fig. 4.17). From the numerical strain-compatibility model, the point at which the concrete reaches its tensile capacity at its bottom-most fiber, f_t, and initiates cracking can be determined; this point is depicted graphically on the load-deflection diagrams in Fig. 4.22. Based on the comparison of the test data and the analytical model assuming no deck slip, the point where the test data diverges from the numerical model is near the point where the two curves diverge. This further indicates that the deck slip bond occurs and is influenced by the cracking of the concrete.

Fig. 4.22(a) Load-deflection model with no slip comparison with test specimen.

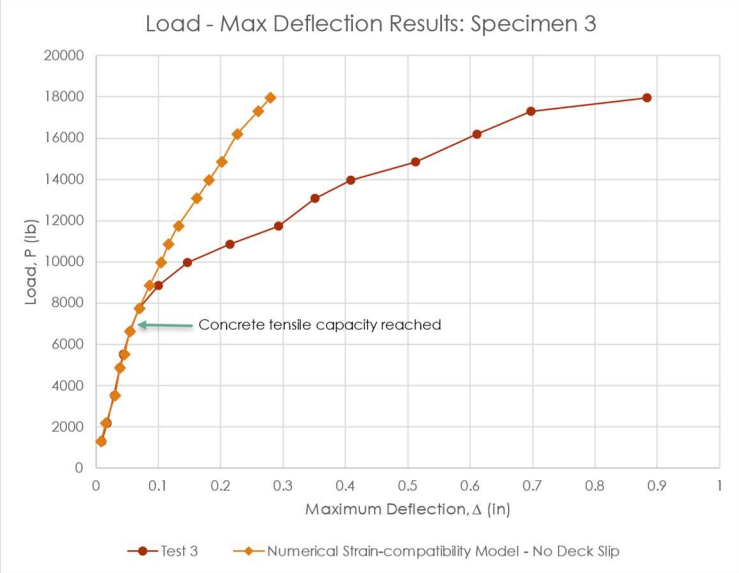

Fig. 4.22(b) Load-deflection model with no slip comparison with test specimen 3.

Fig. 4.22(c) Load-deflection model with no slip comparison with test specimen 4.

Fig. 4.22(d) Load-deflection model with no slip comparison with test specimen 5.

Fig. 4.22(e) Load-deflection model with no slip comparison with test specimen 6.

Fig. 4.22(f) Load-deflection model with no slip comparison with test specimen 7.

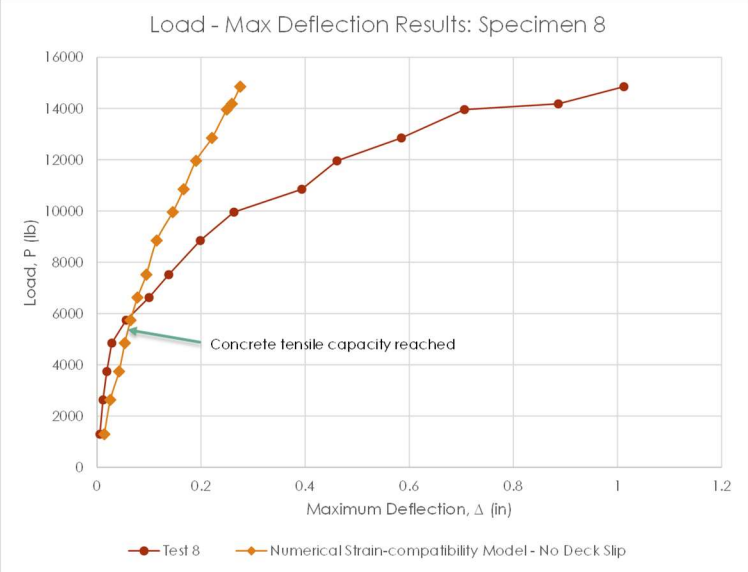

Fig. 4.22(g) Load-deflection model with no slip comparison with test specimen 8.

4.4.1 Computation of Deck Slip Strain

The numerical value of deck-slipping strain, ε_{sl}, is an unknown variable in the computational model; the value and rate of increase of the deck-slip strain can therefore be calibrated to the results of the flexural tests to determine the amount of deck-slip required to match the load-deflection measurements from those tests. The assumptions regarding the deck slip strain include: 1) the stress-strain relationship of the decking is simplified to occur at a single point in the profile of the composite located at the centroid of the decking, y_d; 2) the deck strain slip occurs at the time of or immediately after the concrete's initial flexural

crack; 3) as the concrete flexural crack progresses through the composite concrete deck profile with increasing flexural strain, the deck slip can only increase and not decrease.

To accomplish the deck-slip calibration, a column was added to the analytical model spreadsheet for deck slip, ε_{sl}, which deducted from the initially calculated deck strain, ε_d, in very small increments. The deck slip value was incrementally increased at each calculation row until the resulting calculated deflection (recall the deflection is calculated using the moment-area method) closely matched the test deflection results for maximum deflection. The strain slipping of the concrete-deck interface results in a reduced strain and therefore a reduced stress in the metal decking; to maintain equilibrium of the system, the flexural resisting moment is less than without the slip and the curvature angle is also more than it would have been without the deck-slip.

The final calibrated deck-slip, ε_{sl}, was plotted against various parameters to determine relationships, if any. The results of these comparisons confirmed that the effective stiffness of the system, *EI*, exponentially decreases, as slipping of the deck-concrete interface increases (Fig. 4.23); the deck slip therefore has a significant impact on the overall softening of the flexural behavior of the composite slab.

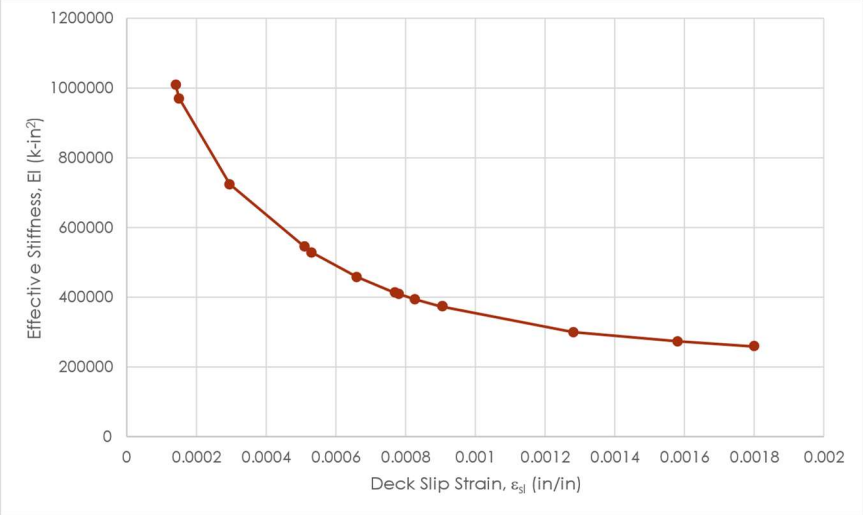

Fig. 4.23 Deck slip strain relationship with corresponding effective stiffness of composite slab, results from specimen 3.

A strong linear relationship was discovered from this study by comparing the deck slip strain, ε_{sl}, with the corresponding flexural curvature angle, ψ, of the composite profile. A linear trend analysis using the least squares method to best fit data to find the slope and intercept of the trendline, was utilized to calculate the linear equation and the coefficient of determination of the data, r^2. Fig. 4.24 depicts the graphical results of the data from a deck-slip calibration of one of the slab specimens, and a trendline analysis with a coefficient of determination of 0.994; this is significantly high r^2 value indicating that there indeed is a high

probability of a linear relationship between the deck slip strain, ε_{sl}, and the corresponding curvature angle, ψ, of the slab.

The relationship between the deck slip and the flexural curvature angle is summarized in the following equation where the resulting slope of the line, which this study will refer to as the *deck slip factor*, s_d, and the negative of the intercept which this study will refer to as the *deck slip adjustment value*, ε_a, predicts the deck slip at all flexural increments at the inception of and after the initial cracking of the concrete:

$$\varepsilon_{sl} = s_d(\psi) - \varepsilon_a \tag{17}$$

ε_{sl}: deck slip
s_d: deck slip factor
ψ: flexural curvature angle (rad)
ε_a: deck slip adjustment value

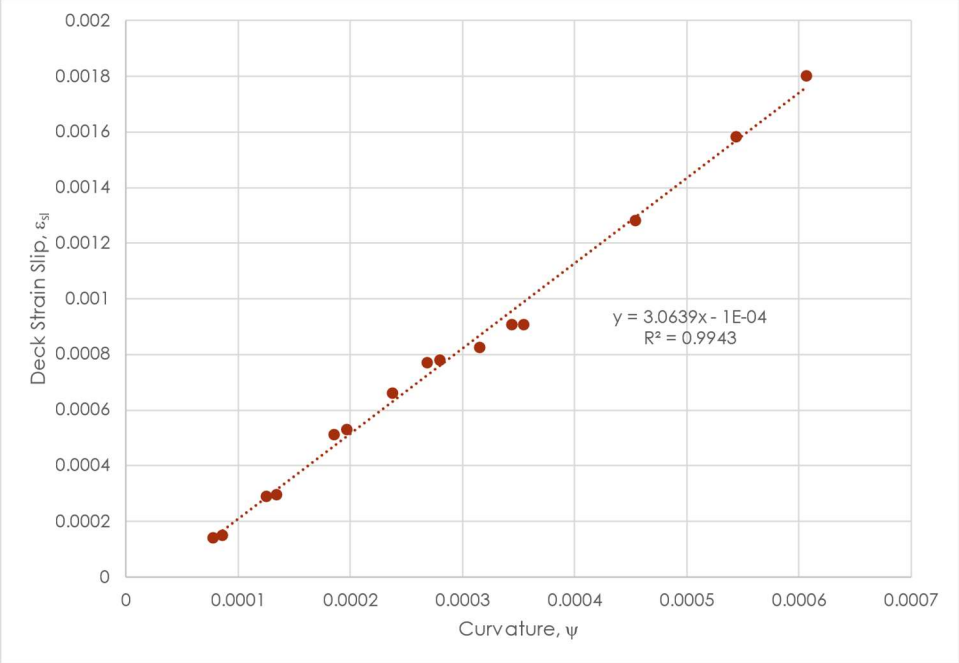

Fig. 4.24 Deck slip strain relationship with corresponding flexural curvature angle of composite slab, results from specimen 3.

For specimen 3, which has a total slab depth of 6.75" (171 mm), the deck slip factor, s_d, was determined to be 3.06 and the deck slip adjustment variable, ε_a, was determined to be 9.8×10^{-5}. It was noted that the linear relationship of deck slip, ε_{sl}, with curvature angle, ψ, is valid for the test specimens from initial tensile cracking of the concrete up until there is a global slipping of the deck noted as *end slip*. The *end slip* becomes measurably apparent as a differential movement between the decking and the concrete and occurs at very high

curvatures, which is outside the serviceable load range of the composite slabs. When end slip occurs on the test specimens, the applied load is within approximately 85% of its calculated strength capacity; consequently, the measured deflection increases above the model's predicted deflection as this new variable related to laminar shear frictional failure between the concrete and steel is introduced into the system. The end slip occurrence can be prevented through rational design by cantilevering the end of the slab, by making the slab a continuous slab over intermediate supports where the decking transitions from a tension element to a compression element, or other similar methods. Because the focus of this study is the serviceable deflection accuracy of the long-span composite dove-tail deck systems, the *end slip* occurrence is duly noted, but not a critical factor for these long-span slabs in the serviceable loading range. It also does not affect the rate of deck slip, ε_{sl}, which was noted to be related to flexural cracking and flexural curvature, as revealed through this study.

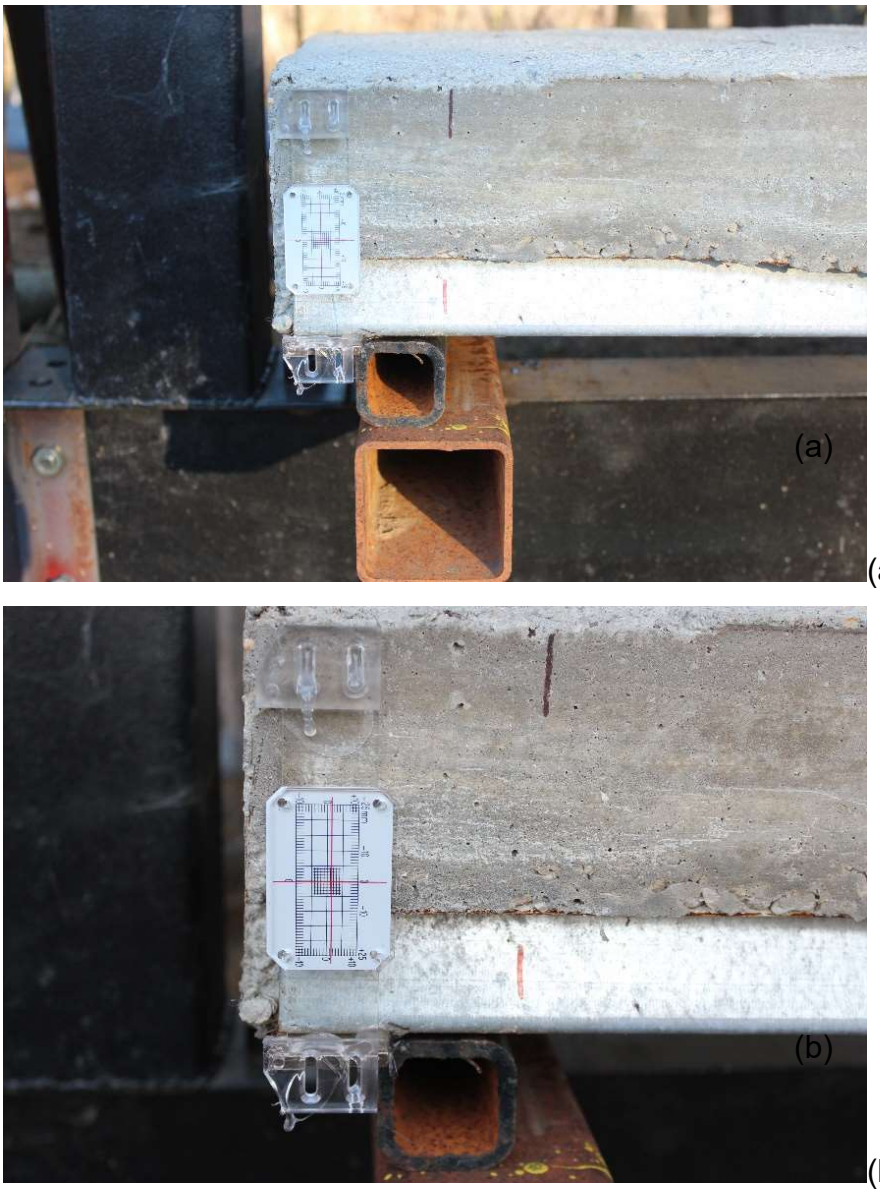

Fig. 4.25 Specimen end slip movement differential from (a) zero at initiation of test and (b) 1 mm at final loading of test.

To validate the linear relationship of the deck slip strain with the other specimens tested under flexural loading, the deck slip strain column was populated with strain slip values using the newly defined equation (17). The deck slope factor, s_d, and the deck slip adjustment variable, ε_a, was incrementally attuned in the numerical strain-compatibility model until a reasonable fit was established with the test data; the final value of s_d and ε_a selected was the one which provided the lowest possible percent root mean square error (RMSE), which is a quantitative measure of how well the proposed model fits the test dataset. The root mean square error is defined by the following equation:

$$RMSE = \sqrt{\frac{\sum(\Delta_{observed} - \Delta_{calculated})^2}{N}} \tag{18}$$

RMSE: Root mean square error

$\Delta_{observed}$: deflection from test data at a specific load level

$\Delta_{calculated}$: deflection from a calculated model at a specific load level

N: number of data points in the sample

The following diagrams provide a visual representation of the new analytical method load-deflection curves compared to its corresponding test dataset. Recall that the each of the samples have slight variations of thickness due to the fabrication process of casting the concrete into the wood formwork

(Section 3.1Experimental Test Overview), and therefore each graph includes the actual depth, *d*, of the specimen represented.

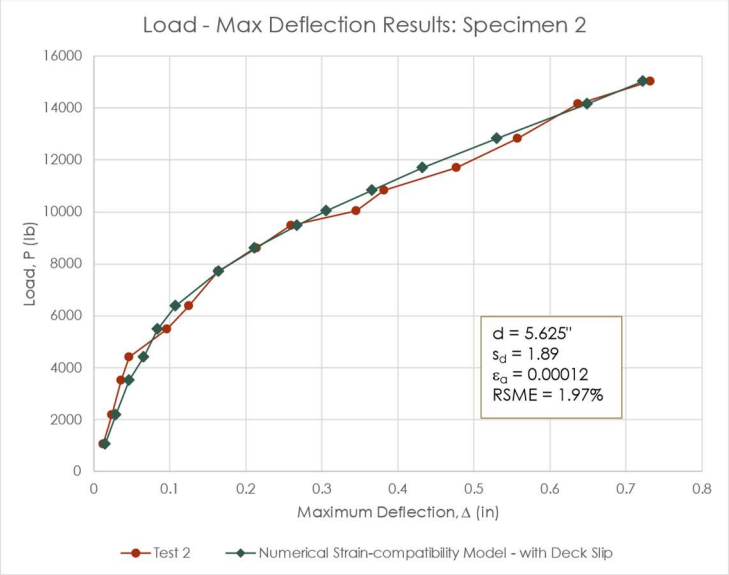

Fig. 4.26(a) Load-deflection model comparison with test specimen 2.

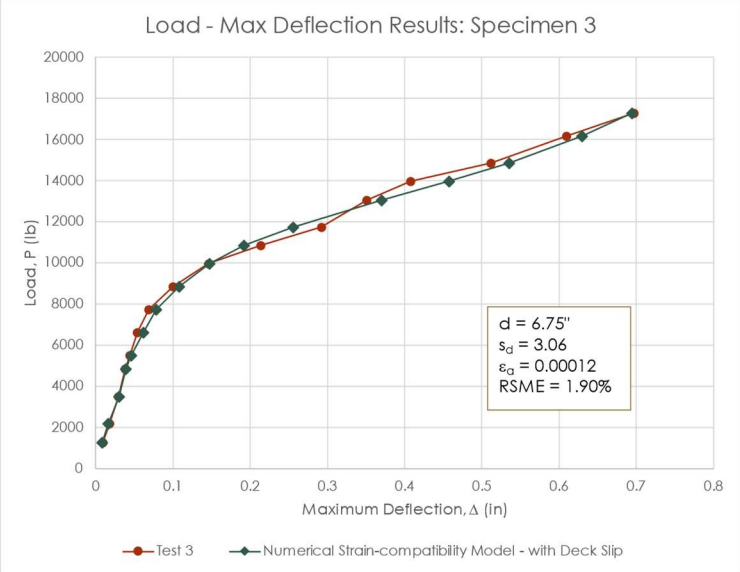

Fig. 4.26(b) Load-deflection model comparison with test specimen 3.

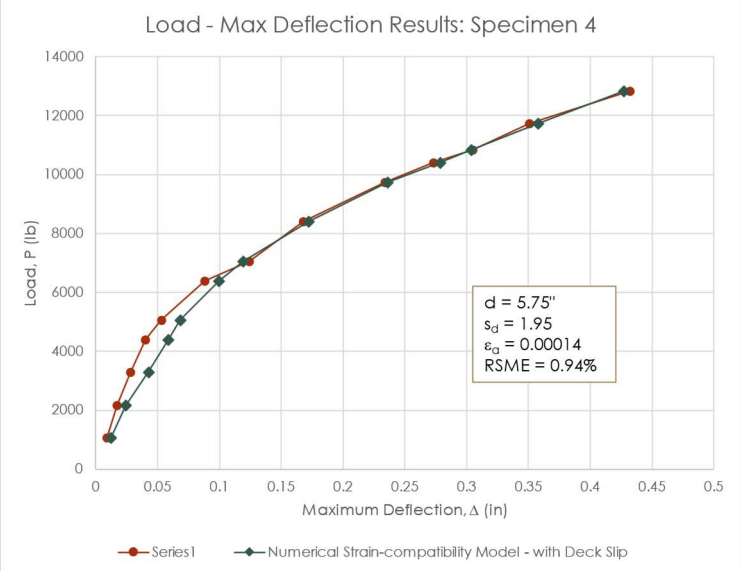

Fig. 4.26(c) Load-deflection model comparison with test specimen 4.

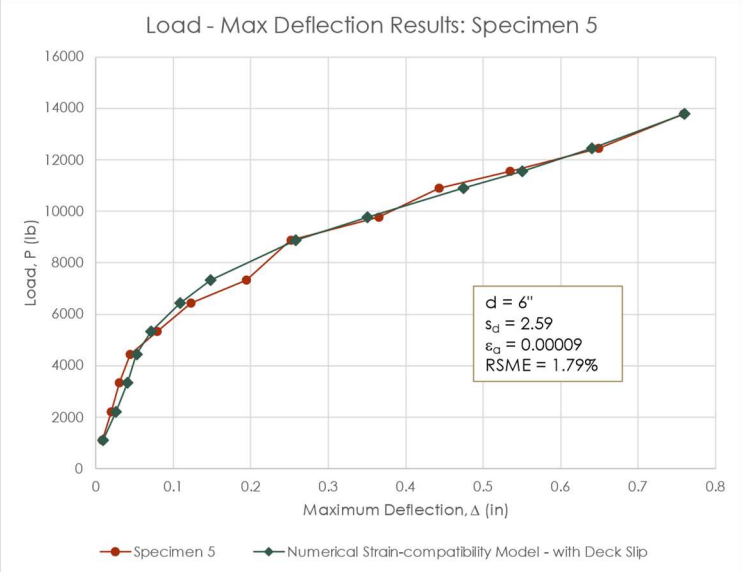

Fig. 4.26(d) Load-deflection model comparison with test specimen 5.

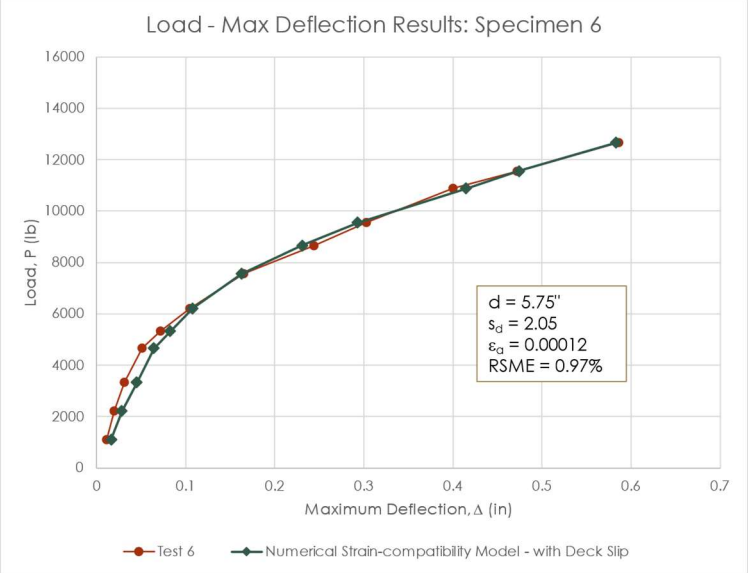

Fig. 4.26(e) Load-deflection model comparison with test specimen 6.

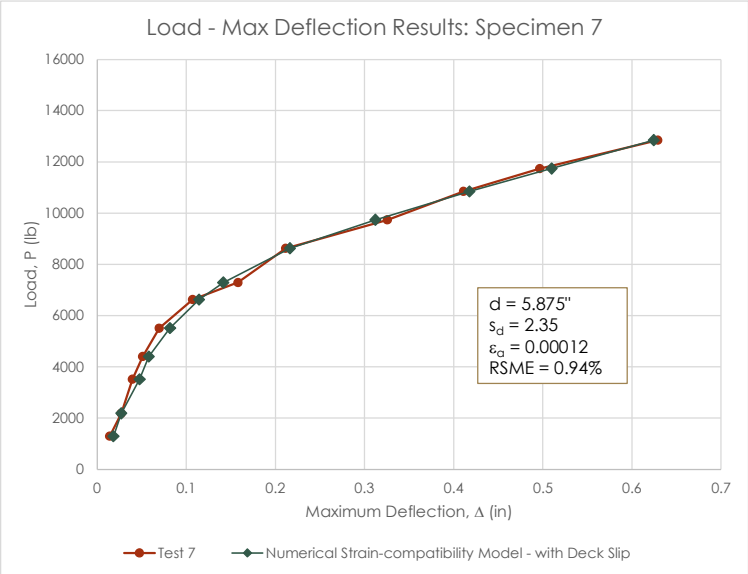

Fig. 4.26(f) Load-deflection model comparison with test specimen 7.

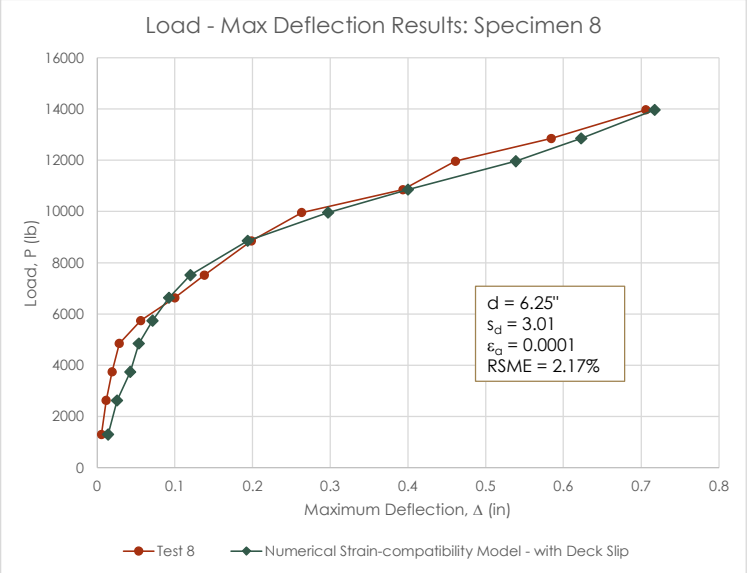

Fig. 4.26(g) Load-deflection model comparison with test specimen 8.

A summary of the deck slip factors calculated based on fitting the analytical models to the test data is summarized in the following table (Table 4.6) and shown in Fig. 4.27. Based on the results of the comparative analysis, the deck slip factor increases as the total depth of slab increases. The slip adjustment variable stays relatively small and is similar to the strain in the deck just before the concrete reaches its tensile strength, which is just before deck slip initiates, regardless of slab depth. This is occurrence is confirmed by the fact that there is no noticeable jump or retracting strain of the deck, based on the test results, as it holds its strain almost constant while the concrete slips against it.

Table 4.6. Deck Slip Factors

Measured Depth (in)	Deck Slip Factor, s_d	Deck Slip Adjustment Value, ε_a	Specimen #
5.625	1.89	0.00012	2
5.75	1.95	0.00014	4
5.75	2.05	0.00012	6
5.875	2.35	0.00012	7
6	2.59	0.00009	5
6.25	3.01	0.0001	8
6.75	3.06	0.00012	3

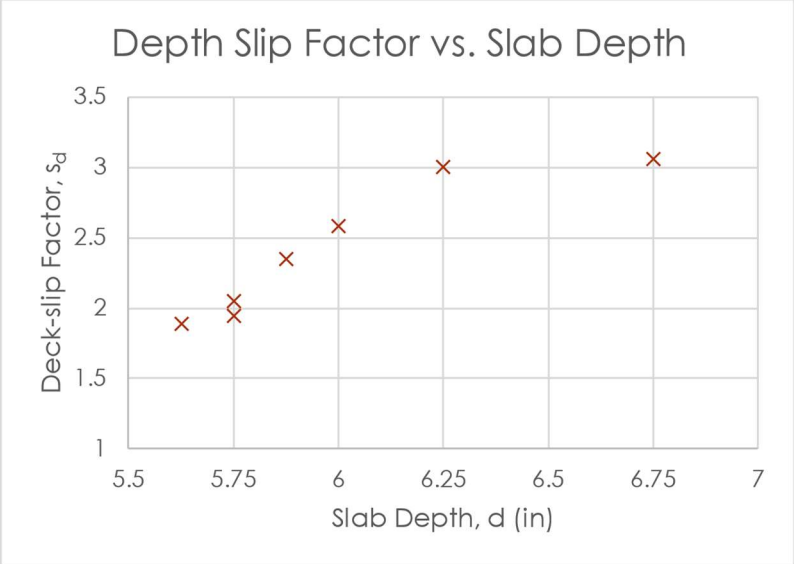

Fig. 4.27 Deck slip factor vs. depth of composite dovetail decking slab.

The numerical strain-compatibility method of modeling the flexural stiffness behavior of the dove-tail composite slab using a computational solver provides an acceptably accurate result within the serviceable range of loading, where the RSME of the specimens tested have a low error value. Discovering a linear relationship between the curvature angle, ψ, and the deck slip strain, ε_{sl}, led to quantifying and implementing the deck slip phenomenon into the analytical solver model with ease. The deck slip factor can be applied to any proposed dovetail composite slab design to accurately calculate its flexural behavior; if an exact value of deck-slip factor is unknown for a specific slab depth, *d*, selecting

the more conservative value (the higher value) of deck slip for design purposes is an acceptable engineering practice.

4.5 Practical Applications of Numerical Strain-compatibility Model for Dovetail Composite Slabs

The numerical strain-compatibility method for calculating the flexural behavior of dovetail composite concrete slabs is a fast and intuitive tool to produce a quick and thorough overview of the stresses, strains, cracking behavior, and equivalent stiffness for use in real-world engineering applications. This tabular analytical model of the behavior of the dovetail composite decking system can be used to create a variety of design tables for engineering and construction applications. And its versatility means that an engineer can change a single variable such as thickness of decking, height of concrete, width of the lower flute in the geometry, and so forth, to produce a unique design table without the time and expense of a finite element model or a test. These types of design tables are valuable features for manufacturers of composite metal decking to quickly and easily demonstrate the strength and functionality range of their products; it can also function as a tool to quickly determine the efficiency of the composite slab system as changes in metal gauge, concrete strength, weight

of concrete, etc. may or may not have a noticeable economic impact on the design of the floor system.

Beyond the development of design tables from this numerical strain-compatibility model, the effective stiffness derived from the moment-curvature diagram can be used to define the effective stiffness in a finite element analyses of floor diaphragms; this is demonstrated with a comparative analysis of a flexural test of an in-situ floor slab in Section 5.

The moment-curvature relationship of the dovetail composite slab derived from numerical strain-compatibility model is a beneficial and versatile engineering aid for the creation of quick lookup design tables, and for use in simplified finite element plate analyses.

5 Analysis of In-Situ Dovetail Composite Slab

Prior observations of buildings using concrete composite dovetail decking floor systems were anecdotally noted to deflect less than the simplified prediction calculations using the simplified SDI and ACI methods. The flexural behavior of a particular floor slab came into question on a composite floor built with dovetail decking with clear spans up to 28'-6" (8.69 m) (Fig. 5.1). This slab was constructed with 20 gauge dovetail decking with the geometry defined in Fig. 1.1 from Section 1.1. The total height of slab was 7 inches (178 mm) as measured from the bottom flute of the metal decking to the top of the slab; the light-weight concrete had an average as-built density of 125 lb/ft^3 (2,002 kg/m^3); the measured strength of concrete was 4,030 psi (27.8 MPa); additional #5 bar reinforcement was laid at bottom of flutes spaced every 12 inches (305 mm).

Because the as-built slab is continuous across load-bearing wall supports, making it an indeterminate structure, the flexural deflection solution for this nonlinear composite slab requires advanced techniques. A performance test was developed and implemented to determine its flexural behavior for comparison with different stiffness calculation methods. The numerical strain-compatibility modeling method developed in Section 4 was used to determine the

slab's moment-curvature relationship, as compared to the in-situ test deflection data.

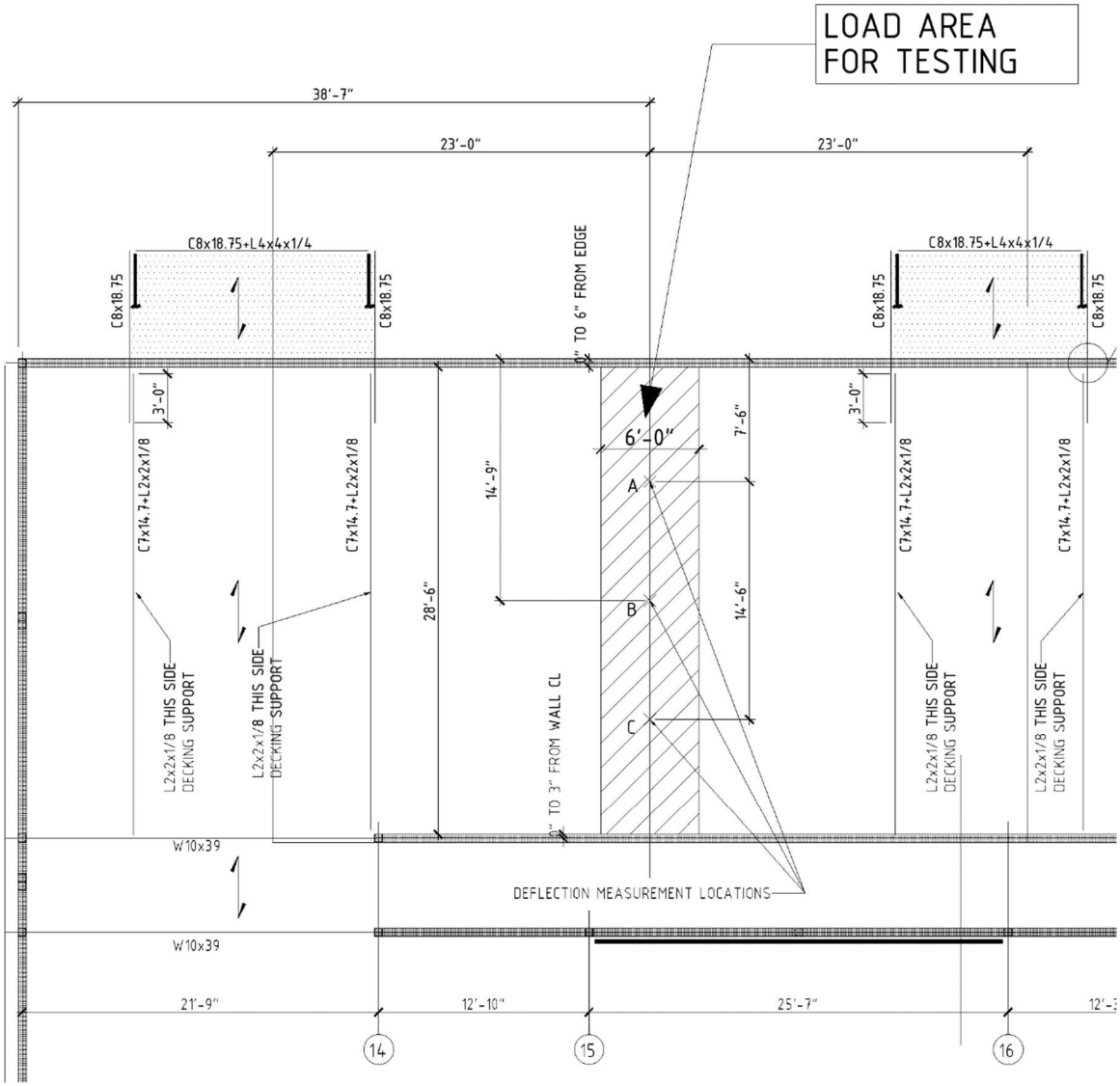

Fig. 5.1 Structural floor plan of in-situ composite slab.

5.1 5.1 In-situ Test Procedure

The slab was not allowed to be load-tested to failure because of the requirement that it must remain functional after the completion of the physical test; therefore, a stiffness performance test was conducted on the structural slab to determine its flexural behavior. The condition of the construction site at the time of the test comprised of the floor slab, erected with shoring, and a total cure time of the concrete greater than 6 months. Three points of erection shoring at the quarter points were removed immediately prior to testing (Fig. 5.2) and the floor slab was documented for existing cracks or anomalies. Formwork for a water holding tank was installed with elevation marks at 2 inch intervals. Because of the large scale of the slab and access to water at the site, the whole slab could not reasonably be filled with water, and therefore the water tank was limited to a 6 ft (1.83 m) width. This load size limitation caused the slab to behave with two-way action instead of a simpler one-way slab action, and therefore the deflection results must be comparatively analyzed using an orthogonal slab finite element model to verify the stiffness of the composite slab system.

The three deflection locations to be monitored were marked at the quarter points on the underside of the slab, labeled “A”, “B”, and “C”; A is the quarter point closest to the exterior wall where the slab end terminates, B is the middle of the span, and C is the quarter point closest to the corridor wall, which is a continuous slab support. The shoring supporting the floor slab was removed and the area was cleared for the set-up of the dial gauges.

Three dial Indicators with flex stands and clamps were mounted to stand-alone tripod shoring, and positioned at locations “A,” “B,” and “C.” The dial indicators measure at a precision of 0.001 inch (0.0254 mm) increments; Fig. 5.3 depicts the dial indicators setup in place, tared to zero. The slab is a pin support at the exterior wall and a continuous support at the interior wall, and location “A” is closest to the exterior wall.

Fig. 5.2 Initial condition of composite slab.

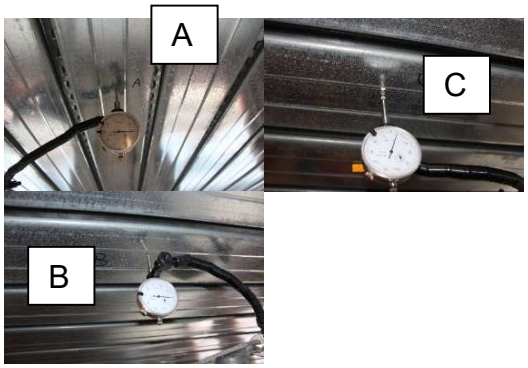

Fig. 5.3 Initial placement and tare of dial indicators.

The performance testing of the in-situ slab was done in conformance with ASCE 3-91, the American “Standard for the Structural Design of Composite Slabs” (American Society of Civil Engineers, 1994). The total distributed load required per this standard is no less than 85% of the factored loads, which equates to 72 psf (3.45 kPa) of additional loading on this floor slab. A water tank was fabricated to apply this distributed load on the slab up to 14 inches (356 mm) in height; instantaneous deflection measurements were taken at 2 inch (51 mm) increments.

5.2 In-situ Test Results

The resulting deflected shape at each measured load increment is shown in Fig. 5.4. Fig. 5.5 portrays the load-deflection (P-Δ) relationship at each of the measured locations, and highlights the instantaneous deflection.

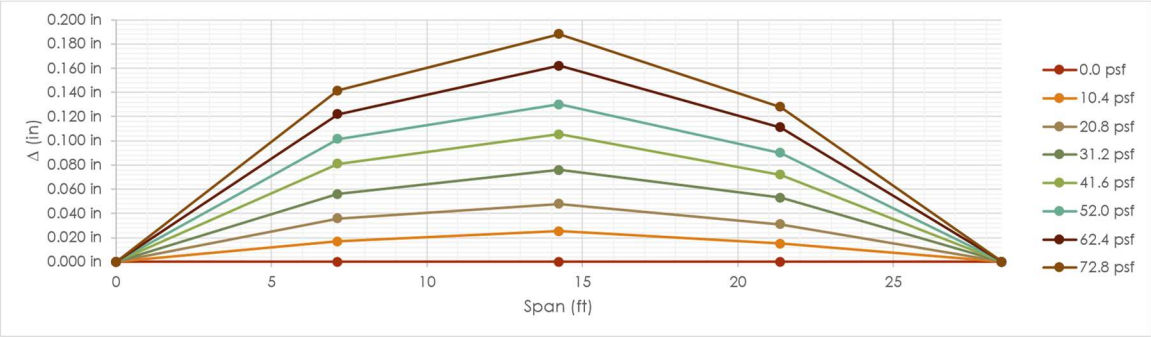

Fig. 5.4 Measured deflection vs vertical load across in-situ composite slab.

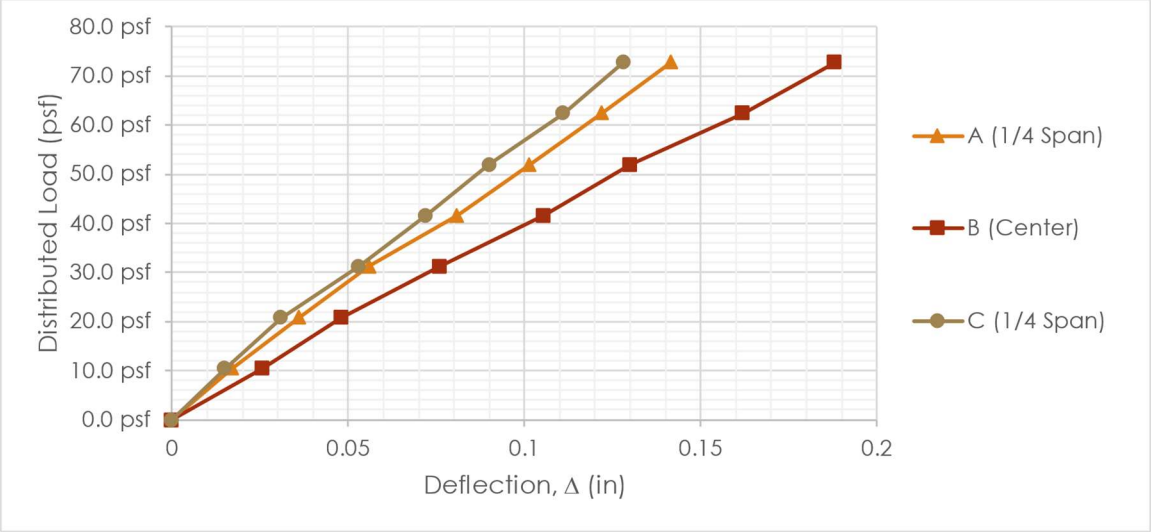

Fig. 5.5 Load deflection relationship at each quarter point, "A," "B," and "C," along the composite slab span.

5.3 Comparison of Numerical Strain-Compatibility Model with Other Simplified Methods

5.3.1 ASCE 3-91 Stiffness Calculation Method

The ASCE 3-91 simplified deflection calculation method uses the transformed section properties and calculates both the uncracked moment of inertia and the cracked moment of inertia and interpolates evenly between the two values (American Society of Civil Engineers, 1994). The uncracked moment of inertia calculation assumes no contribution of the concrete below the neutral

axis, similar to the ACI calculation for traditional reinforced concrete slabs. An additional criteria of ACI for the usage of light-weight concrete is to substitute all 28-day strength of concrete, f'_c, values in elasticity, tension fracture, and other equations for 75% of the strength ($0.75 \cdot f'_c$).

Utilizing the simplified ASCE 3-91 method for the serviceability deflection calculation on this constructed slab, the instantaneous load-deflection diagram for the slab at maximum load is depicted in Fig. 5.5. The transformed geometric properties calculated for this as-constructed case are as follows:

Uncracked moment of inertia, I_u:

$$I_u = 425 \ in^4/ft \tag{19}$$

Cracked moment of inertia, I_c:

$$I_c = 247 \ in^4/ft \tag{20}$$

Moment of inertia of composite section, I_d:

$$I_d = \frac{I_u + I_c}{2} = 336 \ in^4/ft \tag{21}$$

The estimated stiffness, EI, of the composite section is therefore the product of the elastic modulus, E_c, and the calculated I_d of a 12 in wide strip.

$$E_c I_d = 2714\ ksi \cdot 336\ in^4 = 911440\ k \cdot in^2 \tag{22}$$

5.3.2 Other Equations for Stiffness Calculation

An effective moment of inertia equation for reinforced concrete members by Branson (Branson, 1963) was extended to be used in calculating the moment of inertia of composite slabs by Tenhovuori, et al. (1996). Because concrete composite slabs are nonlinear, the value of the effective moment of inertia changes as the applied moment changes along the length of the slab, while the elasticity of the composite slab is assumed to be taken as the elasticity of the concrete, E_c. This effective moment of inertia, $I_{eff,ten}$, could then be applied to the various composite slab parameters to estimate the deflection behavior of a composite slab under flexural loads.

$$I_{eff,ten} = I_u \left(\frac{M_{cr}}{M_a}\right)^3 + I_c \left[1 - \left(\frac{M_{cr}}{M_a}\right)^3\right] \leq I_u \tag{23}$$

$I_{eff,ten}$: Tenhovuori et al. effective moment of inertia
I_u: uncracked moment of inertia
I_c: cracked moment of inertia
M_{cr}: the cracking moment
M_a: the bending moment of the member

Later research by Souza Neto (2001) determined that the Tenhovuori equation for I_{eff} was too high and proposed a modification to the equation based on their experiments:

$$I_{eff,souza} = I_u \left(\frac{M_{cr}}{M_a}\right)^3 + \frac{I_c}{20}\left[1 - \left(\frac{M_{cr}}{M_a}\right)^3\right] \leq I_u \tag{24}$$

$I_{eff,souza}$: Souza Neto's effective moment of inertia
I_u: uncracked moment of inertia
I_c: cracked moment of inertia
M_{cr}: the cracking moment
M_a: the bending moment of the member

A recent study by Costa, et al. (2021) determined that the Souza Neto equation calculated inertia values should be modified to better fit their experimental data; additionally the study differentiated the equation for brittle versus ductile slabs.

$$I_{eff,costa-d} = I_u \left(\frac{M_{cr}}{M_a}\right)^3 + \frac{I_c}{10}\left[1 - \left(\frac{M_{cr}}{M_a}\right)^3\right] \leq I_u \tag{25}$$

$$I_{eff,cost} \quad = I_u \left(\frac{M_{cr}}{M_a}\right)^3 + \frac{I_c}{20}\left[1 - \left(\frac{M_{cr}}{M_a}\right)^3\right] \leq \frac{(I_u + I_c)}{2} \tag{26}$$

$I_{eff,costa\text{-}d}$: Costa et al. effective moment of inertia for ductile slabs
$I_{eff,costa\text{-}b}$: Costa et al. effective moment of inertia for brittle slabs
I_u: uncracked moment of inertia
I_c: cracked moment of inertia
M_{cr}: the cracking moment
M_a: the bending moment of the member

It is worth nothing that the test composite slab samples used to develop and validate these other simplified effective inertia, I_{eff}, equations were made with variations of the trapezoidal profiled decking and not the dovetail decking.

5.3.3 Stiffness Calculation with Numerical Strain-compatibility Model

The moment-curvature diagram for the material and geometric properties of this in-situ composite slab is used to derive the variable stiffness of the loaded slab (Fig. 5.6). Its stiffness varies greatly depending on the applied moment; whereas the ACI estimated stiffness, *EI*, calculation overly simplifies this inelastic flexural behavior, the computational analysis of the moment-curvature diagram provides the complete picture of the composite slab's behavior.

The stiffness, EI, is equal to the moment divided by the curvature, as discussed previously in Section 4.1, Equation (5). By creating a unique table of

Moment vs. Stiffness from the computational analysis, the stiffness can be more accurately defined as it reduces, nonlinearly, with increasing flexural forces (Table 5.1).

Table 5.1. Calculated moment-curvature-stiffness relationship of the in-situ composite slab

M (k-ft)/ft	ψ (rad/in)	EI_{eff} (k-in^2)/ft
2.44E-06	2.62E-11	1.12E+06
1.48	1.59E-05	1.11E+06
2.45	2.65E-05	1.11E+06
3.42	3.71E-05	1.11E+06
4.36	4.79E-05	1.09E+06
5.43	7.19E-05	9.07E+05
6.70	1.05E-04	7.64E+05
…	…	…
26.67	1.86E-03	1.72E+05

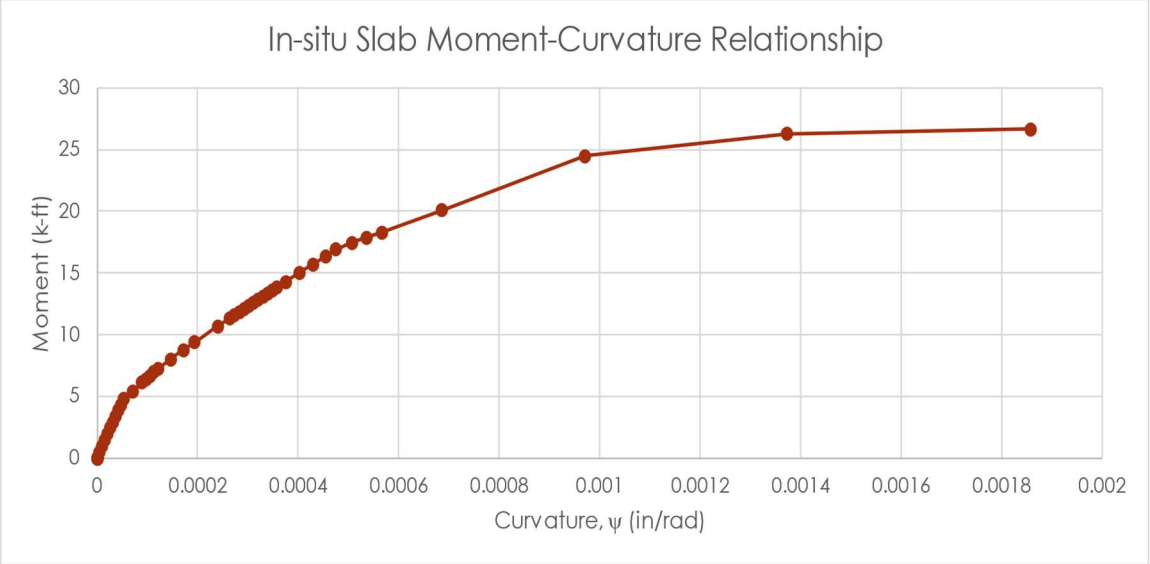

Fig. 5.6 Calculated moment-curvature diagram of in-situ composite slab.

5.3.4 Comparison of Calculated Stiffness Models

The parameters of the in-situ composite concrete slab were applied to the new analytical method proposed in this study, and also to the empirically based equations from ASCE and other prior studies. A graphical comparison of the stiffness behavior at increasing moments for this in-situ slab illustrates the differences for the various calculations Fig. 5.7; it is noted on the graph the load range applied to the in-situ slab.

For small flexural loads, before the bottom fiber of concrete cracks, the stiffness calculation of the proposed new analytical method is approximately 97%

to 94% of what would be calculated as the gross moment of inertia of the uncracked composite concrete slab, $(E_c I_u)$. Graphically, this difference is noticeable, however, the variances in the deflection calculation at this very low flexural load would not be easily noticed because the curvature is still very small in this range. However, the inaccuracy of the deflection calculations using the other methods (Souza Neto, Costa) would be greatly noticed at higher moments, post concrete cracking, where the stiffness of the composite slab calculates much softer than what was determined through testing of the dovetail composite decking. The simplified ASCE calculation would overestimate the deflections up to cracking, and then underestimate deflections for higher moments post cracking; a single stiffness estimate has a very narrow range of accuracy. Note that the other equations were developed using trapezoidal decking, not the dovetail decking, and this comparison shows how they largely differ after cracking has occurred.

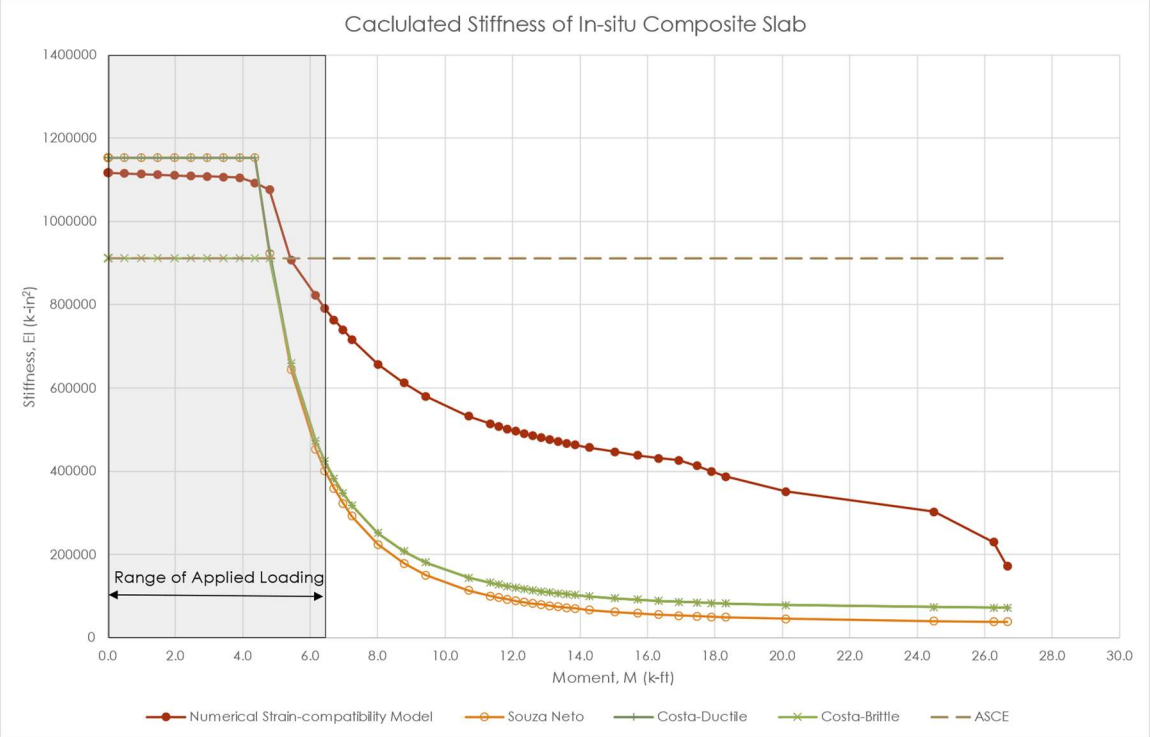

Fig. 5.7 Calculated stiffness, EI, of in-situ composite slab.

5.4 Finite Element Plate Model of In-situ Composite Dovetail Decking Slab Implementing the Numerical Strain-compatibility Model

The in-situ slab, as it was only partially loaded and the parallel edges were not free to deflect, behaves as a two-way slab and therefore a simple finite element analysis is the best method to determine the deflection under the tested loading. The stiffness calculated using the new analytical solver developed in

section 4 and implemented in section 5.3.2 provides the stiffness estimation of the main or strong-axis bending for comparison with the test data. The weak-axis flexural stiffness will be established using an orthotropic equivalent flat plate method implemented by El-Dardiry & Tianjian (2006) for modelling stiffness of a slab; their study specifically addressed finite element modelling that was tested with dynamic frequencies of a composite slab instead of deflection behavior from static loading, however its method of estimating weak axis bending can be applied toward this static study, because it is in the serviceable load range for flexure.

The finite element analysis program, RISA 3D v20, was selected to create the flat plate, orthotropic model (Fig. 5.8). The slab was laid out with constraints and integrated steel members, as observed in the constructed condition. The composite slab was modeled as rectangular plate/shell elements capable of transferring moments and shear at all four nodes. The user inputs available for the plate/shell elements in RISA 3D are: a thickness, *t*; elasticity in the strong axis, *E1*, and in the weak axis, *E2*; shear modulus, *G;* and moment of inertia, *I*. For this orthotropic model, the stiffness in the weak axis and the strong axis, $(EI)_x$ and $(EI)_y$, respectively, are modeled by altering the elasticity variable in RISA, *E1* and *E2*, while providing a constant moment of inertia, *I*, for both axes. The plates

are given a thickness, t_{eq}, estimated from the stiffness of the slab in the weak-axis direction, I_y, which is determined from a finite element analysis of the composite slab in Ansys Workbench 2021 R2 to determine $(EI)_y$.

$$I_y = \frac{b \cdot {t_{eq}}^3}{12} \tag{27}$$

I_y: Moment of inertia in the weak-axis direction of a section of the composite slab

b: width of the slab analyzed

t_{eq}: simplified equivalent thickness

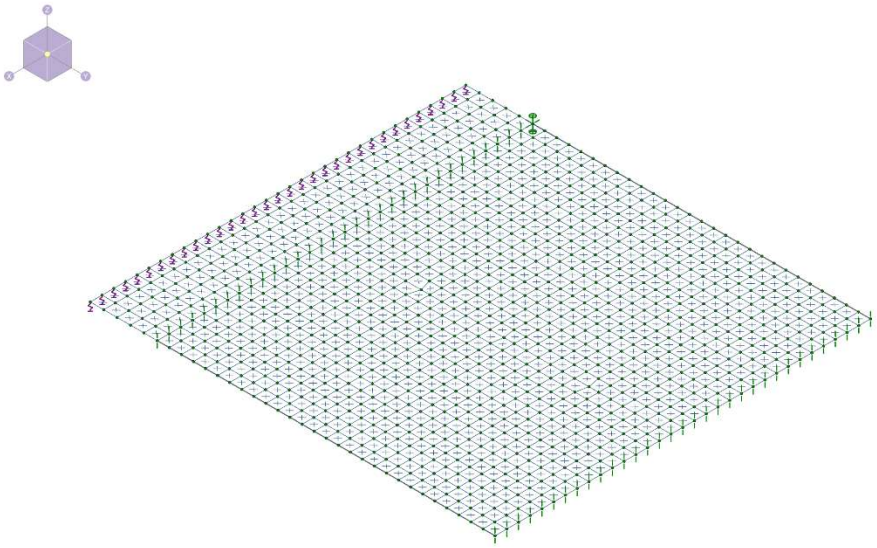

Fig. 5.8 Flat plate model of in-situ slab in RISA 3D.

The solid model weak-axis bending was evaluated in the elastic range of the concrete material in Ansys Workbench. The maximum deflection solution was obtained from Ansys from a ramped vertical surface pressure applied at the top of the slab; the boundary conditions were placed at the longitudinal edges of the composite slab to create a weak-axis bending condition (Fig. 5.9). The resulting load-deflection results mimic a simply-supported beam in elastic flexure from a constant distributed load, and therefore the stiffness, $(EI)_y$, can be calculated from the equation for maximum deflection for this load condition of an elastic member:

$$(EI)_y = \frac{w \cdot L^4}{384 \cdot \Delta_{max}} \tag{28}$$

Δ_{max}: maximum vertical deflection of the member
L: total length of the member between supports
w: constant distributed load
$(EI)_y$: stiffness of the composite slab in weak-axis bending

If the elasticity of the concrete is assumed to be set as E_c, the elasticity of the concrete in the linear range, the weak-axis moment of inertia, I_y, is calculated from the stiffness property, $(EI)_y$, and the resulting thickness, t_{eq}, is then calculated from the equation relating thickness to I_y, Eqn. (27).

Table 5.2. Weak-axis flexural properties for in-situ composite slab.

$(EI)_y$	4.19E+05	k-in^2
Ec	2714	ksi
I_y	154	in^4
t_{eq}	5.37	in

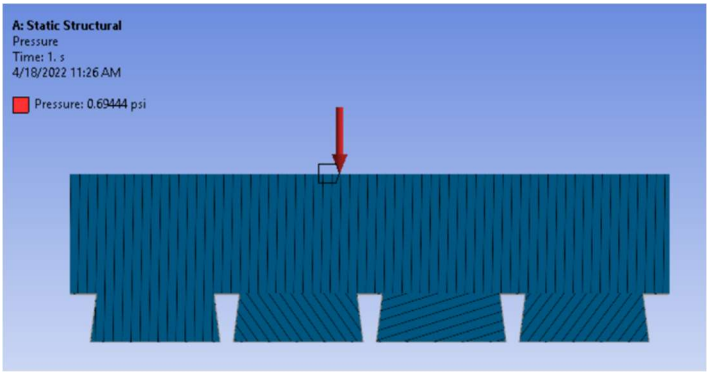

Fig. 5.9 Weak-axis bending of in-situ composite slab in Ansys.

To determine the best shear modulus estimate for the orthotropic flat-plate equivalent modeling of a composite concrete slab, El-Dardiry & Ji (2006) tested four different possible equations for shear modulus, *G*. They determined that the following shear modulus calculation provided the most universally accurate results:

$$G = \frac{E_y \sqrt{E_y / E_x}}{2\left(1 + \nu \sqrt{E_x / E_y}\right)} \tag{29}$$

G: Shear modulus for orthotropic model

E_y: Elastic modulus in the weak axis for orthotropic model

E_x: Elastic modulus in the strong axis for orthotropic model

ν: Poisson's ratio for concrete

The strong-axis effective elasticity, *E1*, is determined from $(EI)_x$ calculated from the analytical method proposed in this study using a constant I_x, calculated from the equivalent thickness, t_{eq}, similar to the weak-axis stiffness calculation. The internal bending moment of the slab varies under the self-weight and the test load; it is therefore inaccurate to assign the same single material attribute to all finite elements in the flat-plate model. Therefore, as a finite element reaches a given flexural moment, its material stiffness properties are adjusted to model the appropriate stiffness at that load.

The in-situ slab is part of a continuous slab, such that there is an intermediate bearing wall support. This intermediate support causes the flexural moment to change from positive bending to negative bending. Fig. 5.10 shows a simplified free-body diagram and moment diagram of the continuous slab condition that is similar to the in-situ composite slab; a more realistic boundary

condition is modeled at the exterior wall is a rotational spring with some rotational resistance instead of a perfect pin because the upper floor's load-bearing wall sandwiches the end 6 inches (152 mm) of the slab preventing free rotation. Over the wall, the in-situ slab was constructed with top reinforcement bars, sized #6 spaced at 6 inches (152 mm), positioned at approximately 2.5 inches (64 mm) from the top of the slab to resist the negative bending of the composite slab (Fig. 5.11). The stiffness of the composite slab in negative flexural moment, EI_{neg}, is calculated neglecting the concrete material in tension, as is typical with a common reinforced concrete slab. The equivalent thickness value, t_{eq}, and its associated inertia, I, is then divided out of the EI_{neg} equation providing an effective E_{neg} for this negative flexure portion of the composite slab.

Table 5.3 summarizes the calculated effective elasticity, E, values and shear modulus, G, values of the in-situ composite concrete slab with dovetail decking.

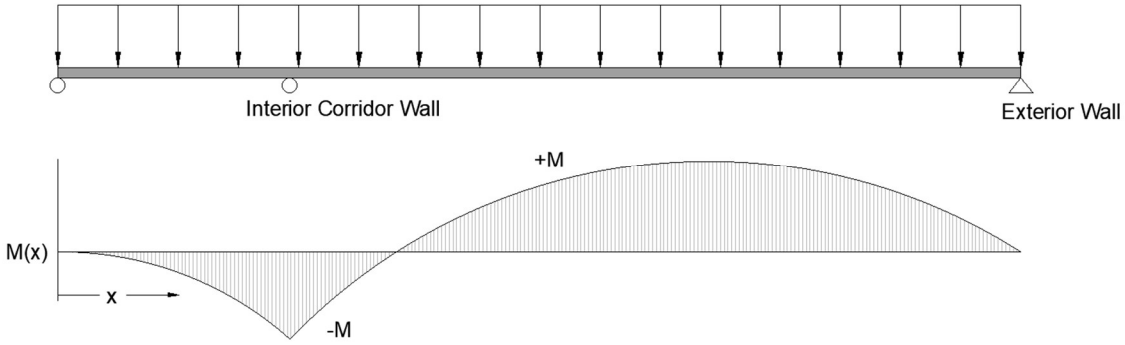

Fig. 5.10 Strong-axis simplified moment diagram of continuous composite slab.

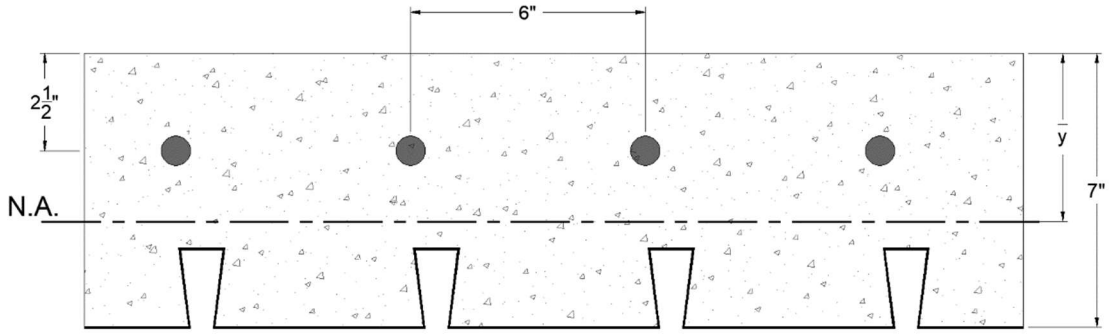

Fig. 5.11 Composite slab reinforced for negative flexure.

Table 5.3. In-situ composite dovetail decking slab effective stiffness for FE model

Material Label	Moment k-ft/ft	(EI)x $k\text{-}in^2$	Ex* ksi	Ey* ksi	Ex*/Ey*	G*[1] ksi
neg.	<0	4.06E+05	2628	2628	1.00	1095
0	1.0	1.11E+06	7212	2714	0.38	628
1	4.8	1.08E+06	6967	2714	0.39	641
2	5.5	9.11E+05	5901	2714	0.46	711
3	6.2	8.27E+05	5352	2714	0.51	754
4	6.5	7.77E+05	5033	2714	0.54	783
					[1] ν =	0.2

The first load step is modeled in RISA 3D with the stiffness assigned based on the strong axis flexural moment from the table, Table 5.3. The total flexural moment in the slab to determine the corresponding material stiffness includes the self-weight of the composite slab, 72 psf (3.2 kPa) applied to the entire surface, and the first applied load condition, 10.4 psf (0.50 kPa) applied along the 6 ft (1.8 m) strip. A graphic portrayal of the slab plate element stiffness set under the first load step is depicted in Fig. 5.12. The directional deflection at the nodes corresponding to data points, “A”, “B”, and “C” were extracted from the finite element solution data for comparison to the data collected from the in-situ test.

The same process was repeated for all successive load steps, 2 through 7. The final deflection data at the specified locations are plotted against the raw data for a visual comparison in Fig. 5.19, and summarized in Table 5.4. The proposed analytical method detailed in this study for determining the composite dovetail decking slab flexural behavior provides adequate deflection results when compared to test results from real-world construction. The calculated RSME was 0.25%, 0.36%, and 0.27%, for locations A, B, and C, respectively. This analysis comparing the numerical strain-compatibility model with physical testing shows very good results for the stiffness model up to and 45% beyond the cracking moment of the slab.

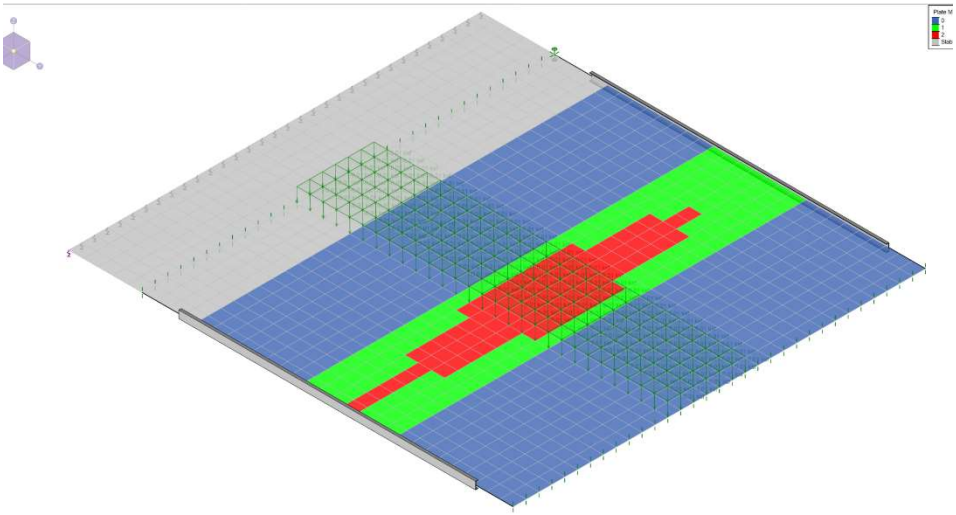

Fig. 5.12 In-situ slab material stiffness variations under self-weight and first load step.

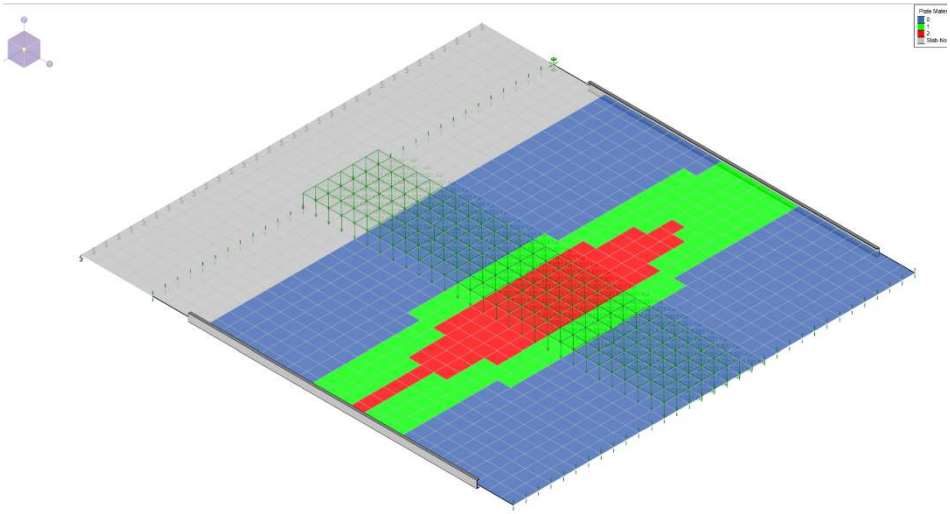

Fig. 5.13 In-situ slab material stiffness variations under self-weight and second load step.

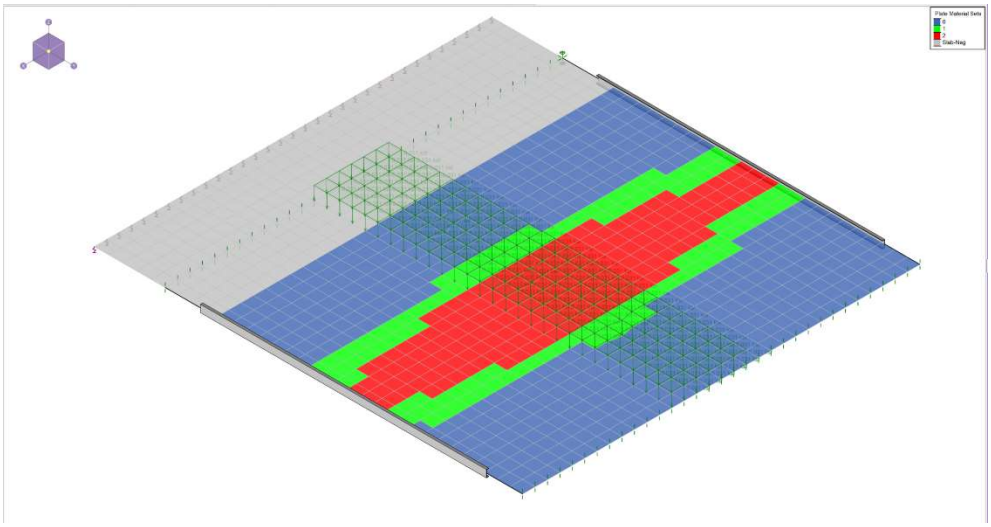

Fig. 5.14 In-situ slab material stiffness variations under self-weight and third load step.

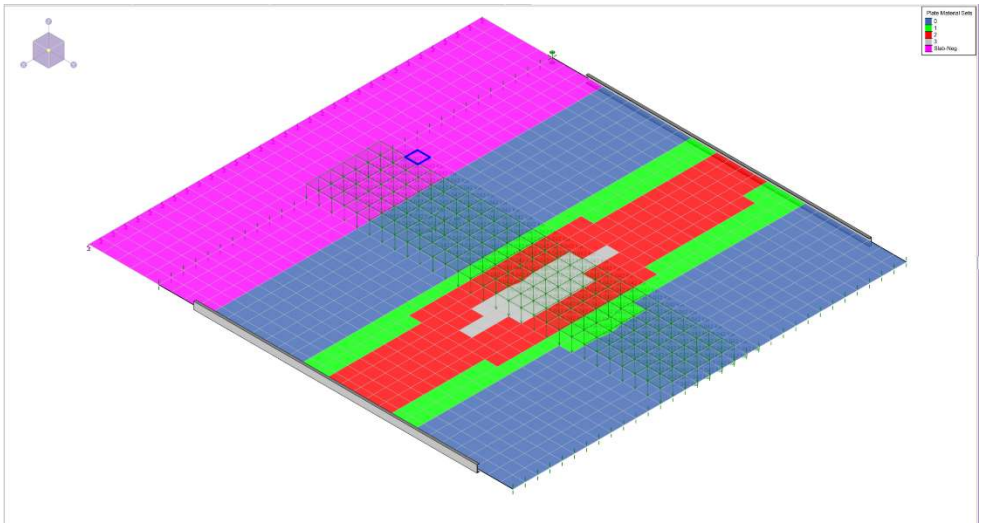

Fig. 5.15 In-situ slab material stiffness variations under self-weight and fourth load step.

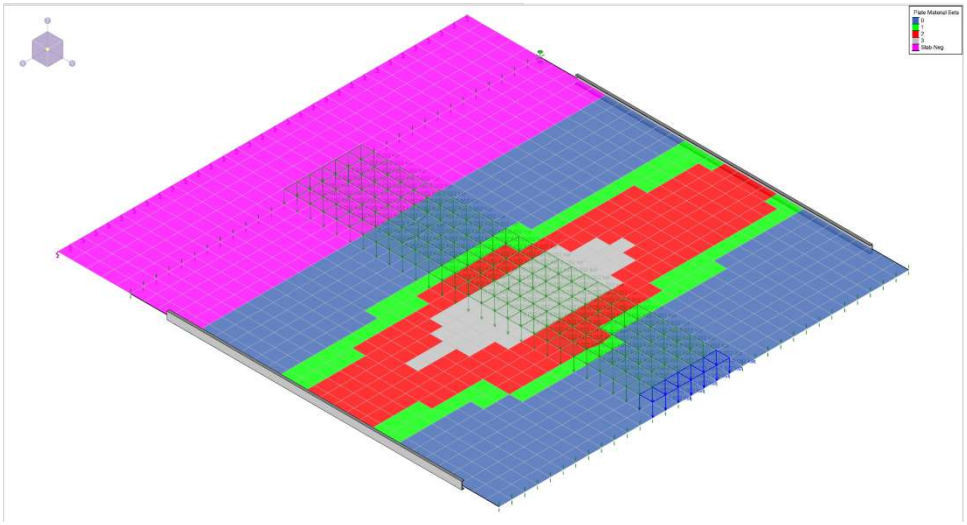

Fig. 5.16 In-situ slab material stiffness variations under self-weight and fifth load step.

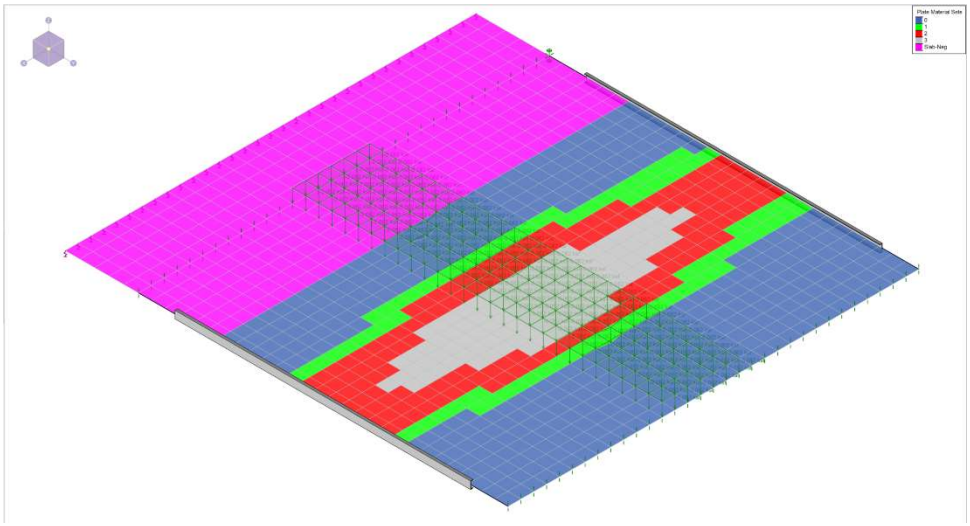

Fig. 5.17 In-situ slab material stiffness variations under self-weight and sixth load step.

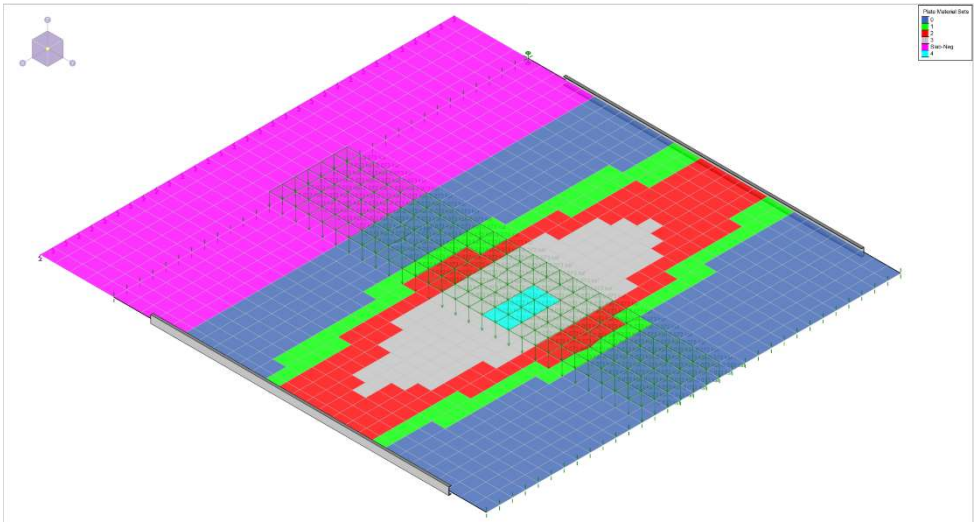

Fig. 5.18 In-situ slab material stiffness variations under self-weight and seventh load step.

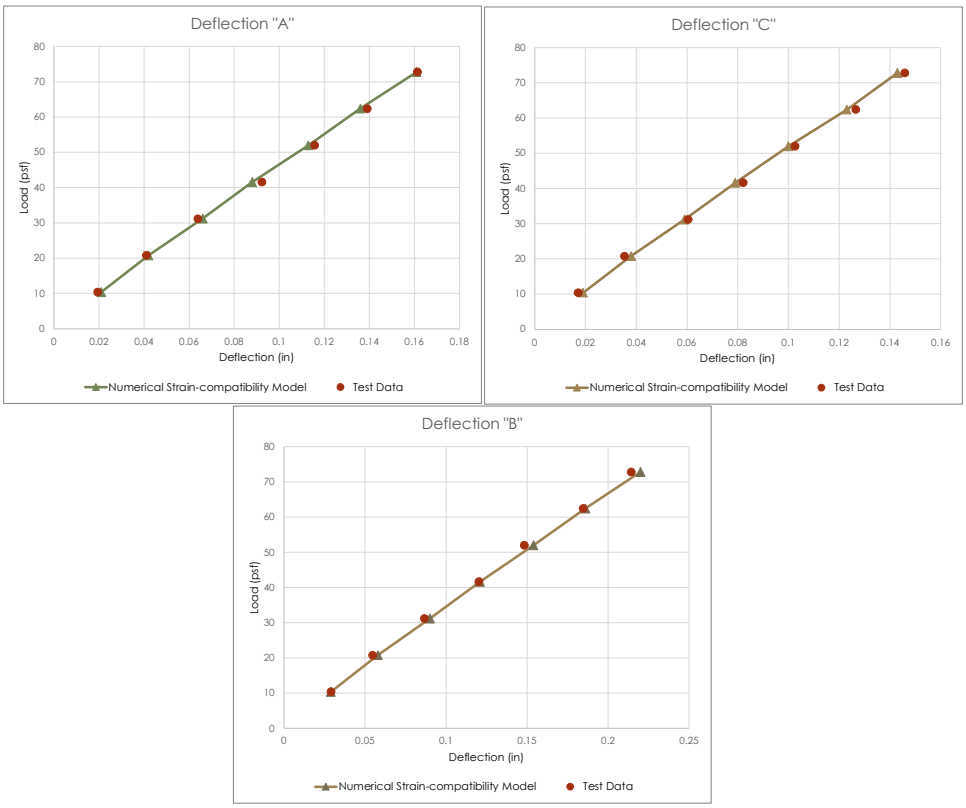

Fig. 5.19 Numerical Strain-compatibility Model vs. In-situ Test Data

Table 5.4. Numerical Strain-compatibility Method FE Deflection vs. In-situ Test Data

	Load	Strain-compatibility Model (EI)			In-situ Test Data			Error Calc		
	w	Δ_A	Δ_B	Δ_C	Δ_A	Δ_B	Δ_C	$(\Delta_{obs}-\Delta_{calc})^2$		
	(psf)	(in)	(in)	(in)	(in)	(in)	(in)			
1	10.4	0.021	0.029	0.019	0.0194	0.0291	0.0171	2.62E-06	4.90E-09	3.61E-06
2	20.8	0.042	0.058	0.038	0.0410	0.0547	0.0353	9.22E-07	1.08E-05	7.08E-06
3	31.2	0.066	0.09	0.059	0.0638	0.0866	0.0604	4.67E-06	1.13E-05	2.02E-06
4	41.6	0.088	0.121	0.079	0.0923	0.1203	0.0821	1.88E-05	5.33E-07	9.49E-06
5	52	0.113	0.154	0.1	0.1157	0.1482	0.1026	7.34E-06	3.36E-05	6.76E-06
6	62.4	0.136	0.186	0.123	0.1391	0.1847	0.1265	9.49E-06	1.74E-06	1.25E-05
7	72.8	0.161	0.22	0.143	0.1613	0.2143	0.1459	9.61E-08	3.23E-05	8.53E-06
							RSME =	**0.25%**	**0.36%**	**0.27%**

6 Development of Design Tables Utilizing the Numerical Strain-compatibility Model

The versatility of a complete, easily and quickly computed flexural behavior model for dovetail composite decking extends to the derivation of an technical design table for various common configurations of the composite slab. The following discusses the process of implementation of the numerical strain-compatibility model to derive a custom design table for engineering purposes.

6.1 Design Table Introduction

The final calculated moment-curvature diagram calculation method can be utilized to produce a robust and versatile design table for a various decking gauges, slab thickness values, concrete strength ranges, and so forth. The purpose for the design table is to provide a design guide for practicing structural engineers to aid in the specification of composite concrete slabs in building projects.

Engineers use design tables to quickly reference the design properties needed for strength and serviceability calculations of structural components. It can be a very useful calculation tool in lieu of cumbersome and/or repetitive

manual calculations, therefore it has become common for decking manufacturers to provide technical design catalogs specific to their feature products (Canam, 2010). These engineering design aids include real-world scenarios of the more common loads, spans, slab depths, etc., but only serve as guidance for the engineer, not a replacement. As such, the limitations and assumptions of the guides are typically discussed in the footnotes of the tables or in a preface page of notes; the final design is up to the design engineer who will have the liability and responsibility of discerning the project requirements and reconciling that with the information gleaned from the manufacturer's technical catalog.

6.2 Practical Scope of the Design Table

The strain-compatibility based analytical model, the New Analytical Model, developed in this study and verified through physical flexural tests and finite element models, determines an accurate moment-curvature relationship for flexural behavior of the dovetail composite decking structural slabs. Recall that each unique composite slab has a given set of geometric and material properties that can vary. By establishing a finite list of common values of concrete strength, slab depth, super-imposed dead load, live load, and span, multiple design guide

tables are produced using this new analytical model solver to fit the common structural scenarios for a building project.

6.2.1 Common Material and Geometric Properties

The dovetail decking material utilized for testing verification and model application in the study is from a manufacturer, Canam. Currently, they provide decking thickness of this product in three different sizes: 22-gauge, 20-gauge, and 18-gauge. Therefore, a design table with three different gauge options would be prudent to include in the technical guide. The grade of the steel, which establishes the yield strength, *Fy*, would also be set based on what the manufacturer offers; the grade of steel of the dovetail decking utilized in this study has a yield strength of 40,000 psi (276 MPa).

Concrete strength varies greatly, but for design purposes is set in increments of 500 psi (3.4 MPa), but more commonly in increments of 1,000 psi (6.9 MPa). Concrete can also be made with typical density aggregate which is called “normal weight concrete”, or with lighter aggregate which is referred to as “light weight concrete.” Prior studies have shown that light weight concrete has a different elasticity in its linear region, and lower tensile strength than normal weight concrete. As such, the American Concrete Institute (ACI) has required a

reduction of 75% that of normal weight concrete to be applied to light weight concrete's tensile strength, f_t, and modulus of elasticity, E_c (American Concrete Institute, 2014). Design tables with different concrete material options for strength and for normal weight vs. light weight concrete is prudent to include in the technical guide.

American architects, engineers, and builders prefer cast-in-place concrete slab thickness measurements to be in either 0.5" or 1" increments, as anything smaller would be impractical in the construction field. A reasonable range of common slab depths in 0.5" to 1" increments would therefore be desirable for an effective engineering design table.

The International Building Code (IBC) provides loading based on the occupational use of the building structure. For the floor of a typical residential and/or commercial building, the most common live loads (loads that are transient and highly unpredictable) are 40 psf (1.9 kPa) and 100 psf (4.8 kPa) (International Code Council, Inc., 2020). The superimposed dead loads (loads that are not part of the structure but are permanent to the building such as floor finishes, hung mechanical ducts, plumbing, etc.) are commonly in the range of 5 psf (0.24 k Pa) to 10 psf (0.48 kPa), but can be more in some cases. Design tables typically provide the most likely loading scenario for the common

occupiable floor to include all combinations of the two common live loads with approximately two common superimposed dead loads.

The International Building Code (IBC) and the American Society of Civil Engineers (ASCE 7) state a structural element must meet both the defined strength and serviceability conditions. The design engineer, in their analysis of the composite structural slab, must check the slab's strength capabilities against the code-required design forces applied to ensure that their design does not exceed the prescribed loads. Therefore, the design table should include the design strength, ϕM_n, of the composite slab. They must also check that the serviceability of the slab is not exceeded; the common serviceability limit codified in the American standards is the maximum deflection limit for live loads () and a deflection limit for dead loads (loads that are part of the permanent structure) and live loads, together (American Society of Civil Engineers, 2016) (International Code Council, Inc., 2020). To create a more versatile design table for this composite system with nonlinear materials and behavior, the deflections at each stage of loading are shown individually such that the engineer can apply the appropriate long-term deflection factors, λ, based on the unique construction conditions of their building project. The maximum deflection can therefore be

compared against the three most common ratios: L/240, L/360, and L/480 where *L* is the length of the span between supports.

It is currently not common to see a graph of the effective stiffness, *EI*, of the slab in a design guide. The benefit to having a convenient reference of the Moment-Stiffness relationship is so that an engineer can use the data for simplified finite element analyses as was done in Section 5.4. It can also be a useful tool to help visually recognize the rate at which the softening of the composite slab occurs and at what flexural loading that should be avoided, should the design project require it.

A sample design table is depicted in Fig. 6.1. This is an example of a 5.5" composite slab with dovetail decking, made from grade 40 steel, whose geometry is defined previously in Fig. 3.1; the concrete is 5,000 psi strength and it is normal weight. The corresponding moment-stiffness diagram for this exact slab design is shown in Fig. 6.2.

f'c = 5000 psi

Normal Weight Concrete

Slab Depth	Gauge *Thickness*	Self Weight	Unshored Span (max)
5.5 in	20 *0.0358 in*	64.5 lb/ft	9 ft

ϕV_n = 12.8 k-ft

Superimposed Dead = 5 psf, Live = 40 psf

	Span (Single) 8 ft	10 ft	12 ft	14 ft	16 ft	18 ft	20 ft
Δ_{wt}	0.006 in	0.017 in	0.032 in	0.066 in	0.112 in	0.205 in	0.300 in
Δ_{SD}	0.001 in	0.002 in	0.002 in	0.007 in	0.019 in	0.007 in	0.031 in
Δ_L	0.005 in	0.011 in	0.029 in	0.051 in	0.082 in	0.171 in	0.409 in
Mu/ϕMn	0.09	0.14	0.21	0.28	0.37	0.47	0.58
L/240	0.400 in	0.500 in	0.600 in	0.700 in	0.800 in	0.900 in	1.000 in
L/360	0.267 in	0.333 in	0.400 in	0.467 in	0.533 in	0.600 in	0.667 in
L/480	0.200 in	0.250 in	0.300 in	0.350 in	0.400 in	0.450 in	0.500 in

Superimposed Dead = 5 psf, Live = 100 psf

	Span (Single) 8 ft	10 ft	12 ft	14 ft	16 ft	18 ft	20 ft
Δ_{wt}	0.006 in	0.017 in	0.032 in	0.066 in	0.112 in	0.205 in	0.300 in
Δ_{SD}	0.001 in	0.002 in	0.002 in	0.007 in	0.019 in	0.007 in	0.031 in
Δ_L	0.012 in	0.030 in	0.068 in	0.137 in	0.321 in	0.795 in	1.700 in
Mu/ϕMn	0.15	0.24	0.34	0.47	0.61	0.77	0.95
L/240	0.400 in	0.500 in	0.600 in	0.700 in	0.800 in	0.900 in	1.000 in
L/360	0.267 in	0.333 in	0.400 in	0.467 in	0.533 in	0.600 in	0.667 in
L/480	0.200 in	0.250 in	0.300 in	0.350 in	0.400 in	0.450 in	0.500 in

Superimposed Dead = 10 psf, Live = 40 psf

	Span (Single) 8 ft	10 ft	12 ft	14 ft	16 ft	18 ft	20 ft
Δ_{wt}	0.006 in	0.017 in	0.032 in	0.066 in	0.112 in	0.205 in	0.300 in
Δ_{SD}	0.001 in	0.003 in	0.010 in	0.012 in	0.024 in	0.017 in	0.066 in
Δ_L	0.006 in	0.012 in	0.020 in	0.050 in	0.081 in	0.192 in	0.436 in
Mu/ϕMn	0.10	0.15	0.22	0.29	0.38	0.49	0.60
L/240	0.400 in	0.500 in	0.600 in	0.700 in	0.800 in	0.900 in	1.000 in
L/360	0.267 in	0.333 in	0.400 in	0.467 in	0.533 in	0.600 in	0.667 in
L/480	0.200 in	0.250 in	0.300 in	0.350 in	0.400 in	0.450 in	0.500 in

Superimposed Dead = 10 psf, Live = 100 psf

	Span (Single) 8 ft	10 ft	12 ft	14 ft	16 ft	18 ft	20 ft
Δ_{wt}	0.006 in	0.017 in	0.032 in	0.066 in	0.112 in	0.205 in	-
Δ_{SD}	0.001 in	0.003 in	0.010 in	0.012 in	0.024 in	0.017 in	-
Δ_L	0.012 in	0.031 in	0.061 in	0.139 in	0.346 in	0.863 in	-
Mu/ϕMn	0.16	0.24	0.35	0.48	0.62	0.79	-
L/240	0.400 in	0.500 in	0.600 in	0.700 in	0.800 in	0.900 in	-
L/360	0.267 in	0.333 in	0.400 in	0.467 in	0.533 in	0.600 in	-
L/480	0.200 in	0.250 in	0.300 in	0.350 in	0.400 in	0.450 in	-

#.## in Does not meet Δ_L < L/240
#.## in Does not meet Δ_L < L/360
#.## in Does not meet Δ_L < L/480

Fig. 6.1 Sample design table for dovetail decking composite slab.

Fig. 6.2 Moment - effective stiffness diagram for sample design of dovetail decking composite slab.

7 Conclusions

The dovetail composite decking can be accurately modeled using a numerical strain-compatibility analysis based on the physical testing performed in this study. Historically, the dovetail decking profile did not have available research and universal design guidance compared to the more common trapezoidal composite decking and this lack of a more accurate design standard had made the calculation of the non-linear stiffness behavior of the dovetail composite deck floor systems under small to intermediate strains inaccurate.

The objective of this research was met with the development of an analytical model of the flexural behavior of re-entrant dovetail composite decking called the numerical strain-compatibility model. The flexural behavior of the composite metal deck is modeled based on its material properties and the following base assumptions: the composite slab is in pure bending; plane sections remain plane and are orthogonal to the neutral axis; the laws of static equilibrium apply; and loads are assumed to be static. Application of this composite theory to determine the moment-curvature relationship using a numerical strain-compatibility computer-based solver was compared against physical tests to validate and calibrate the theoretical assumptions that make up the basis for the calculations. The resulting flexural behavior derived from this

numerical strain-compatibility method has a multitude of uses including but not limited to: the derivation of a robust design table for a number of decking gauges, common slab thickness values, concrete strength ranges, and so forth; and variable stiffness properties for use in simplified finite element plate models.

The computational model was verified with physical testing of slab specimens in four-point flexural loading. By numerically calibrating the deck-slip strain experienced under bending to the test data, a strong linear correlation was discovered between the curvature angle of the slab and the deck-slip strain; this discovery led to a simple linear equation to be added to the computational solver program to adjust the deck strain after cracking has occurred and thereby produce an adequate moment-curvature relationship for a variety of slab depths.

The versatility of having a known moment-curvature relationship computation for any particular dovetail decking composite slab was demonstrated by calculating the flexural behavior of a constructed floor slab, which had been tested in flexural loading. Applying the stiffness relationship calculated from the numerical strain-compatibility model of the as-built slab to a finite element plate model showed adequate deflection results when compared to the physical test data.

Additionally the numerical strain-compatibility model was implemented in the development of a robust design guide table for engineering use. The computational model provides an accurate history of stiffness under increasing flexural loads that have a significant impact on design for longer spans where deflection calculations are more critical in controlling the design.

The numerical strain-compatibility model developed and verified in this study has multiple benefits including but not limited to: it is faster to calculate for each unique composite dovetail decking slab than a detailed finite element model; it is more accurate than other current simplified calculation standard; it provides a detailed strain and stress profile at each incremental bending curvature angle; it provides a moment-curvature relationship that can be directly utilized in simplified finite element plate models of floor slabs; multiple variables can be adjusted to customize the composite slab required for analysis.

The real-world purpose for this new numerical strain-compatibility model is to provide an intuitive and accurate design guidance and engineering resources for practicing structural engineers, without a time-consuming and expensive finite element model. With the numerical strain-compatibility analysis, an engineer can accurately analyze and specify composite concrete slabs in building projects

without being limited by shorter spans or thicker slabs due to inaccuracies in deflection calculations.

8 References

Abdullah, R., & Easterling, W. S. (2008). Elemental Bending Test and Modeling of Shear Bond in Composite Slabs. *International Conference on Composite Construction in Steel and Concrete* (pp. 138-150). American Society of Civil Engineers.

Abdullah, R., & Easterling, W. S. (2009). New evaluation and modeling procedure for horizontal shear bond in composite slabs. *Journal of Constructional Steel Research*, 891-899.

Ahmed, I. M., & Tsavdaridis, K. D. (2019). The evolution of composite flooring systems: applications, testing, modelling and eurocode design approaches. *Journal of Constructional Research*, 286-300.

American Concrete Institute. (2014). Building Code Requirements for Structural Concrete (ACI 318-14).

American Concrete Institute. (2014). Commentary on Building Code Rquirements for Structural Concrete (ACI 318R-14).

American Society of Civil Engineers. (1992). *Standard Practice for Construction and Inspection of Composite Slabs.* New York: ANSI/ASCE 9-91.

American Society of Civil Engineers. (1994). *Standard for the Structural Design of Composite Slabs ANSI/ASCE 3-91.* New York: American Society of Civil Engineers.

American Society of Civil Engineers. (2016). *Minimum Design Loads and Associate Criteria for Buildings and Other Structures ANSI/ASCE 7-16.* New York.

Bazant, Z., & Oh, B. H. (1983). Crack band theory for fracture of concrete. *Materials and Structures*, 155-177.

Beer, F. P., & Johnston, E. R. (1992). *Mechanics of Materials.* New York: McGraw Hill.

Bortolotti, L. (1994). Influence of Concrete Tensile Ductility on Compressive STrength of Confined Columns. *Journal of Materials in Civil Engineering*, 542-563.

Branson, D. E. (1963). *Instantaneous and Time-dependent Deflections of Simple and Continuous Reinforced Concrete Beams.* Alabama: State Highway Department.

Canam. (2010). *Steel Deck*. Canam Steel Corporation.

Canam. (2016). *Reveal Series Architectural Deck Products*. Canam Group Inc.

Chen, S. (2010). Discussion of "Determination of Composite Slab Strength Using a New Elemental Test Method" by Redzuan Abdullah and W. Samuel Easterling. *Journal of Structural Engineering*, 1032-1033.

Comite Euro-International du Beton. (1993). *CEB-FIP Model Code 1990.* Lausanne, Switzerland: Thomas Telford Services Ltd, Thomas Telford House.

Costa, R. S., Lavall, A. C., da Silva, R. G., Viana, H. F., Rodrigues, F. C., & Andrade, E. L. (2021). New equations to establish the effective moment of inertia of composite slabs with profiled steel sheeting for delection calculation. *Journal of Building Engineering*, 1-15.

Crisnel, M., & Edder, P. (2006). New Method for the Design of Composite Slabs. *Composite Construction in Steel and Concrete V*, 166-177.

Dally, J. W., & Riley, W. F. (1978). *Experimental Stress Analysis.* New York: McGraw Hill Book Company.

Damjanic, F., & Owen, D. R. (1984). Practical considerations for modeling of postcracking concrete behavior for finite element analysis of reinforced concrete structures. *International Conference on Computer Aided Analysis of the Design of Concrete Structures.* Pineridge, Swansea, U.K.

De Schutter, G. (1999). Extension towards Early Age Concrete of CEB-FIP Model Code 1990 Stress-Strain Relation for Short-Term Compressive Loading. *ACI Materials Journal*, 95-100.

El-Dardiry, E., & Tianjian, J. (2006). Modelling of the dynamic behaviour of profiled composite floors. *Engineering Structures*, 567-579.

Favre, R., & Charif, H. (1994). Basic Model and Simplified Calculations of Deformations According to the CEB-FIP Model Code 1990. *ACI Structural Journal*, 169-177.

Gholamhoseini, A. (2018). Experimental and finite element study of ultimate strength of continuous composite concrete slabs with steel decking. *International Journal of Advanced Structural Engineering*, 85-97.

Gholamhoseini, A., Gilbert, R. I., Bradford, M. A., & Chang, Z. T. (2014). Longitudinal shear stress and bond-slip relationships in composite concrete slabs. *Engineering Structures*(69), 37-48.

International Code Council, Inc. (2020). *2021 International Building Code.* Country Club Hills, IL: ICC Publications.

Kumar, S., & Barai, S. V. (2011). *Concrete Fracture Models and Applications.* New York: Springer.

Kumar, S., & Barai, S. V. (2011). *Concrete Fracture Models and Applications.* New York: Springer.

Lamport, W. B., & Porter, M. L. (1990). Deflection Predicitons for Concrete Slabs Reinforced with Steel Decking. *ACI Structural Journal*, 564-570.

Levinson, I. J. (1971). *Statics and Strength of Materials.* Englewood Cliffs, NJ: Prentice-Hall.

Mander, J. B., Priestley, M. J., & Park, R. (1988). Theoretical Stress-Strain Model for Confined Concrete. *Journal of Structural Engineering*, 1804-1826.

Norhalim, A. F., Jaini, Z. M., Abd Ghafar, N., Majid, M. A., & Ahwang, A. (2020). Dynamic Serviceability of Lightweight Composite Deck as Floor System Under Huma Excitation. *IOP Conference Series: Master Science Engineering*, (p. 713).

Norhalim, A. F., Jaini, Z. M., Ghafar, N. A., Majid, M. A., & Ahwang, A. (2020). Dynamic Serviceability of Lightweight Composite Deck as Floor System Under Human Excitation. *IOP Conf. Series: Materials Science and Engineering.* IOP Publishing.

Patrick, M. (1990). Long-spannning Composite Members with Steel Decking. *Tenth International Specialty Conference on Cold-formed Steel Structures* (pp. 81-102). St. Louis: University of Missouri-Rolla.

Rackham, J. W., Couchman, G. H., & Hicks, S. J. (2009). Composite Slabs and Beams using Steel Decking: Best Practice for Design and Construction. United Kingdom: The Steel Construction Institute and The Metal Cladding & Roof Manufacturers Association.

Simoes, R., & Pereira, M. (2019). Vertical shear behavior of steel-concrete composite slabs. *The 14th Nordic Steel Construction Conference* (pp. 289-294). Copenhagen: Nordic Steel.

Souza Neto, A. S. (2001). *Analysis of the behavior and resistance of a composite slab system with end anchorage with considerations on steel decking and friction in supports.* Brazil: Federal University of Minas Gerais.

Steel Deck Institute. (2014). *Celerating 75 years of deck*. Retrieved from Steel Deck Institute Web site: http://www.sdi.org/75th-anniversary

Steel Deck Institute. (2017). C-2017 Standard for Composite Steel Floor Deck-Slabs. American national Standards Institute / Steel Deck Institute.

Steel Deck Institute. (2017). T-CD-2017 Test Standards for Composite Steel Deck-Slabs. American National Standards Institute/ Steel Deck Institute.

Stramandinoli, R. S., & La Rovere, H. L. (2008). An efficient tension-stiffeneing model for nonlinear analysis of reinforced concrete members. *Engineering Structures*, 2069-2080.

Tenhovuori, A., Karkkainen, K., & Kanerva, P. (1996). Parameters and definitions for classifying the behaviour of composite slabs. *Composite Construction Steel Concrete III*, 752-765.

Thorne, R. (2009). Reviewed Work: Corrugated Iron: Building on the Frontier by Adam Mournment and Simon Holloway. *Construction History Vol. 24*. The Construction History Society.

Torres, L., Lopez-Almansa, F., & Bozzo, L. M. (2004). Thension-Stiffening Model for Cracked Flexural Concrete Members. *Journal of Structural Engineering*, 1242-1251.

van Mier, J. G. (1986). Multiaxial strain-softening of concrete, Part 1: Fracture. *Materiaux et Constructions*, 179-190.